UNIVERSITY OF AMSTERDAM

UvA-DARE (Digital Academic Repository)

Measurements of inclusive and differential cross-sections of $t\bar{t}\gamma$ production in pp collisions at $\sqrt{s}$ = 13 TeV with the ATLAS detector

ATLAS Collaboration

DOI
10.1007/JHEP10(2024)191

Publication date
2024

Document Version
Final published version

Published in
Journal of High Energy Physics

License
CC BY

Link to publication

Citation for published version (APA):
ATLAS Collaboration (2024). Measurements of inclusive and differential cross-sections of $t\bar{t}\gamma$ production in *pp* collisions at $\sqrt{s}$ = 13 TeV with the ATLAS detector. *Journal of High Energy Physics*, *2024*(10), Article 191. https://doi.org/10.1007/JHEP10(2024)191

General rights
It is not permitted to download or to forward/distribute the text or part of it without the consent of the author(s) and/or copyright holder(s), other than for strictly personal, individual use, unless the work is under an open content license (like Creative Commons).

Disclaimer/Complaints regulations
If you believe that digital publication of certain material infringes any of your rights or (privacy) interests, please let the Library know, stating your reasons. In case of a legitimate complaint, the Library will make the material inaccessible and/or remove it from the website. Please Ask the Library: https://uba.uva.nl/en/contact, or a letter to: Library of the University of Amsterdam, Secretariat, P.O. Box 19185, 1000 GD Amsterdam, The Netherlands. You will be contacted as soon as possible.

UvA-DARE is a service provided by the library of the University of Amsterdam (https://dare.uva.nl)

Download date:07 Sept 2026

Published for SISSA by Springer

Received: *March 15, 2024*
Accepted: *September 16, 2024*
Published: *October 25, 2024*

Measurements of inclusive and differential cross-sections of $t\bar{t}\gamma$ production in pp collisions at $\sqrt{s} = 13$ TeV with the ATLAS detector

The ATLAS collaboration

E-mail: atlas.publications@cern.ch

Abstract: Inclusive and differential cross-sections are measured at particle level for the associated production of a top quark pair and a photon ($t\bar{t}\gamma$). The analysis is performed using an integrated luminosity of 140 fb^{-1} of proton-proton collisions at a centre-of-mass energy of 13 TeV collected by the ATLAS detector. The measurements are performed in the single-lepton and dilepton top quark pair decay channels focusing on $t\bar{t}\gamma$ topologies where the photon is radiated from an initial-state parton or one of the top quarks. The absolute and normalised differential cross-sections are measured for several variables characterising the photon, lepton and jet kinematics as well as the angular separation between those objects. The observables are found to be in good agreement with the Monte Carlo predictions. The photon transverse momentum differential distribution is used to set limits on effective field theory parameters related to the electroweak dipole moments of the top quark. The combined limits using the photon and the Z boson transverse momentum measured in $t\bar{t}$ production in associations with a Z boson are also set.

Keywords: Hadron-Hadron Scattering

ArXiv ePrint: 2403.09452

Open Access, © The Authors.
Article funded by SCOAP^3.

https://doi.org/10.1007/JHEP10(2024)191

JHEP10(2024)191

Contents

1 Introduction **1**

2 ATLAS detector **3**

3 Simulation of signal and background processes **4**

4 Event reconstruction and selection **7**

5 Background estimation **9**

6 Systematic uncertainties **11**

7 Signal discrimination **12**

8 Cross-section definition **15**

9 Inclusive cross-section **16**
9.1 Results for the $t\bar{t}\gamma$ production measurement 16
9.2 Results for the total $t\bar{t}\gamma$ production and decay measurement 19

10 Differential cross-sections **20**
10.1 Differential distributions for the $t\bar{t}\gamma$ production 21
10.2 Differential distributions for the total $t\bar{t}\gamma$ production and decay process 30

11 EFT interpretation **36**

12 Conclusion **41**

A Variables used in the training of the neural networks **44**

B Differential cross-sections for the $t\bar{t}\gamma$ production process **47**

C Differential cross-sections for the combined $t\bar{t}\gamma$ production and decay process **50**

The ATLAS collaboration **58**

1 Introduction

Precise measurements of the associated production of a top quark pair ($t\bar{t}$) with a high-energy photon provide crucial information about the predictions of the Standard Model (SM) in the top quark sector, specifically of the top-photon electroweak coupling. Therefore, measurements of the inclusive and differential cross-sections of the $t\bar{t}\gamma$ process are a probe for possible extensions of the SM, being sensitive to new physics through anomalous dipole moments of the top quark [1–3], studied in the context of effective field theories (EFT) [4].

The first evidence for the production of $t\bar{t}\gamma$ was reported by the CDF Collaboration [5], while the observation of the $t\bar{t}\gamma$ process was established by the ATLAS Collaboration with

JHEP10(2024)191

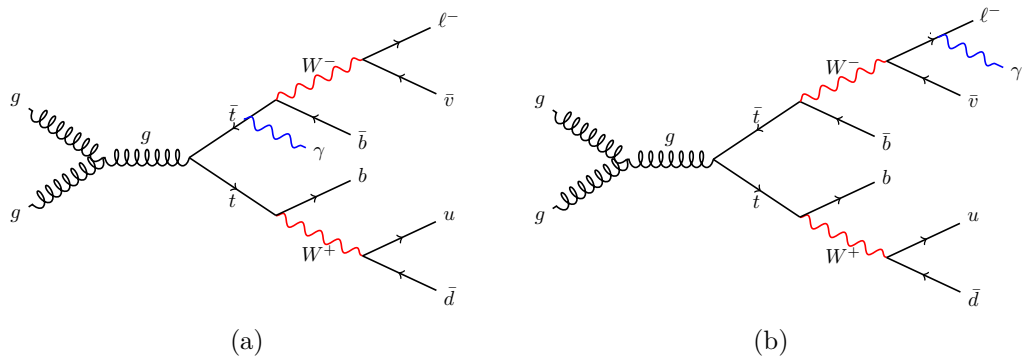

Figure 1. Examples of leading-order Feynman diagrams for (a) $t\bar{t}\gamma$ production and (b) $t\bar{t}\gamma$ decay in the single-lepton final state. The diagrams correspond to the cases where the photon is radiated by an off-shell top quark and by a charged lepton, respectively.

the data collected at $\sqrt{s} = 7$ TeV [6]. Since those measurements were published, efforts have concentrated on improving the precision and extending the scope of the inclusive and differential cross-section measurements [7–12] and the study of the production properties [13].

In $t\bar{t}\gamma$ final states, the photon can be emitted in the top quark production stage or in the decay stage (including the W boson and W boson decay products). Theoretical studies [14, 15] show that in the narrow-width approximation, which is valid in the considered kinematic regime as shown in ref. [15], the cross-section of the $t\bar{t}\gamma$ process with a high p_{T} photon in the final state can be factorised into two contributions: the first one describes the photon emission in the production part of the process, while the second corresponds to the emission from the top quark decay products. The interference among the production and decay contributions is negligible, both in the SM case and when considering the EFT effects. Of the two contributions the production one is the most sensitive to the top-photon coupling.

The main focus of this paper is the measurement of the inclusive and differential cross-sections of top quark pair production with an additional photon where the photon is radiated in the production part, i.e., from an initial-state parton or from an off-shell top quark, referred to as $t\bar{t}\gamma$ production, following the notation of ref. [13]. Thus, the analysis strategy is designed to improve the separation of the $t\bar{t}\gamma$ production events from the $t\bar{t}\gamma$ events where the photons are radiated from any of the charged decay products of the top quark (including the W boson), referred to as $t\bar{t}\gamma$ decay. Examples of Feynman diagrams at leading order for $t\bar{t}\gamma$ production and $t\bar{t}\gamma$ decay are illustrated in figure 1. In the simulation of the processes, all possible diagrams are considered. This approach enhances the sensitivity of the measurement to the top-photon coupling. The cross-sections of the $t\bar{t}\gamma$ process, regardless of the origin of the photon, are also measured to facilitate the comparison with a previous measurement using a partial data set at 13 TeV [9].

The measurements are performed using the data sample collected during Run 2 with the ATLAS detector at the Large Hadron Collider (LHC), between 2015 and 2018, corresponding to an integrated luminosity of 140 fb^{-1}, exploiting both the single-lepton and dilepton $t\bar{t}$ channels at stable particle level in a fiducial phase space. The differential cross-sections are measured in the same fiducial region as functions of photon kinematic variables, angular

JHEP10(2024)191

variables related to the photon and the leptons or the jets, and, in the dilepton channel, as functions of angular separations between the two leptons in the event.

In the single-lepton channel, events with exactly one photon, one lepton and at least four jets, with at least one jet identified as coming from the hadronisation of a b-quark (b-tagged), are selected. In the dilepton channel, the events are required to contain exactly one photon, two oppositely charged leptons (electrons or muons), and at least two jets with at least one of them being b-tagged. To separate the $t\bar{t}\gamma$ signal from the main background sources, multivariate discriminants are built using neural networks (NNs). They are used to define signal and control regions, enriched in signal or in background events, respectively. In the single-lepton channel, a multi-class approach is used, considering three different background categories, while in the dilepton channel a binary classifier is trained due to the smaller contribution of background processes.

The inclusive cross-section is obtained via a profile-likelihood fit to the discriminating variables in the signal and control regions. The differential cross-sections are corrected to stable particle level using a profile-likelihood unfolding approach. The results are interpreted in the context of EFT, testing the sensitivity of the $t\bar{t}\gamma$ production process to possible modifications of the coupling between the top quark and the photon. The limits on the relevant Wilson coefficients in the SM effective field theory (SMEFT) framework [4] are obtained from the differential cross-section measurement of the photon p_{T}. The production of $t\bar{t}$ in association with a Z boson ($t\bar{t}Z$) is also sensitive to modifications of the electroweak couplings between the Z boson and the top quark. The combined limits are extracted from the simultaneous measurement of the photon p_{T} and Z boson p_{T}, presented in ref. [16].

This paper is organised as follows. The ATLAS detector is described in section 2. The simulation of signal and background processes and the event reconstruction and selection are discussed in sections 3 and 4, respectively. The estimate of the background processes is summarised in section 5. The sources of systematic uncertainties considered in the measurements are described in section 6. Details of the analysis strategy and the NNs employed to discriminate between signal and background events are given in section 7. The definition of the fiducial regions and the results of the inclusive and differential cross-section measurements are presented in sections 8, 9 and 10, respectively. The combination with the $t\bar{t}Z$ process and the EFT interpretation are discussed in section 11. Finally, a summary of the results is given in section 12.

2 ATLAS detector

The ATLAS detector [17] at the LHC covers nearly the entire solid angle around the collision point.[1] It consists of an inner tracking detector surrounded by a thin superconducting

[1]ATLAS uses a right-handed coordinate system with its origin at the nominal interaction point (IP) in the centre of the detector and the z-axis along the beam pipe. The x-axis points from the IP to the centre of the LHC ring, and the y-axis points upwards. Polar coordinates (r, ϕ) are used in the transverse plane, ϕ being the azimuthal angle around the z-axis. The pseudorapidity is defined in terms of the polar angle θ as $\eta = -\ln\tan(\theta/2)$ and is equal to the rapidity $y = \frac{1}{2}\ln\left(\frac{E+p_z c}{E-p_z c}\right)$ in the relativistic limit. Angular distance is measured in units of $\Delta R \equiv \sqrt{(\Delta y)^2 + (\Delta\phi)^2}$.

JHEP10(2024)191

solenoid, electromagnetic and hadronic calorimeters, and a muon spectrometer incorporating three large superconducting air-core toroidal magnets.

The inner-detector system (ID) is immersed in a 2 T axial magnetic field and provides charged-particle tracking in the range $|\eta| < 2.5$. The high-granularity silicon pixel detector covers the vertex region and typically provides four measurements per track, the first hit generally being in the insertable B-layer (IBL) installed before Run 2 [18, 19]. It is followed by the SemiConductor Tracker (SCT), which usually provides eight measurements per track. These silicon detectors are complemented by the transition radiation tracker (TRT), which enables radially extended track reconstruction up to $|\eta| = 2.0$. The TRT also provides electron identification information based on the fraction of hits (typically 30 in total) above a higher energy-deposit threshold corresponding to transition radiation.

The calorimeter system covers the pseudorapidity range $|\eta| < 4.9$. Within the region $|\eta| < 3.2$, electromagnetic calorimetry is provided by barrel and endcap high-granularity lead/liquid-argon (LAr) calorimeters, with an additional thin LAr presampler covering $|\eta| < 1.8$ to correct for energy loss in material upstream of the calorimeters. Hadronic calorimetry is provided by the steel/scintillator-tile calorimeter, segmented into three barrel structures within $|\eta| < 1.7$, and two copper/LAr hadronic endcap calorimeters. The solid angle coverage is completed with forward copper/LAr and tungsten/LAr calorimeter modules optimised for electromagnetic and hadronic energy measurements respectively.

The muon spectrometer (MS) comprises separate trigger and high-precision tracking chambers measuring the deflection of muons in a magnetic field generated by the superconducting air-core toroidal magnets. The field integral of the toroids ranges between 2.0 and 6.0 T m across most of the detector. Three layers of precision chambers, each consisting of layers of monitored drift tubes, cover the region $|\eta| < 2.7$, complemented by cathode-strip chambers in the forward region, where the background is highest. The muon trigger system covers the range $|\eta| < 2.4$ with resistive-plate chambers in the barrel, and thin-gap chambers in the endcap regions.

The luminosity is measured mainly by the LUCID-2 [20] detector that records Cherenkov light produced in the quartz windows of photomultipliers located close to the beampipe.

Events are selected by the first-level trigger system implemented in custom hardware, followed by selections made by algorithms implemented in software in the high-level trigger [21]. The first-level trigger accepts events from the 40 MHz bunch crossings at a rate below 100 kHz, which the high-level trigger further reduces in order to record complete events to disk at about 1 kHz.

A software suite [22] is used in data simulation, in the reconstruction and analysis of real and simulated data, in detector operations, and in the trigger and data acquisition systems of the experiment.

3 Simulation of signal and background processes

A set of Monte Carlo (MC) simulated samples described in detail in ref. [13] is used in this paper to model the different signal and background processes. The response of the ATLAS detector was simulated [23] with GEANT4 [24]. Some of the alternative samples used to evaluate systematic uncertainties and in the EFT interpretation were processed using a fast

JHEP10(2024)191

simulation (AtlFast-II), which relies on a parameterisation of the calorimeter response [25]. All samples were reconstructed using the same software as for the data.

Two samples to model the $t\bar{t}\gamma$ process were simulated with the MadGraph5_aMC@NLO [26] generator. The first MC sample of $t\bar{t}\gamma$ events with the photon produced from the top quark or from initial-state radiation was simulated as a $2 \to 3$ process at next-to-leading (NLO) accuracy in quantum chromodynamics (QCD) with the on-shell top quarks in the final state being decayed at leading order (LO) using MadSpin [27, 28] to preserve spin correlations. The interference effects between initial-state photon radiation (from the incoming partons) and the final-state photon radiation (from the off-shell top quarks) were taken into account in the simulation. This sample is referred to as the '$t\bar{t}\gamma$ production sample' in the following. The second $t\bar{t}\gamma$ sample, where the photon arises from any of the decay products of the top quarks or from one of the on-shell top quarks, was simulated with the same version of MadGraph5_aMC@NLO but at LO precision as a $2 \to 2$ process followed by the decay of the top quarks, also simulated with MadGraph5_aMC@NLO at LO precision. This sample is referred to in the following as the '$t\bar{t}\gamma$ decay sample'. Both samples were generated by using the NNPDF3.0nlo [29] parton distribution function (PDF) set. The renormalisation and factorisation scales were set to $0.5 \times \sum_i \sqrt{m_i^2 + p_{\mathrm{T},i}^2}$, where m_i and $p_{\mathrm{T},i}$ are the masses and transverse momenta of the particles generated from the matrix element (ME) calculation. In both samples, photons were required to have $p_{\mathrm{T}} > 15$ GeV and to be isolated according to a smooth-cone hadronic isolation criterion [30], which avoids infrared divergences. The $t\bar{t}\gamma$ production sample is normalised to the NLO cross-section given by the MC simulation, while the normalisation of the $t\bar{t}\gamma$ decay sample is corrected by a NLO/LO inclusive K-factor of 1.5 obtained in ref. [13].

The $tW\gamma$ events were generated at LO accuracy with the MadGraph5_aMC@NLO generator in the five-flavour scheme (5FS). To simulate the full process, two complementary samples were generated: one as a $2 \to 3$ process assuming a stable top quark and the other as a $2 \to 2$ process, where the photon is radiated from any other final-state charged particle. The decay of the top quarks is also simulated with MadGraph5_aMC@NLO. To avoid infrared divergences, the photon was required to have $p_{\mathrm{T}} > 15$ GeV and $|\eta| < 5.0$ and to be separated by $\Delta R > 0.2$ from any parton. Both samples make use of the NNPDF2.3lo PDF set [31] and are normalised to the cross-section provided by the MC simulation.

The production of $t\bar{t}$ and single-top-quark events (tW, t- and s-channels) was modelled at NLO in QCD using Powheg-Box [32–35]. For the $t\bar{t}$ sample, the h_{damp} parameter that controls the p_{T} of the first additional emission, was set to 1.5 times the top quark mass [36]. The $t\bar{t}$ and single-top-quark simulated samples are normalised to the cross-sections calculated at next-to-next-to-leading order (NNLO) in QCD including the resummation of next-to-next-to-leading-logarithmic (NNLL) soft-gluon terms [37] at NNLO or approximated NNLO [38–40], respectively. The overlap between the $t\bar{t}$ and the single top tW final states is removed using the diagram-removal scheme [41].

The production of $V\gamma$, diboson processes (VV) with leptonic final states and V+jets processes with $V = W, Z$ were simulated using Sherpa [42, 43] at NLO in QCD with the NNPDF3.0nnlo PDF set. The $V\gamma$ production is normalised to the cross-section provided by the MC simulation. The diboson processes are normalised to NLO QCD cross-sections [44],

JHEP10(2024)191

and the W and Z boson samples are normalised to the cross-sections calculated at NNLO in QCD [45]. Events with a $t\bar{t}$ pair produced in association with a W or Z boson ($t\bar{t}V$) were simulated at NLO in QCD with MadGraph5_aMC@NLO using the NNPDF3.0nlo PDF set.

Two $t\bar{t}\gamma$ MC samples used in previous publications [9, 10] as nominal and to determine the parton shower uncertainty are used in this paper for comparison with the unfolded data in section 10.2. These samples were simulated at LO using the MadGraph5_aMC@NLO v2.3.3 generator [26] and the NNPDF2.3lo PDF set and were interfaced either to Pythia 8 or Herwig 7. The $t\bar{t}\gamma$ events were generated as a doubly resonant $2 \to 7$ process. Diagrams where the photon is radiated from the initial state, from the intermediate top quarks, b-quarks, the intermediate W bosons, and from the decay products of the W bosons, were included. The LO MC samples are re-scaled to the NLO prediction using the K-factors derived in ref. [9].

Additional MC samples were simulated at LO in QCD for the $t\bar{t}\gamma$ and $t\bar{t}Z$ production processes to perform the EFT interpretation. They were generated by using the MadGraph5_aMC@NLO generator with the same set-up as those discussed in ref. [16], including as universal FeynRules output the `SMEFTsim 3.0` model [46], in the M_W electroweak input scheme [47] with the `top` flavour restrictions (5FS). The renormalisation and factorisation scales were set to $\mu = \sum_i m_i$, where i indicates the massive final state resonances. The events were generated as the SM process, and the MadGraph5_aMC@NLO reweighting module was used to obtain alternative event weights to model the dimension-6 EFT vertices and propagators. Further details can be found in ref. [16].

All samples generated with Powheg-Box and MadGraph5_aMC@NLO were interfaced to Pythia 8 [48] to simulate the parton shower, fragmentation, and underlying event. The A14 set of tuned parameters (tune) [49] and the NNPDF2.3lo PDF set were used in Pythia. The heavy-flavour hadron decays were modelled by EvtGen [50]. All samples generated with Sherpa used the Sherpa parton shower based on the Catani-Seymour dipole factorisation with a dedicated tune provided by the authors [51]. The top quark mass was set to 172.5 GeV. The overlap between the samples in which events were generated without explicitly including a photon in the ME in the final state and the samples where photons were included, such as $t\bar{t}\gamma$, $tW\gamma$ and $V\gamma$, was removed following the same procedure as described in ref. [13]. In particular, events with parton-level photons with $p_{\mathrm{T}} > 15$ GeV and separated by $\Delta R > 0.2$ from any charge lepton are discarded. The number of the events from the inclusive samples subject to the overlap removal amounts to a few per cent of the total number of events.

Additional pp collisions in the same or neighbouring bunch crossings (pile-up) were modelled by overlaying minimum bias events, simulated using Pythia 8 with the A3 tune [52] and the NNPDF2.3lo PDF set, on events from hard-scatter processes. The MC events were reweighted to reproduce the distribution of the average number of interactions per bunch crossing observed in the data.

Corrections to the trigger, reconstruction and selection efficiencies, and the energy scales and resolutions, are applied to the MC simulated events to match the performance in the data.

JHEP10(2024)191

4 Event reconstruction and selection

This analysis is performed using the pp collision data collected with the ATLAS detector between 2015 and 2018 at $\sqrt{s} = 13\,\text{TeV}$. After the application of data-quality requirements [53], the data sample corresponds to an integrated luminosity of 140 fb^{-1} [54]. Events were selected using single-lepton triggers with variable electron and muon transverse momentum (p_{T}) thresholds, and various identification and isolation criteria depending on the lepton flavour and the data-taking period [55–58]. The events are also required to have at least one reconstructed collision vertex with two or more associated tracks with $p_{\text{T}} > 0.5$ GeV. The primary vertex is chosen as the vertex with the highest $\sum p_{\text{T}}^2$ of the associated tracks and consistent with the average beam-spot position.

Photon candidates are reconstructed from energy deposits (clusters) in the central region of the electromagnetic calorimeter. Two types of photon candidates are considered: the unconverted, with the cluster not matched to any reconstructed track in the ID system, and the converted, with the cluster matched to reconstructed tracks consistent with originating from a photon conversion and with a reconstructed conversion vertex. Both types of photons are required to satisfy a *tight* identification criteria [59] and to be isolated [59] fulfilling the criteria $E_{\text{T}}^{\text{iso}}|_{\Delta R=0.4} < 0.022 \cdot E_{\text{T}}(\gamma) + 2.45\,\text{GeV}$ and $p_{\text{T}}^{\text{iso}}|_{\Delta R=0.2} < 0.05 \cdot E_{\text{T}}(\gamma)$, where $E_{\text{T}}^{\text{iso}}|_{\Delta R=0.4}$ is the calorimeter isolation within a cone of radius $\Delta R = 0.4$ in the direction of the photon candidate, $p_{\text{T}}^{\text{iso}}|_{\Delta R=0.2}$ is the track isolation within $\Delta R = 0.2$ and $E_{\text{T}}(\gamma)$ is the transverse energy of a photon.[2] Photon candidates are selected if they satisfy $E_{\text{T}}(\gamma) > 20$ GeV, $|\eta_{\text{cluster}}| < 2.37$ and $|\eta_{\text{cluster}}| \notin [1.37, 1.52]$, the transition region between the barrel and the endcap calorimeters.

Electron candidates are reconstructed from energy deposits in the central region of the electromagnetic calorimeter associated with reconstructed tracks from the ID system, and are required to satisfy the *MediumLH* identification criteria [59] and have a pseudorapidity of $|\eta_{\text{cluster}}| < 2.47$, excluding candidates in the transition region ($|\eta_{\text{cluster}}| \notin [1.37, 1.52]$).

Muon candidates are reconstructed with a combined algorithm, using the track segments in the various layers of the muon spectrometer and the tracks in the ID system. Muons are required to satisfy the *Medium* identification quality criteria and to have $|\eta| < 2.5$ [60].

The electron and muon candidates are required to have $p_{\text{T}} > 25$ GeV ($p_{\text{T}} > 20$ GeV for the subleading lepton in the dilepton channel) and meet the loose working point (WP) of the prompt-lepton isolation discriminant [61], trained to separate prompt and non-prompt leptons. The transverse impact parameter divided by its estimated uncertainty, $|d_0|/\sigma(d_0)$, is required to be less than five (three) for electron (muon) candidates. The longitudinal impact parameter must satisfy $|z_0 \sin(\theta)| < 0.5$ mm for both lepton flavours.

Jets are reconstructed using the anti-k_t algorithm [62] in the FastJet implementation [63] with a radius parameter $R = 0.4$ using particle flow objects [64]. The jet energy scale (JES) and resolution are calibrated using simulations with in situ corrections obtained from data [65].

[2] The calorimeter isolation $E_{\text{T}}^{\text{iso}}\big|_{\Delta R=0.4}$ is calculated as the sum of the transverse energy of the topological clusters in the calorimeter in a cone of $\Delta R = 0.4$ around the barycentre of the photon candidate, with the core energy of the photon candidate subtracted. The track isolation $p_{\text{T}}^{\text{iso}}\big|_{\Delta R=0.2}$ is obtained by adding the p_{T} of the tracks with $p_{\text{T}} > 1\,\text{GeV}$ within $\Delta R = 0.2$ around the photon cluster. The tracks associated with photon conversions are excluded from the calculation.

JHEP10(2024)191

They are required to have $p_{\mathrm{T}} > 25\,\mathrm{GeV}$ and $|\eta| < 2.5$. To reject jets from pile-up or other primary vertices, a *jet vertex tagger* (JVT) discriminant [66] is required to be larger than 0.59 for jets with $p_{\mathrm{T}} < 60\,\mathrm{GeV}$ and $|\eta| < 2.4$. Jets arising from b-quark hadronisation, referred to as b-jets, are identified using the DL1r b-tagging algorithm [67]. The b-tagged jets are required to satisfy the WP corresponding to 70% or 85% efficiency for identifying b-quark initiated jets in $t\bar{t}$ simulated events in the single-lepton or dilepton channels, respectively. To fully exploit the b-tagging information of an event, each jet is assigned a pseudo-continuous b-tagging score that defines if a jet satisfies a given WP but fails to satisfy the adjacent tighter one. A score of two, three, four or five is assigned to a jet satisfying the 85%, 77%, 70% or 60% WP, respectively. If a jet does not satisfy any WP, a score of one is assigned.

The missing transverse momentum vector, with magnitude $E_{\mathrm{T}}^{\mathrm{miss}}$, is defined as the negative sum of the transverse momenta of the reconstructed and calibrated physical objects, plus a 'soft term' built from all other tracks not matched to a reconstructed object that are associated with the primary vertex [68].

An overlap removal procedure is applied to avoid the double counting of detector signatures. Electron candidates sharing a track with a muon candidate are first removed. The closest jet found within a $\Delta R = 0.2$ cone of an electron is removed and electrons within a $\Delta R = 0.4$ cone of a remaining jet are rejected. Jets with less than three associated tracks and within $\Delta R = 0.2$ of the muon and muons within $\Delta R = 0.4$ of a jet with more than two associated tracks are rejected. Photons within a $\Delta R = 0.4$ cone of a remaining lepton are removed. Finally, jets found in a $\Delta R = 0.4$ cone around a photon are removed.

Events in the single-lepton channel are selected if they contain exactly one photon and one isolated electron or muon, fulfilling the requirements described above and matched to the corresponding trigger-level object. The p_{T} thresholds for the matched leptons are 25 GeV in 2015 data, 27 GeV in 2016 data, and 28 GeV in 2017 and 2018 data, which are at least 1 GeV above the p_{T} thresholds of the single-lepton triggers. Events are rejected if there are additional lepton candidates with $p_{\mathrm{T}} > 7$ GeV. Additionally, only events where the invariant mass of the electron and the photon is outside a Z boson mass window of ± 5 GeV are kept to reduce the background contribution from $Z \to ee$ events, where an electron is misidentified as a photon. Events are required to contain at least four reconstructed jets, and at least one of these jets is required to be tagged as a b-jet using a 70% WP. In the dilepton channel, events are selected if they contain exactly two isolated leptons (ee, $e\mu$, $\mu\mu$) of opposite electric charges and at least one is matched to the corresponding trigger-level object, and at least two jets out of which at least one is b-tagged using a WP with 85% efficiency. In the same lepton flavour channels, events with an invariant mass of the lepton pair smaller than 15 GeV are rejected to suppress contribution from the decays of heavy-flavour resonances and low-mass Drell-Yan processes. Events in the ee and $\mu\mu$ channels are also required to have an invariant mass outside a Z boson mass window of $\pm$ 5 GeV, and to have $E_{\mathrm{T}}^{\mathrm{miss}} > 30$ GeV to further reject backgrounds from $Z\gamma$ processes.

JHEP10(2024)191

5 Background estimation

Background processes are divided into categories based on the photon origin into the prompt and fake or misidentified photon background, where the photon is mimicked by another object, such as a misreconstructed hadron or electron. The contribution of events with prompt photons is estimated by using MC simulation while the fake backgrounds are estimated by using data-driven methods. In the following, the background categories and the methods used to estimate them are briefly summarised. Further details can be found in ref. [13].

The largest prompt photon background contribution arises from $t\bar{t}\gamma$ decay events, about 30% (45%) of the total number of events in the single-lepton (dilepton) channel. All other background processes with a prompt photon ($tW\gamma$, single-top quark, $V\gamma$, VV, $t\bar{t}V$ and $t\bar{t}$), referred to as the 'Other γ' background category, constitute about 15% of the selected events in both channels.

The contribution from processes with an electron mimicking a photon signature, 'e-fake', is estimated in data from the numbers of electron-positron candidates from $Z \to e^+e^-$ decays that are reconstructed as ee or $e\gamma$ pairs [69]. Two control regions are defined: one containing events with an electron-positron pair and the other, enriched in e-fake events, selecting events with an electron and a photon satisfying the selection criteria of the signal region. The e-fake rate is determined by comparing the observed ee and $e\gamma$ invariant mass spectra around the Z boson peak in these two regions, after having subtracted the respective background contributions, estimated from the sidebands around the Z boson peak. It is measured as a function of photon η and p_{T}, separately for converted and unconverted photons. The systematic uncertainty in the e-fake background estimate arises from the choice of the function describing the Z boson mass peak and the mass range considered as well as from the assumed function for the background description. The ratio of the e-fake rates in data and simulation measured in ref. [13] is used to correct the e-fake background predicted by the simulation in the signal regions. The e-fake background originates mainly from dilepton $t\bar{t}$ events where an electron from the top quark decay chain is identified as a photon resulting in the same signature as the single-lepton $t\bar{t}\gamma$ channel. It represents about 15% of the total number of selected events in this channel, while the e-fake contribution is below 1% in the dilepton channel.

The background contribution from events where the photon signature arises from hadronic energy depositions in the electromagnetic calorimeter or from hadron decays, referred to as 'h-fake', is estimated from data using the 'ABCD' data-driven method [70]. In this approach, three orthogonal regions enriched with h-fake photon events are defined either by inverting the photon isolation or by loosening some of the identification criteria. Counting the number of selected data events in these regions, after subtracting the prompt photon and e-fake background contributions, allows the number of h-fake events in the signal region to be evaluated and the correction factors relative to the MC prediction to be determined. These correction factors are obtained as a function of photon p_{T} and η, separately for converted and unconverted photons, and applied to the simulation to determine the h-fake background contribution. Since around 90% of h-fake events originate from $t\bar{t}$ production, all modelling uncertainties considered for the $t\bar{t}$ process and described in section 6 are propagated to the correction factors and constitute the dominant source of the uncertainty. Additional contributions arise from the normalisation uncertainties in the prompt photon backgrounds and the

JHEP10(2024)191

Category	Single-lepton channel	Dilepton channel
$t\bar{t}\gamma$ production	12450 ± 740	2400 ± 99
$t\bar{t}\gamma$ decay	13400 ± 3100	3100 ± 640
h-fake	3600 ± 1200	220 ± 82
e-fake	6900 ± 980	57.9 ± 7.0
$W\gamma$	2700 ± 1400	—
$tW\gamma$	1180 ± 580	290 ± 150
Other prompt γ	2500 ± 600	820 ± 170
Lepton fake	640 ± 110	—
Total	43900 ± 4600	6900 ± 710
Data	47767	7379

Table 1. The observed data and the expected event yields for the signal and backgrounds in the single-lepton and dilepton channels. All data-driven corrections are included. The $t\bar{t}\gamma$ decay sample is scaled by the NLO K-factor. The $W\gamma$ contribution is included in the Other prompt γ category in the dilepton channel. Lepton fakes in the dilepton channel are negligible and are included in the corresponding MC yields. The uncertainties correspond to the sum of the statistical and systematic uncertainties (see section 6). The uncertainty of the $t\bar{t}\gamma$ decay events includes the uncertainty in the K-factor.

uncertainties in the data-driven e-fake background entering the h-fake enriched regions. This category corresponds to about 7% (3%) of the events in the single-lepton (dilepton) channel.

An additional small background contribution arising from events with a non-prompt or misidentified lepton, referred to as 'lepton fake', is also obtained from data with the 'matrix method' [71]. The contribution of this process in the single-lepton channel is estimated from the data events, satisfying lepton selection requirements with looser identification and isolation, corrected by a weight that depends on the efficiency of a real prompt and a fake or misidentified loose lepton to satisfy tight lepton selection criteria. Systematic uncertainties in the fake lepton background estimate arise from the statistical uncertainties and the choice of parameterisation of real and fake lepton efficiencies. This contribution is negligible in the dilepton channel. It is taken from simulation and is not treated as a separate category.

The observed data and the expected event yields for the signal and background processes in both channels after applying all data-driven corrections are given in table 1. The 'Other prompt γ' category corresponds to Other γ background excluding the $tW\gamma$ and $W\gamma$ contribution in the single-lepton channel.

JHEP10(2024)191

6 Systematic uncertainties

Several sources of systematic uncertainty, arising from detector effects or theoretical assumptions, and uncertainties due to the limited number of events in the MC simulations, are considered in the inclusive and differential measurements in both channels. They affect the event yields and the shapes of the distributions of the observables of interest.

The correction factors applied to the simulated samples to improve the description of the photon and lepton identification and isolation efficiencies, momentum scale and resolution [59, 60], and lepton trigger efficiencies are varied within their uncertainties to estimate the corresponding systematic uncertainty. The JES uncertainty [65] accounts for contributions from jet-flavour composition, η-intercalibration, punch-through, single-particle response, calorimeter response to different jet flavours, and pile-up, resulting in 30 uncorrelated JES uncertainty subcomponents. The jet energy resolution has been measured separately for data and MC using two in situ techniques [65]. The systematic uncertainty is defined as the quadratic difference between the jet energy resolutions for data and simulation and split into 13 uncorrelated uncertainty components. Additionally, the uncertainty associated with the JVT discriminant for pile-up jet rejection is obtained by varying the efficiency correction factors [66]. The uncertainties in the b-jet tagging calibration are determined separately for b-jets, c-jets and light-flavour jets [72–74] and are decomposed into several uncorrelated components for each category. Additionally, a 50% normalisation uncertainty is applied to events with high-p_{T} jets above the p_{T} limit where the b-jet tagging algorithm is calibrated. The fractions of such events with high-p_{T} b-jets, c-jets or light jets are about 0.3%, 0.8% and 3.5%, respectively. The uncertainty in $E_{\mathrm{T}}^{\mathrm{miss}}$ results from the propagation of the uncertainties in the energy scales and resolutions of photons, leptons and jets, and from the modelling of its soft term [68].

The uncertainty in the integrated luminosity is 0.83% [54], obtained using the LUCID-2 detector [20] for the primary luminosity measurements. The uncertainty in the pile-up modelling is obtained by varying the pile-up reweighting applied to match the distribution in the simulation to the data within its uncertainties.

The signal and background modelling uncertainties account for effects from the choice of QCD scales, parton shower (PS), amount of QCD initial-state radiation (ISR), and PDF set. They are treated as uncorrelated sources of uncertainty between different processes. The effect of the QCD scale uncertainty for each of the $t\bar{t}\gamma$, $tW\gamma$ and $t\bar{t}$ processes is obtained by separately varying the renormalisation and factorisation scales relative to their nominal values by a factor of two up and down. The uncertainty from the PS and hadronisation is estimated by comparing the nominal simulated samples interfaced to Pythia 8 with samples interfaced to Herwig 7.2.1 [75, 76]. The uncertainty in the modelling of the ISR is estimated by varying the amount of radiation corresponding to the *var3c* eigentune uncertainty [49] in the A14 tune. The impact of the ME corrections applied to all emissions is evaluated by comparing the nominal sample to a dedicated Powheg + Pythia 8 sample with the corrections turned off. An additional uncertainty is applied to the $t\bar{t}$ process by comparing the nominal sample to the alternative one simulated with h_{damp} parameter in Powheg, increased by a factor of two [77]. The uncertainty in the PDFs for the signal and background $t\bar{t}\gamma$ processes is estimated by using the 30 PDF variations of the PDF4LHC15

JHEP10(2024)191

prescription [78]. Each PDF variation is considered as a separate nuisance parameter in the fit.

The total uncertainties associated with the data-driven estimates of the e-fake, h-fake, and lepton-fake backgrounds are propagated to the final result. A normalisation uncertainty of 20% is assigned to the $t\bar{t}\gamma$ decay process, based on the estimated uncertainty in the NLO K-factor [9], in the case of the measurement of the total, production and decay, $t\bar{t}\gamma$ cross-section. The uncertainty in the normalisation of the background processes estimated from MC is 6% for $t\bar{t}$ [37], 50% for $W\gamma$ [13] and for all other minor background processes contributing to the Other γ category, i.e., single top quark, $t\bar{t}V$, diboson, and $Z\gamma$.

7 Signal discrimination

To separate the signal from the background processes multivariate analysis techniques are employed, in particular fully connected feed forward NNs. In the single-lepton channel, a multi-class NN is used to separate the $t\bar{t}\gamma$ production signal from the background, which is divided into three categories: $t\bar{t}\gamma$ decay, fake photon processes (e-fake photons and h-fake photons) and other prompt photon backgrounds. In the dilepton channel, where the background contribution from sources other than $t\bar{t}\gamma$ decay is much smaller, a binary classification NN is employed to separate the $t\bar{t}\gamma$ production signal from all background sources.

A total of 40 and 16 variables are used as input to the NN training in the single-lepton and the dilepton channels, respectively. These variables describe the kinematic properties of the photon and the leptons, the kinematic and flavour properties of the jets, and the invariant masses and angular distances between different combinations of objects. Additionally, in the single-lepton channel, to improve the discrimination between the $t\bar{t}\gamma$ production and $t\bar{t}\gamma$ decay processes, the $t\bar{t}\gamma$ event is reconstructed. The two jets with the highest b-tagging score in the event are considered to be the two b-jets from a $t\bar{t}$ decay. If two b-tagged jets have the same score, the one with the largest p_{T} is chosen. The rest of the jets are used to find a pair with an invariant mass closest to the W boson mass to reconstruct the hadronically decaying W boson ('hadronic W boson'). The leptonically decaying W boson ('leptonic W boson') is reconstructed using the W boson mass constraint, lepton and $E_{\mathrm{T}}^{\mathrm{miss}}$ information, and solving the quadratic equation to determine the z-component of the neutrino momentum. For real solutions, the smallest value is chosen, while in the case of complex solutions, the real part of the solution is considered. The reconstructed W bosons, b-jets and a photon are used to reconstruct the top quark and antiquark. Out of the four possible permutations corresponding to an assignment of b-jets and a photon to the hadronic or leptonic W boson decay, the one that minimises the value of $\Delta m^2 = (m_1 - m_t)^2 + (m_2 - m_t)^2$, where m_1 and m_2 are the invariant masses of the two reconstructed top quarks and $m_t = 172.5$ GeV, the top quark mass in the simulation, is selected as the best solution. Several variables related to the reconstructed W bosons, such as the invariant masses of the leptonic and hadronic W bosons and Δm^2, are used in the NN training. Since the selected photon is included in the event reconstruction as one of the $t\bar{t}$ decay products, these variables are expected to behave differently and provide separation between $t\bar{t}\gamma$ decay and $t\bar{t}\gamma$ production events, where the photon is not emitted by the decay products of the $t\bar{t}$ system. The list of variables used in

JHEP10(2024)191

the NN training in each channel and examples of the variables with the largest separation power can be found in appendix A.

The training of the NNs is performed using Keras [79] with the TensorFlow backend [80] and categorical or binary cross-entropy as a loss function in the single-lepton and dilepton channels, respectively. All MC simulated samples described in section 3 with the corresponding data-driven scale factors, if applicable, are used in the training. It is verified that the shapes of the input variables in the inclusive region and in each of the categories are well described by the simulations. The resulting output distributions are shown in figure 2 for the four NN nodes ($t\bar{t}\gamma$ production, $t\bar{t}\gamma$ decay, photon fakes and other prompt photon) in the single-lepton channel and for the binary NN in the dilepton channel. The shape of the distributions is well described by the simulation in all the categories. A slight underestimate of the data by the SM prediction in the regions where the fraction of $t\bar{t}\gamma$ production events is significant is likely due to a smaller $t\bar{t}\gamma$ production cross-section in MC simulation than in data that was observed in the previous measurements [9, 12].

JHEP10(2024)191

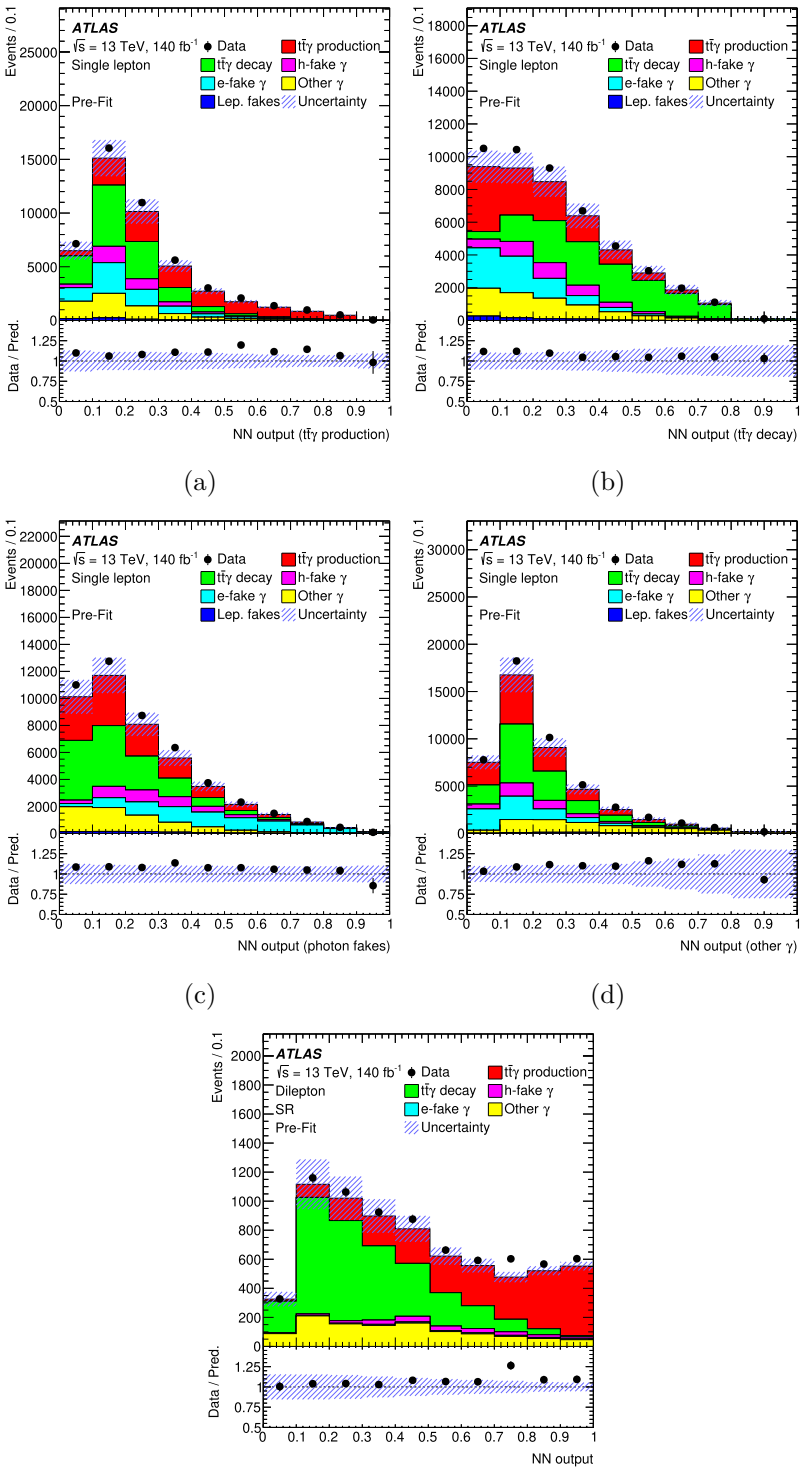

Figure 2. Distributions of the four NN output classifiers in the single-lepton channel: (a) $t\bar{t}\gamma$ production node, (b) $t\bar{t}\gamma$ decay node, (c) photon fakes and (d) other prompt γ, and (e) the NN output in the dilepton channel. The lower panels show the ratios of the data to the predictions. The uncertainty band represents the total uncertainties before the fit to data.

JHEP10(2024)191

To enhance the separation of the $t\bar{t}\gamma$ production process from the different background categories and to better constrain the uncertainties in the different processes and increase the overall sensitivity, a signal and three control regions are defined based on the four NN output classifiers in the single-lepton channel. The $t\bar{t}\gamma$ production signal region (SR) is defined first, followed by the control region (CR) enriched in $t\bar{t}\gamma$ decay events, and the CR enriched in h-fake photons and e-fake photons processes. The remaining events form the other prompt photon CR. The detailed criteria to define the signal and the control regions based on the requirements on the NN output classifiers are summarised in table 2.

8 Cross-section definition

Although the focus of this paper is to consider only the $t\bar{t}\gamma$ production process as a signal, the cross-sections are also measured including the $t\bar{t}\gamma$ decay process as part of the signal for completeness and for a comparison with the previous measurements. The inclusive and differential cross-sections are measured in all scenarios at particle level in a fiducial region, defined by the kinematic properties of the signal process, in which all selected final-state objects are produced within the detector acceptance.

Particle level refers to a collection of objects that are considered stable in MC simulation (lifetime $\tau \geq 30$ ps) but without any simulation of the interaction of these particles with the detector components or additional pp interactions. The objects at particle level are defined in the following.

Photons are required to not originate from a hadron decay, satisfy $E_{\mathrm{T}} > 20\,\mathrm{GeV}$ and $|\eta| < 2.37$, and that the sum of transverse momenta of all charged particles surrounding the photon within $\Delta R = 0.2$ is less than 5% of its own p_{T}. Muons and electrons are required to have $p_{\mathrm{T}} > 25$ GeV and $|\eta| < 2.5$, and must not originate from hadron decays. The momenta of nearby photons, within a $\Delta R = 0.1$ cone, are added to the lepton before applying the selection. Particle-level jets are clustered with the anti-k_t algorithm with a radius parameter of $R = 0.4$. All stable particles are considered in the clustering, except for the selected electrons, muons and photons, and the neutrinos originating from the top quarks. Jets are required to satisfy $p_{\mathrm{T}} > 25$ GeV and $|\eta| < 2.5$. A jet is identified as a b-jet if a hadron with $p_{\mathrm{T}} > 5\,\mathrm{GeV}$ containing a b-quark is matched to the jet through a ghost-matching method [81]. Muons and electrons with separation $\Delta R < 0.4$ from a jet are excluded. Jets are removed if they are within $\Delta R = 0.4$ of an isolated photon candidate. Events are additionally required to satisfy $\Delta R(\gamma, \ell) > 0.4$, where ℓ is the electron or muon.

The fiducial phase space in the single-lepton channel is defined by requiring exactly one photon, exactly one electron or muon, and at least four jets, and in the dilepton channel by requiring exactly one photon and exactly two leptons, and at least two jets. In both cases, at least one jet must be a b-tagged jet. Events are rejected if there are additional leptons with $p_{\mathrm{T}} > 7$ GeV. For the combination of the channels, a union of the single-lepton and dilepton fiducial phase spaces is used.

In the case of the measurement of $t\bar{t}\gamma$ production, the efficiency of selecting and reconstructing events that are generated within the fiducial phase space is about 31% in the single-lepton channel and about 35% in the dilepton channel, while the fractions of events

JHEP10(2024)191

Category	$t\bar{t}\gamma$ decay classifier	fake γ classifier	other prompt γ classifier	purity
SR $t\bar{t}\gamma$ production	< 0.15	< 0.2	< 0.5	73%
CR $t\bar{t}\gamma$ decay	> 0.25	—	< 0.4	71%
CR fake γ	< 0.15	> 0.2	< 0.5	50%
CR Other γ		remaining events		26%

Table 2. Summary of the criteria to define the signal and the control regions in the single-lepton channel, based on the requirements on the NN output classifiers. The last column of the table corresponds to the purity of the target processes (signal or specific background processes) in the particular region.

that satisfy the selection at the reconstruction level but fail to satisfy the particle-level requirements are about 17% and 19%, respectively.

9 Inclusive cross-section

The fiducial inclusive $t\bar{t}\gamma$ production cross-sections are obtained using a binned profile-likelihood fit. The expected signal and background distributions are modelled by template histograms from the MC simulated samples corrected by the data-driven estimates where applicable. The sum of signal and background contributions is fitted to the data. The likelihood function consists of Poisson terms for the event yields and Gaussian functions to constrain the nuisance parameters which represent the systematic uncertainties described in section 6. For the uncertainties related to the finite number of simulated MC events, the Gaussian terms in the likelihood are replaced by Poisson terms, following the Barlow-Beeston 'light' approach [82].

In the single-lepton channel, the fit is performed in the four regions defined in section 7. In the $t\bar{t}\gamma$ production and the $t\bar{t}\gamma$ decay regions, the output of the corresponding NN classifiers are used as fitted distributions while in the photon fakes CR and in the other prompt photon CR the distributions of the second largest pseudo-continuous b-tagging score are used. The choice of the fitted variable in the photon fakes CR and in the other prompt photon CR is motivated by a requirement to have bins that are sufficiently well populated by the targeted processes that are statistically limited. Additionally, since most of the other prompt photon backgrounds have fewer b-jets than the signal, the second largest b-tagging score distribution provides a reasonably good discrimination. In the dilepton channel the NN output is used in the fit. The binning of the NN output distributions in both channels is chosen to avoid bins with large statistical uncertainties and to ensure that distributions of the small backgrounds are smooth, while keeping a good separation between the process of interest and the backgrounds.

9.1 Results for the $t\bar{t}\gamma$ production measurement

For the $t\bar{t}\gamma$ production cross-section measurement, the normalisation of the $t\bar{t}\gamma$ decay process is a free parameter in the profile-likelihood fit. Figures 3 and 4 show the distributions of the fitted variables in the single-lepton and dilepton channel after the fit. Good agreement

JHEP10(2024)191

is observed between data and the prediction in both channels. The uncertainty bands are calculated taking into account the full post-fit correlation matrix.

The measured fiducial $t\bar{t}\gamma$ production cross-section in the single-lepton channel is

$$\sigma^{\text{Single lepton}}_{t\bar{t}\gamma\text{ production}} = 288^{+21}_{-19}\,\text{fb} = 288 \pm 5(\text{stat})^{+20}_{-19}(\text{syst})\,\text{fb},$$

and, in the dilepton channel, it is

$$\sigma^{\text{Dilepton}}_{t\bar{t}\gamma\text{ production}} = 45.7^{+3.3}_{-3.1}\,\text{fb} = 45.7^{+1.4}_{-1.3}(\text{stat})^{+3.0}_{-2.8}(\text{syst})\,\text{fb}.$$

The value of the normalisation factor of the $t\bar{t}\gamma$ decay contribution determined by the fit is 0.99 ± 0.07 in both channels. The total relative uncertainties in the measurements are 7.6% (7.1%) in the single-lepton (dilepton) channel. The systematic uncertainty is determined by subtracting the statistical uncertainty in quadrature from the total uncertainty. The statistical uncertainty is obtained from a fit where all nuisance parameters are fixed to their post-fit values.

Most of the nuisance parameters are not constrained by the fit and their best-fit values are well within one standard deviation of the prior uncertainties. The fit slightly constrains the $t\bar{t}\gamma$ production parton-shower uncertainty in the single-lepton channel, resulting in an uncertainty 20% smaller than its initial value.

The measured cross-sections are in agreement within the uncertainties with the NLO predictions from MadGraph5_aMC@NLO interfaced to Pythia 8, which correspond to $255^{+25}_{-26}(\text{scale})^{+6}_{-4}(\text{PDF})$ fb and $40.9^{+3.9}_{-4.0}(\text{scale})^{+0.9}_{-0.5}(\text{PDF})$ fb in the single-lepton and dilepton channel, respectively, with a central value about 10% larger than the corresponding predictions.

The $t\bar{t}\gamma$ production cross-section is also obtained from a simultaneous profile-likelihood fit to the data in all the signal and control regions in the single-lepton and the dilepton channels treating all systematic uncertainties as correlated. The result yields:

$$\sigma_{t\bar{t}\gamma\text{ production}} = 319 \pm 15\,\text{fb} = 319 \pm 4\,(\text{stat})\,^{+15}_{-14}(\text{syst})\,\text{fb}.$$

The measured value is slightly lower than the sum of the two channels owing to the correlations among systematic uncertainties. In particular, the fits performed in the dilepton and single-lepton channels separately show different correlations after the fit between the parton-shower uncertainty in the $t\bar{t}\gamma$ production and the cross-section. The difference between the correlations also leads to a reduction of this uncertainty in the combined fit. This observed behaviour of the parton-shower uncertainty is related to the jet-related variables having a different impact on the fitted distributions, also resulting in a reduction of some JES and flavour tagging uncertainties in the combination. The relative uncertainty of the combined $t\bar{t}\gamma$ production cross-section is 5.2%, and the normalisation of the $t\bar{t}\gamma$ decay component determined from the combined fit is 0.98 with an uncertainty of 6%. The expected cross-section given by the NLO MadGraph5_aMC@NLO simulation is $296^{+29}_{-30}(\text{scale})^{+6}_{-4}(\text{PDF})$ fb.

The impact of the systematic uncertainties on the inclusive cross-section in the single-lepton and dilepton channels grouped into different categories is given in table 3. The measurements are limited by the systematic uncertainties. The dominant sources are those related to the modelling of the $t\bar{t}\gamma$ production in both channels and the normalisation of

JHEP10(2024)191

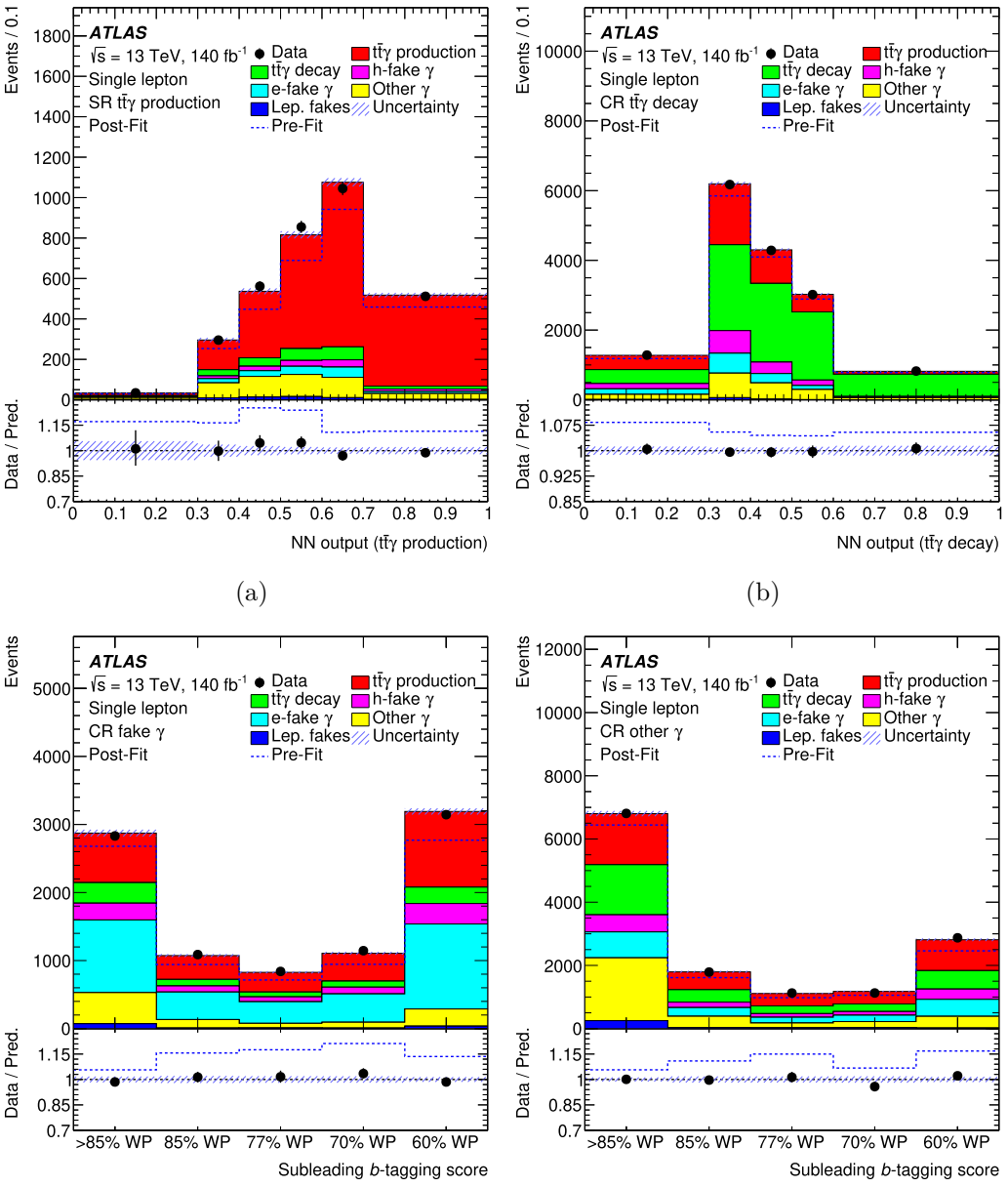

Figure 3. Distributions of (a) the $t\bar{t}\gamma$ production classifier in the SR, (b) the $t\bar{t}\gamma$ decay classifier in the $t\bar{t}\gamma$ decay CR and the second largest pseudo-continuous b-tagging score in (c) the photon fakes CR and (d) the other prompt photon CR after the fit to data for the measurement of the $t\bar{t}\gamma$ production cross-section in the single-lepton channel. The uncertainty band represents the total post-fit uncertainty in the prediction. The lower panels show the ratios of the data to the total post-fit predictions. The dashed lines correspond to the pre-fit prediction (upper panel) and the ratio of the data to the total pre-fit prediction (lower panel).

JHEP10(2024)191

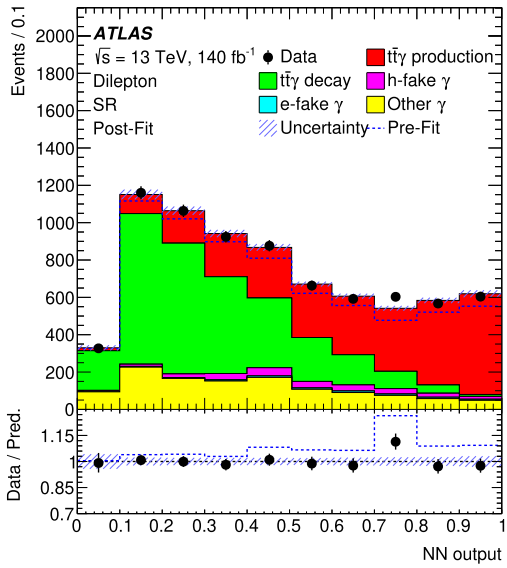

Figure 4. Distribution of the NN output distribution after the fit to data for the measurement of the $t\bar{t}\gamma$ production cross-section in the dilepton channel. The uncertainty band represents the total post-fit uncertainty in the prediction. The lower panel shows the ratio of the data to the total post-fit prediction. The dashed lines correspond to the pre-fit prediction (upper panel) and the ratio of the data to the total pre-fit prediction (lower panel).

the $t\bar{t}\gamma$ decay. Other significant contributions are spread over many different sources of experimental and modelling uncertainties, the largest contributors being the uncertainties associated with jets, b-tagging and the normalisation of the prompt backgrounds.

9.2 Results for the total $t\bar{t}\gamma$ production and decay measurement

For the measurement of the $t\bar{t}\gamma$ process, where all $t\bar{t}\gamma$ events are considered to be a signal regardless of the origin of the photon, the $t\bar{t}\gamma$ production and $t\bar{t}\gamma$ decay templates are added together, and the normalisation of this combined template is treated as a free parameter of the fit. A 20% uncertainty is assigned to the normalisation of the $t\bar{t}\gamma$ decay template [9, 13].

The fiducial cross-sections yield

$$\sigma_{t\bar{t}\gamma}^{\text{Single lepton}} = 704^{+49}_{-46}\,\text{fb} = 704 \pm 5\,(\text{stat})\,^{+49}_{-46}\,(\text{syst})\,\text{fb}$$

in the single-lepton channel and

$$\sigma_{t\bar{t}\gamma}^{\text{Dilepton}} = 116.1^{+8.2}_{-7.7}\,\text{fb} = 116.1 \pm 1.7\,(\text{stat})\,^{+8.0}_{-7.6}\,(\text{syst})\,\text{fb}$$

in the dilepton channel. The combined fiducial cross-section is measured to be

$$\sigma_{t\bar{t}\gamma} = 788^{+38}_{-37}\,\text{fb} = 788 \pm 5\,(\text{stat})\,^{+38}_{-37}\,(\text{syst})\,\text{fb}.$$

As expected, the statistical uncertainty is reduced in this measurement while the total systematic uncertainty is slightly larger compared with the measurement of the $t\bar{t}\gamma$ production cross-section. This difference is related to the $t\bar{t}\gamma$ decay normalisation uncertainty having a larger impact, while there are no significant differences in the impact of the experimental and modelling uncertainties relative to the measurement of $t\bar{t}\gamma$ production.

JHEP10(2024)191

Source	$\Delta\sigma_{t\bar{t}\gamma\text{ production}}/\sigma_{t\bar{t}\gamma\text{ production}}$ (%) Single lepton	Dilepton	Combination
Statistical uncertainty	1.8	3.3	1.5
MC statistical uncertainties	1.5	1.5	1.0
Modelling uncertainties			
$t\bar{t}\gamma$ production PS uncertainty	2.4	3.7	0.9
Other $t\bar{t}\gamma$ production modelling	5.1	1.6	3.0
$t\bar{t}\gamma$ decay modelling	0.3	1.3	0.8
$t\bar{t}\gamma$ decay normalisation	2.4	3.1	2.1
Prompt photon background normalisation	1.5	2.0	2.0
Fake photon background estimate	0.8	1.5	1.6
Fake lepton background estimate	0.4	–	0.1
Other Background modelling	0.7	0.2	0.5
Experimental uncertainties			
Jet uncertainties	3.5	3.0	1.7
B-tagging uncertainties	2.6	2.1	1.0
Photon	0.5	1.5	0.8
Lepton	1.3	1.4	1.3
$E_{\mathrm{T}}^{\mathrm{miss}}$	0.3	0.4	0.4
Pile-up	0.3	0.7	0.5
Luminosity	0.8	1.0	0.8
Total systematic uncertainty	7.6	7.1	5.0
Total uncertainty	7.8	7.7	5.2

Table 3. Summary of the impact of the systematic uncertainties on the $t\bar{t}\gamma$ production fiducial inclusive cross-section in the single-lepton and dilepton channels and their combination grouped into different categories. The category 'Jets' corresponds to the combined effect of JES, jet resolution and JVT uncertainties, while the categories 'Photon' and 'Lepton' correspond to all experimental uncertainties related to photons and leptons (including trigger uncertainties), respectively. The relative uncertainties quoted are obtained by repeating the fit, fixing the set of nuisance parameters of the sources corresponding to each category to their post-fit values, and subtracting in quadrature the resulting uncertainty from the total uncertainty of the nominal fit. The total uncertainty is different from the sum in quadrature of the components due to correlations among nuisance parameters.

10 Differential cross-sections

The measurements of the differential cross-sections of the $t\bar{t}\gamma$ production and the $t\bar{t}\gamma$ process including photons from production and decay, are performed as functions of photon, lepton and jet kinematic properties and angular separations of the photon, leptons and jets. Both absolute and normalised differential cross-sections are measured. The list of all the variables considered is given in table 4. The kinematic properties of the photon are sensitive to the top-photon coupling, in particular the photon p_{T}. Angular distances, such as $\Delta R(\gamma,\ell)_{\mathrm{min}}$, are related to the angle between the top quark and the radiated photon that gives insight into the structure of this coupling and are expected to be less sensitive to the top quark off-shell effects [15]. Since these variables have significant shape differences between the $t\bar{t}\gamma$ production and the $t\bar{t}\gamma$ decay, they are measured for both processes. Following refs. [10, 12], additional differential distributions of leptonic observables are measured in the dilepton

JHEP10(2024)191

Variable	Description
	Both channels
$p_{\mathrm{T}}(\gamma)$	Transverse momentum of the photon
$\lvert\eta(\gamma)\rvert$	Absolute value of the pseudorapidity of the photon
$\Delta R(\gamma,\ell)_{\mathrm{min}}$	Angular separation between the photon and the closest lepton
$\Delta R(\gamma,b)_{\mathrm{min}}$	Angular separation between the photon and the closest b-jet
$\Delta R(\ell,j)_{\mathrm{min}}$	Smallest angular separation between any of the selected leptons and jets
$p_{\mathrm{T}}(j_1)$	Transverse momentum of the leading jet in p_{T}
	Additional variables: dilepton channel
$\Delta R(\gamma,\ell_1)$	Angular separation between the photon and the leading lepton
$\Delta R(\gamma,\ell_2)$	Angular separation between the photon and the subleading lepton
$\lvert\Delta\eta(\ell,\ell)\rvert$	Pseudorapidity difference between the two leptons
$\Delta\phi(\ell,\ell)$	Azimuthal angle difference between the two leptons
$p_{\mathrm{T}}(\ell,\ell)$	Transverse momentum of the dilepton system

Table 4. List of variables measured differentially in the single-lepton and dilepton channels.

channel for the $t\bar{t}\gamma$ total process, in particular, $\Delta\phi(\ell,\ell)$ and $|\Delta\eta(\ell,\ell)|$ that are sensitive to the $t\bar{t}$ spin correlation.

In the single-lepton channel, the same four regions considered in the inclusive measurement are used. In the dilepton channel, all events are split into a signal-enriched region with the value of the NN discriminant above 0.6 and a background-enriched control region with NN below 0.6. This threshold is optimised to minimise the expected total uncertainty in the photon p_{T} differential distribution. The measurements are performed by using the profile-likelihood unfolding [16] in the signal and control regions. The parameters of interest $\vec{\mu}$, the signal strength in each bin of the distribution at particle level, are free parameters of the fit. The same likelihood but with only one parameter of interest is used for the inclusive cross-section measurement. No regularisation is applied due to small bin-to-bin migrations for all the variables considered. In the case of the normalised distribution, the $\vec{\mu}$ is reparametrised such that the last element of the vector is the overall signal normalisation. In this case, the content of the last bin of the unfolded distribution is dropped from the $\vec{\mu}$, since it is no longer a free parameter, and it can be calculated based on the values in other bins and the overall normalisation.

The performance of the unfolding procedure is tested for possible biases from the choice of the input model using pseudodata. The unfolding procedure is performed using the nominal response matrices and modified $t\bar{t}\gamma$ templates where the distributions are linearly reweighted or the shape is modified by the observed differences between data and the MC simulation at reconstruction level. In both cases, the procedure reproduces the altered shapes of the input distributions within the statistical uncertainties.

10.1 Differential distributions for the $t\bar{t}\gamma$ production

The photon p_{T} distributions in the four signal and control regions in the single-lepton channel and the migration matrices are shown for illustration in figures 5 and 6, respectively. The corresponding distributions in the dilepton signal and control regions are given in figure 7. The binning is optimised in the dilepton channel to ensure that the bin width is larger than

JHEP10(2024)191

twice the resolution of the observable and that the expected statistical uncertainty in the distribution at particle level is below 10%. The resulting binning is found to be similar to the one used in ref. [12] for most variables. Therefore, the latter is adopted to simplify the comparisons. The fraction of events reconstructed in the same bin of the differential distribution as the one they were generated in is above 90% in every bin of the p_{T} distributions in all the SRs and CRs. This fraction ranges from 70% for variables involving b-jets up to 99% for the leptonic variables.

The absolute and normalised $t\bar{t}\gamma$ production cross-sections are presented in figure 8 for the single-lepton channel and in figure 9 for the dilepton channel as a function of angular distances between the photon and the closest lepton or b-jet and between the closest lepton-jet pair. The results are compared with the NLO predictions from the MadGraph5_aMC@NLO simulation interfaced to Pythia 8 and Herwig 7. The MC predictions, normalised to the NLO cross-section given by the simulation, slightly underestimate the measured cross-section, in agreement with the measurements of the inclusive cross-section. There are no significant differences between the two MC simulations. Both describe the shape of the distributions well. The total uncertainty in the absolute cross-section in the single-lepton channel ranges from 8% to 20%, depending on the variable and the bin of the distribution. The statistical uncertainty is about 3%–10% for most of the bins. The largest systematic uncertainties arise from the normalisation of the backgrounds with prompt photons, some components of the JES uncertainty and from the $t\bar{t}\gamma$ modelling uncertainties. The total uncertainty in the dilepton channel varies from 8% up to 20%–30% in the tails of the distributions, and it is dominated by the statistical uncertainty in the data.

The precision of the normalised cross-sections is below 10% for most bins of the distributions, owing to a large cancellation of systematic uncertainties that affect the normalisation of the distributions, in particular, the normalisation uncertainties associated with the prompt background and the $t\bar{t}\gamma$ decay contribution.

The photon p_{T} and η distributions are measured in each channel and in the combined fiducial phase space. The combined measurement of photon p_{T} is used as input to obtain limits on the EFT parameters, as described in section 11. The absolute and normalised cross-sections measured in the combined phase space are shown in figure 10, while the individual results and the measured leading jet p_{T} are included in appendix B. As expected, the measured absolute cross-sections are larger than the prediction. The total uncertainty per bin varies between 8% and 12%, the largest single contribution arises from the statistical uncertainty (about 5%). The photon p_{T} distribution in data is somewhat softer than the MC prediction, while there are no significant differences between the shapes of the $|\eta|$ distributions.

The breakdown of the categories of systematic uncertainties and the statistical one is illustrated in figure 11 for the absolute $t\bar{t}\gamma$ production differential cross-sections measured in the combined fiducial phase space of the single-lepton and dilepton channels as a function of the photon p_{T} and η. The systematic uncertainties in the unfolded distributions are decomposed into signal modelling uncertainties, uncertainties related to the different background categories, experimental uncertainties, and statistical uncertainties. Among experimental uncertainties the largest effects come from the jet uncertainties followed by b-tagging and photon uncertainties.

JHEP10(2024)191

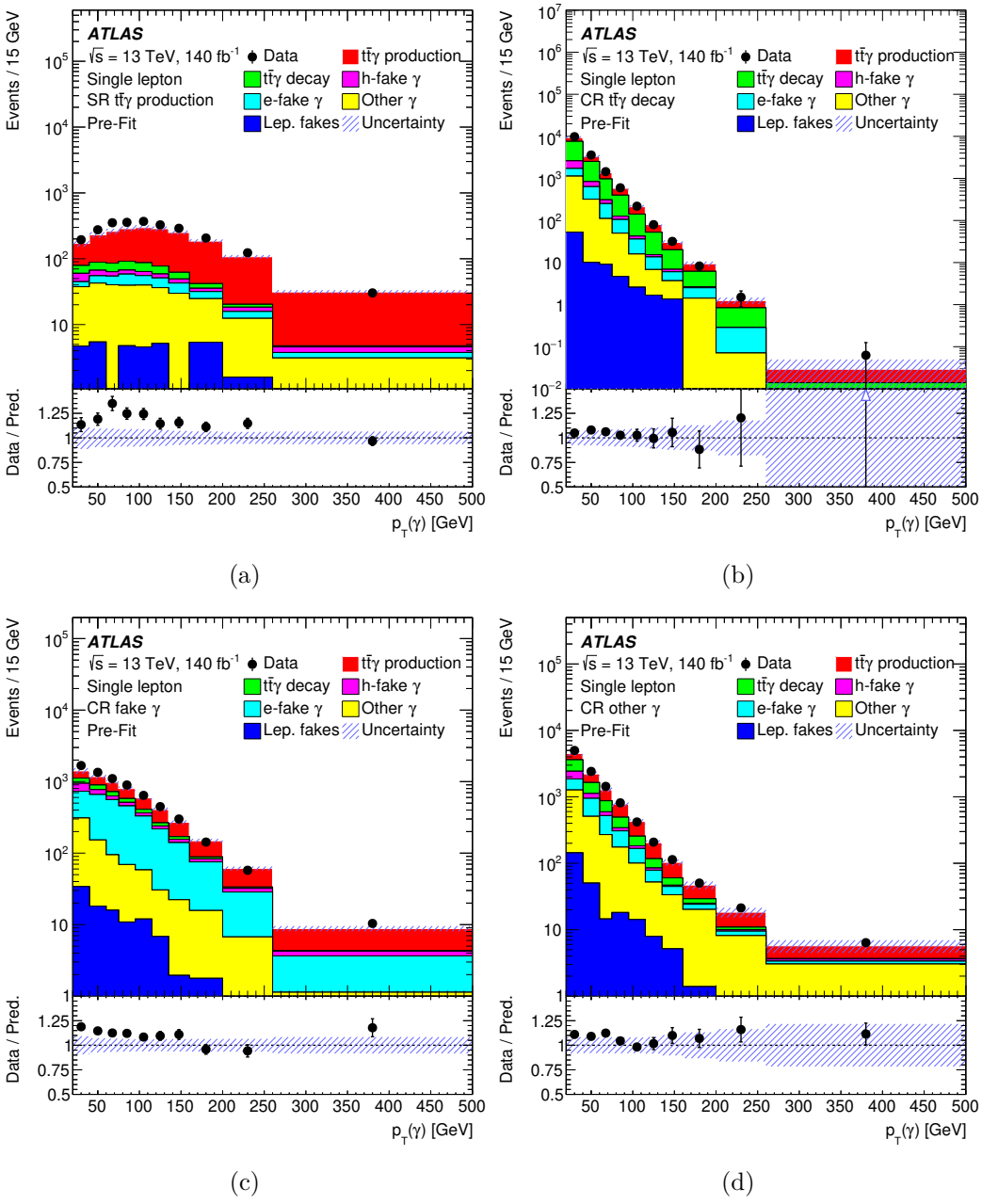

Figure 5. Photon p_{T} distributions at reconstruction level in the four regions of the single-lepton channel: (a) $t\bar{t}\gamma$ production SR, (b) $t\bar{t}\gamma$ decay CR, (c) photon fakes CR and (d) other prompt γ CR. The lower panels show the ratios of the data to the predictions. The uncertainty band represents the total uncertainties before the fit to data. The last bin of the distributions includes the overflow events.

JHEP10(2024)191

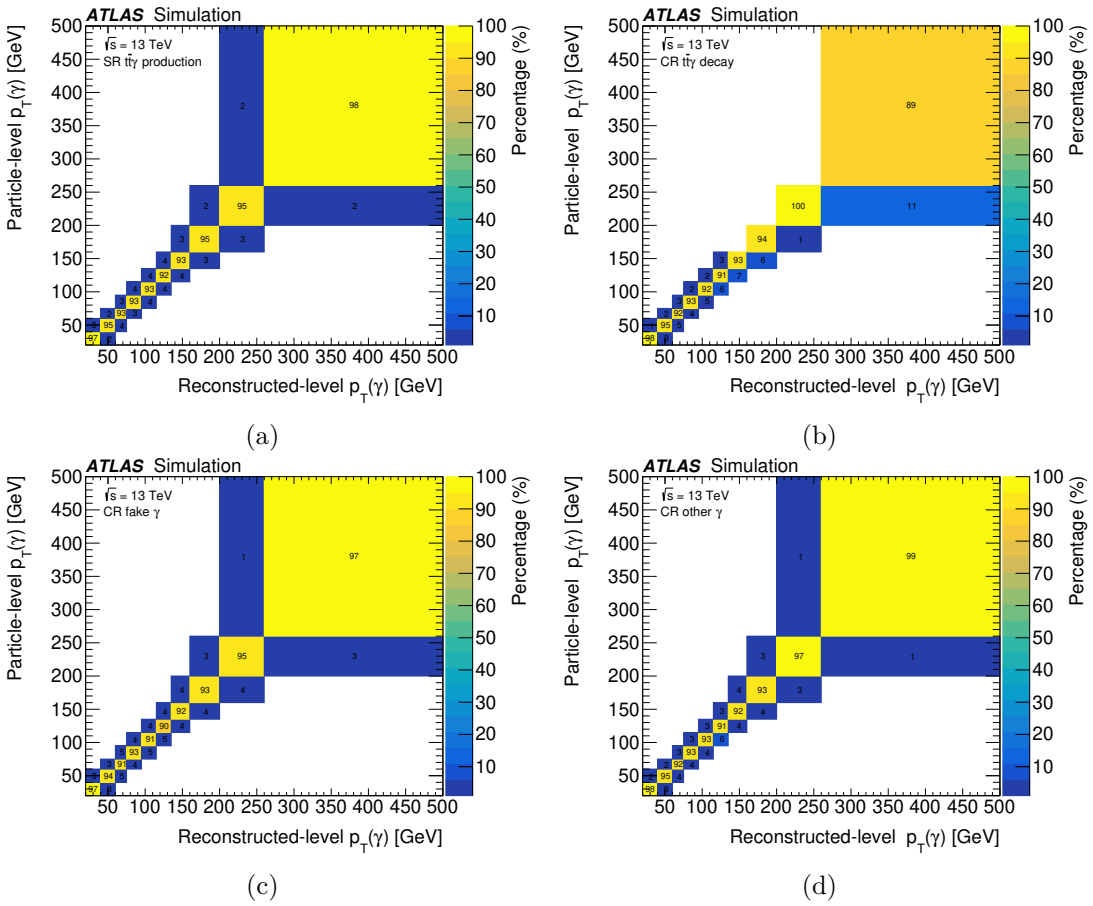

Figure 6. Migration matrices in the four regions of the single-lepton channel: (a) $t\bar{t}\gamma$ production SR, (b) $t\bar{t}\gamma$ decay CR, (c) photon fakes CR and (d) other prompt γ CR, relating the photon p_{T} at the reconstruction and particle levels in the fiducial phase space. The values correspond to the fraction of events in each bin normalised by column and shown as percentage. The last bin of the distributions includes the overflow events.

The compatibility between the measured differential cross-sections and the predictions, evaluated using a ratio of χ^2 to the number of degrees of freedom (ndf) and the corresponding p-values, are summarised in table 5 for all measured variables, including those shown in appendix B. They are evaluated taking into account the statistical and systematic covariance matrices of the measurements and the number of degrees of freedom.

JHEP10(2024)191

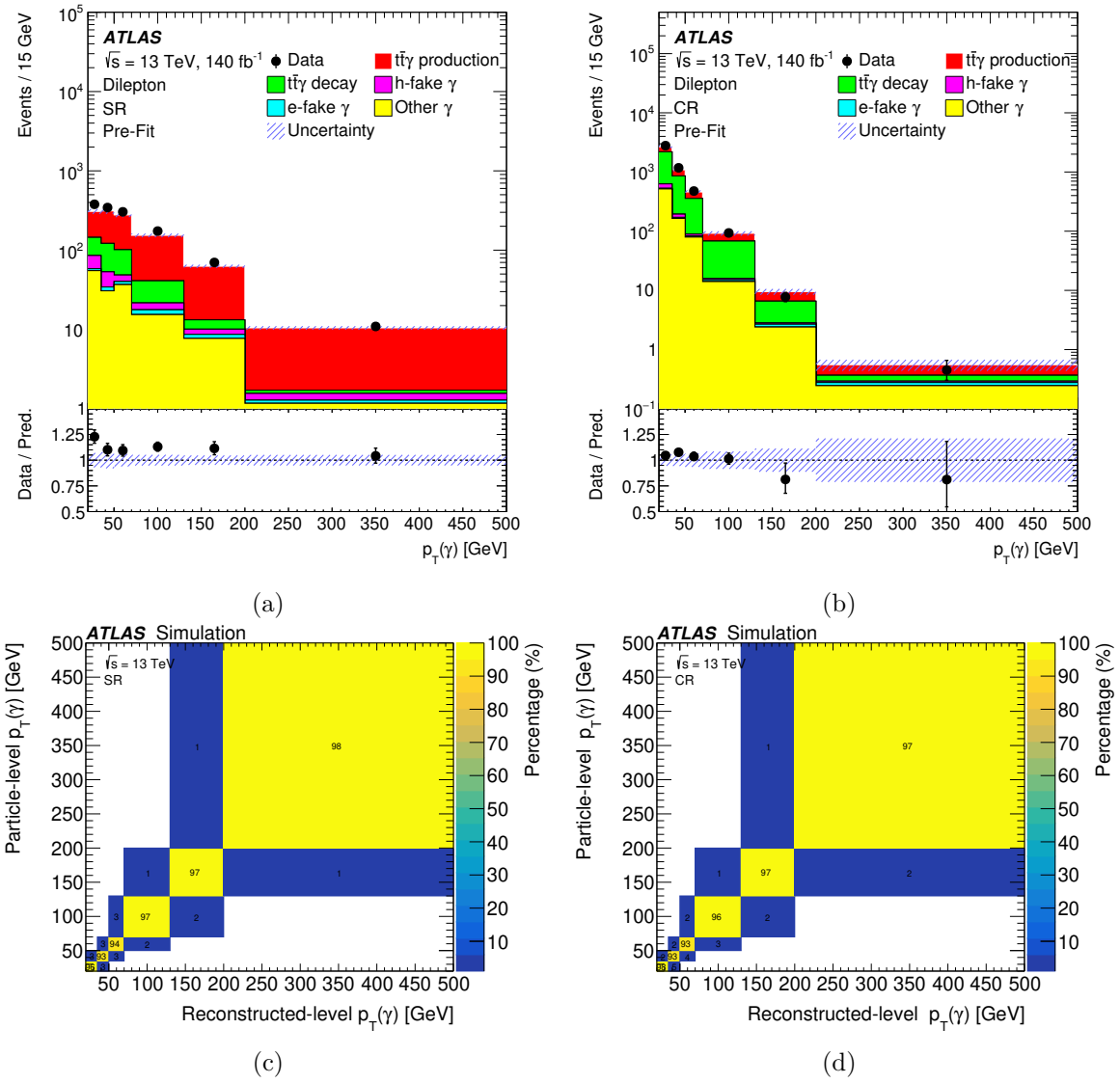

Figure 7. Top row: Photon p_{T} distributions at reconstruction level in the (a) signal and (b) control region defined by the NN output above or below the value of 0.6 in the dilepton channel. The lower panels show the ratios of the data to the predictions. The uncertainty band represents the total uncertainties before the fit to data. Bottom row: Migration matrices relating the photon p_{T} at the reconstruction and particle levels in the fiducial phase space in the (c) signal and (d) control region. The values correspond to the fraction of events in each bin normalised by column and shown as percentage. The last bin of the distributions includes the overflow events.

JHEP10(2024)191

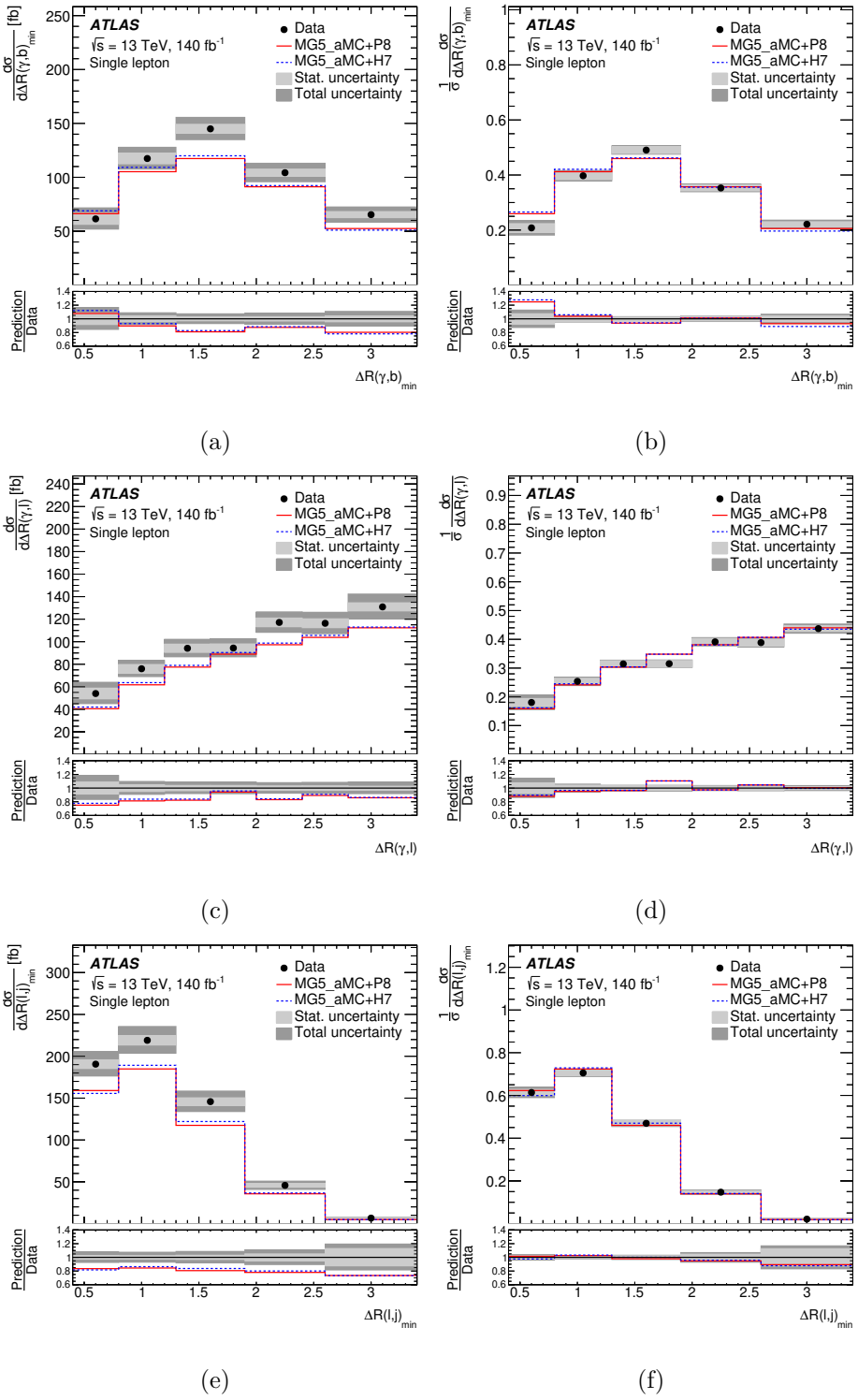

Figure 8. The (a, c, e) absolute and (b, d, f) normalised $t\bar{t}\gamma$ production differential cross-sections measured in the fiducial phase space in the single-lepton channel as a function of (a, b) $\Delta R(\gamma, b)_{\text{min}}$, (c, d) $\Delta R(\gamma, \ell)$ and (e, f) $\Delta R(\ell, j)_{\text{min}}$. Data are compared with the NLO MadGraph5_aMC@NLO simulation interfaced to Pythia 8 and Herwig 7. The lower panels show the ratios of the predictions to the data. The last bin of the distributions includes the overflow events.

JHEP10(2024)191

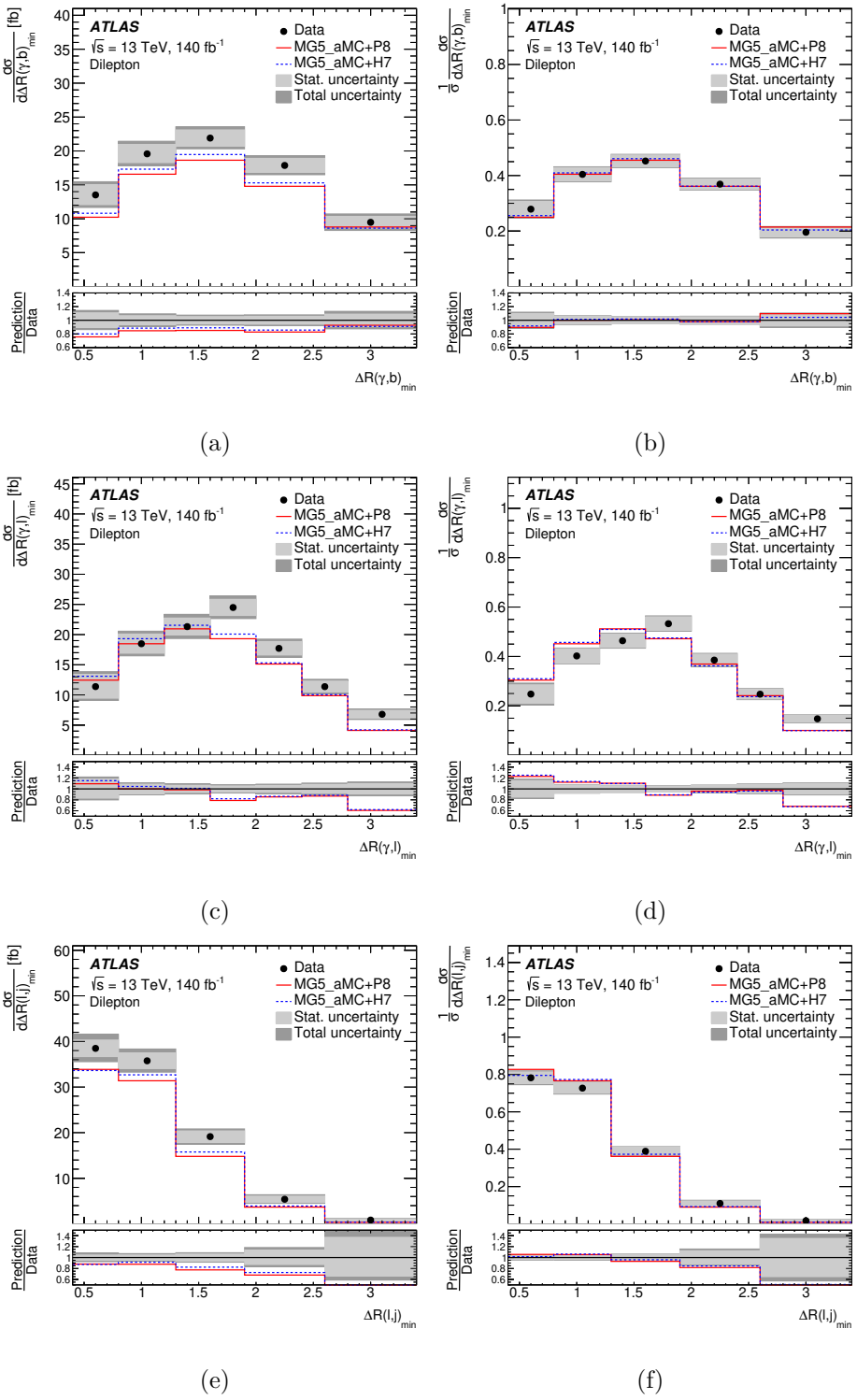

Figure 9. The (a, c, e) absolute and (b, d, f) normalised $t\bar{t}\gamma$ production differential cross-sections measured in the fiducial phase space in the dilepton channel as a function of (a, b) $\Delta R(\gamma, b)_{\text{min}}$, (c, d) $\Delta R(\gamma, \ell)$ and (e, f) $\Delta R(\ell, j)_{\text{min}}$. Data are compared with the NLO MadGraph5_aMC@NLO simulation interfaced to Pythia 8 and Herwig 7. The lower panels show the ratios of the predictions to the data. The last bin of the distributions includes the overflow events.

JHEP10(2024)191

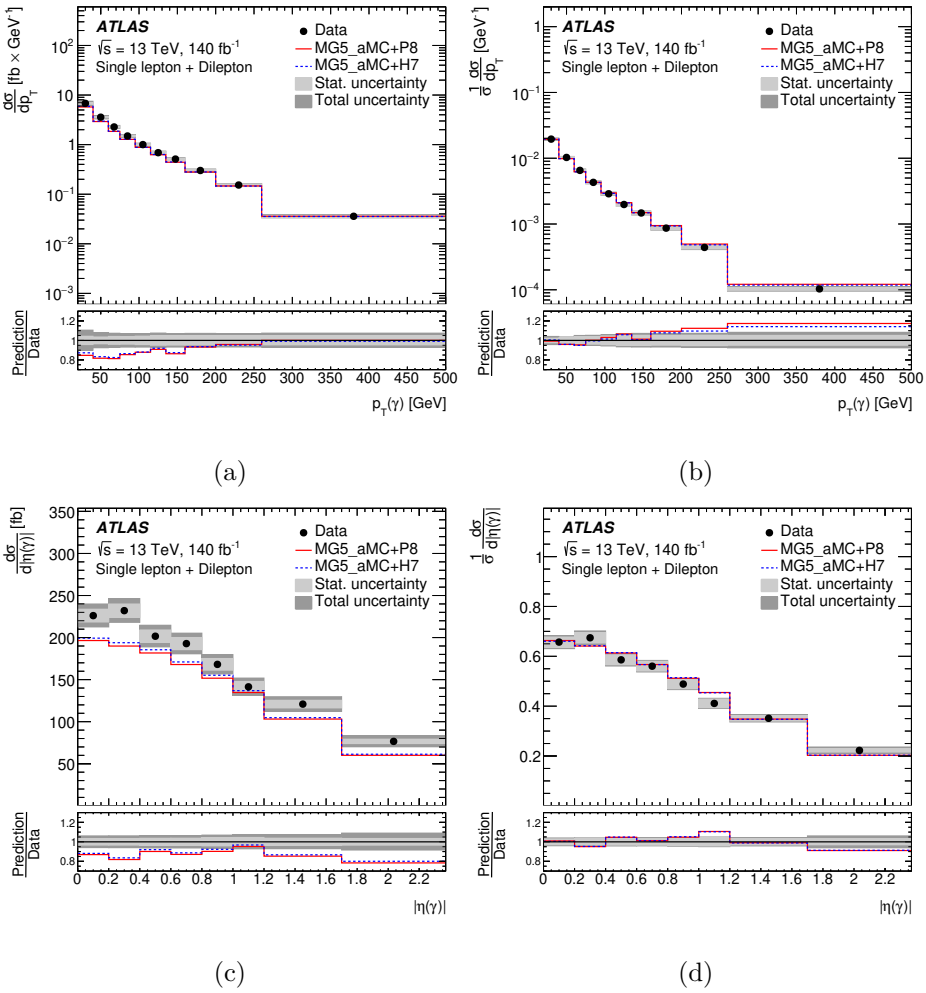

Figure 10. The (a, c) absolute and (b, d) normalised $t\bar{t}\gamma$ production differential cross-sections measured in the combined fiducial phase space of the single-lepton and dilepton channels as a function of the photon (a, b) p_{T} and (c, d) η. Data are compared with the NLO MadGraph5_aMC@NLO simulation interfaced to Pythia 8 and Herwig 7. The lower panels show the ratios of the predictions to the data. The last bin of the photon p_{T} distributions includes the overflow events.

JHEP10(2024)191

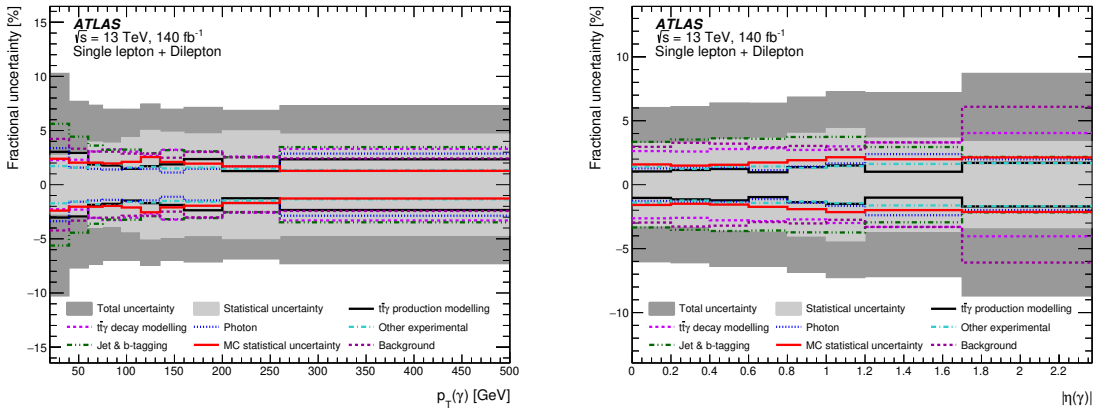

(a) (b)

Figure 11. Contributions of the systematic uncertainties grouped in categories in each bin of the measurement of the absolute $t\bar{t}\gamma$ production differential cross-sections measured in the combined fiducial phase space of the single-lepton and dilepton channels as a function of the photon (a) p_{T} and (b) η. The '$t\bar{t}\gamma$ decay modelling' category includes both the normalisation and modelling uncertainties and the 'Background' category the uncertainties related to other prompt photon, fake photon and fake lepton backgrounds. The 'Other experimental' category corresponds to the combined effect of lepton, $E_{\mathrm{T}}^{\mathrm{miss}}$, luminosity and pile-up uncertainties. The relative uncertainties quoted are obtained by repeating the fit, fixing the set of nuisance parameters of the sources corresponding to each category to their post-fit values, and subtracting in quadrature the resulting uncertainty from the total uncertainty of the nominal fit. The total uncertainty is different from the sum in quadrature of the components due to correlations among nuisance parameters.

	Absolute cross-sections				Normalised cross-sections			
	MG5_aMC@NLO+Pythia 8		MG5_aMC@NLO+Herwig 7		MG5_aMC@NLO+Pythia 8		MG5_aMC@NLO+Herwig 7	
Variables	χ^2/ndf	p-value	χ^2/ndf	p-value	χ^2/ndf	p-value	χ^2/ndf	p-value
Single-lepton and dilepton combined								
$p_{\mathrm{T}}(\gamma)$	10.7/10	0.38	9.3/10	0.50	11.6/9	0.23	8.6/9	0.47
$\lvert\eta(\gamma)\rvert$	15.8/8	0.04	14.2/8	0.08	10.2/7	0.18	10.0/7	0.19
Single-lepton channel								
p_{T} (γ)	11.7/10	0.31	10.4/10	0.40	43.9/9	< 0.01	32.1/9	< 0.01
$\lvert\eta(\gamma)\rvert$	11.8/8	0.16	11.1/8	0.20	8.1/7	0.33	8.1/7	0.32
$\Delta R(\gamma,\ell)$	10.5/7	0.16	9.9/7	0.19	8.8/6	0.19	8.8/6	0.19
$\Delta R(\gamma,b)_{\mathrm{min}}$	12.5/5	0.03	12.3/5	0.03	7.6/4	0.11	9.0/4	0.06
$\Delta R(\ell,j)_{\mathrm{min}}$	6.3/5	0.28	6.6/5	0.25	1.5/4	0.83	2.5/4	0.65
$p_{\mathrm{T}}(j_1)$	12.6/5	0.03	10.8/5	0.06	8.2/4	0.08	9.7/4	0.05
Dilepton channel								
p_{T} (γ)	8.6/6	0.20	7.2/6	0.31	6.5/5	0.26	5.9/5	0.32
$\lvert\eta(\gamma)\rvert$	12.1/8	0.15	9.9/8	0.27	9.2/7	0.24	7.9/7	0.34
$\Delta R(\gamma,\ell)_{\mathrm{min}}$	17.2/7	0.02	16.5/7	0.02	14.2/6	0.03	14.4/6	0.03
$\Delta R(\gamma,b)_{\mathrm{min}}$	7.8/5	0.17	5.0/5	0.42	1.4/4	0.84	0.8/4	0.93
$\Delta R(\ell,j)_{\mathrm{min}}$	9.3/5	0.10	6.4/5	0.27	5.4/4	0.25	3.7/4	0.45
$p_{\mathrm{T}}(j_1)$	10.5/5	0.06	5.0/5	0.42	7.8/4	0.10	3.6/4	0.46

Table 5. The χ^2/ndf and p-values between the measured absolute and normalised cross-sections of $t\bar{t}\gamma$ production and the NLO MadGraph5_aMC@NLO simulations interfaced to Pythia 8 and Herwig 7. They are obtained using the uncertainties of the measured distribution and their correlations.

JHEP10(2024)191

10.2 Differential distributions for the total $t\bar{t}\gamma$ production and decay process

The measurements are also performed for the sum of the $t\bar{t}\gamma$ production and $t\bar{t}\gamma$ decay in the same phase space as the $t\bar{t}\gamma$ production process alone at the stable particle level, similarly to previous measurements. The results are compared with the LO $2 \to 7$ MC simulations of the $t\bar{t}\gamma$ process used in previous publications [9, 10] described in section 3.

The absolute and normalised cross-sections in the single-lepton channel are shown as functions of photon p_{T}, photon $|\eta|$ and leading jet p_{T} in figure 12 and as functions of $\Delta R(\gamma, b)_{\mathrm{min}}$, $\Delta R(\gamma, \ell)$ and $\Delta R(\ell, j)_{\mathrm{min}}$ in figure 13. Overall, the shapes of the ΔR and $|\eta|$ distributions are well described within the total uncertainties of the measurement, while the description of the p_{T} distributions by the LO simulation is poor. Compared to the distributions measured for the $t\bar{t}\gamma$ production process alone, the p_{T} of the photon is softer, while there are no significant differences between the shapes of the photon η. As expected, the ΔR distributions have more events at lower ΔR values when including the $t\bar{t}\gamma$ decay events in the signal, where the photon can be emitted by a lepton. The corresponding distributions measured in the dilepton channel are shown in appendix C.

Following the previous publications by the ATLAS and CMS collaborations [9, 10, 12], the cross-sections in the dilepton channel are measured as a function of additional variables. The absolute and normalised cross-sections as functions of $|\Delta\eta(\ell\ell)|$, $\Delta\phi(\ell\ell)$, and the p_{T} of the dilepton system are presented in figure 14, while figure 15 shows the ΔR distributions between the photon and the leading and subleading lepton ordered by p_{T}. The qualitative description of the $\Delta\phi(\ell, \ell)$ and $|\Delta\eta(\ell\ell)|$ distributions by the simulation is in agreement with the observations of the previous measurements performed in a different phase space at parton [10] or particle level [9].

The compatibility between the measured differential cross-sections and the predictions is also quantified using χ^2/ndf and p-values, which are summarised in table 6 for all variables considered, including those in appendix C. On average, p-values corresponding to the LO $2 \to 7$ simulation are lower than those for the MadGraph5_aMC@NLO simulation presented in table 5 pointing to a somewhat poorer description of the data provided by the LO $2 \to 7$ simulation.

JHEP10(2024)191

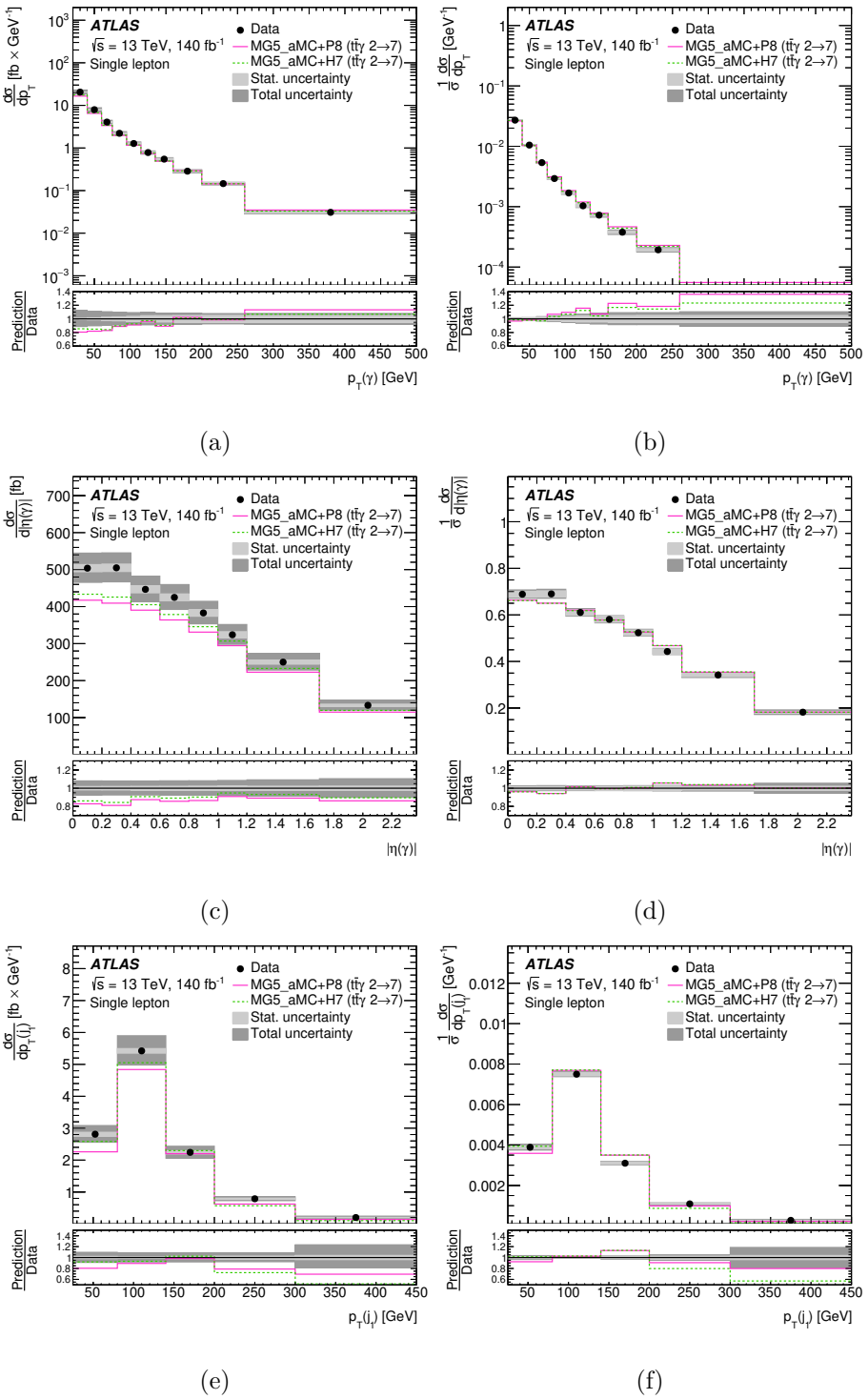

Figure 12. The (a, c, e) absolute and (b, d, f) normalised differential distributions of the total $t\bar{t}\gamma$ production and decay cross-section measured in the fiducial phase space in the single-lepton channel as a function of the (a, b) photon p_{T}, (c, d) photon $|\eta|$ and (e, f) leading jet p_{T}. Data are compared with the $t\bar{t}\gamma$ MadGraph5_aMC@NLO simulation at LO interfaced to Pythia 8 and Herwig 7. The lower panels show the ratios of the predictions to the data. The last bin of the distributions includes the overflow events.

JHEP10(2024)191

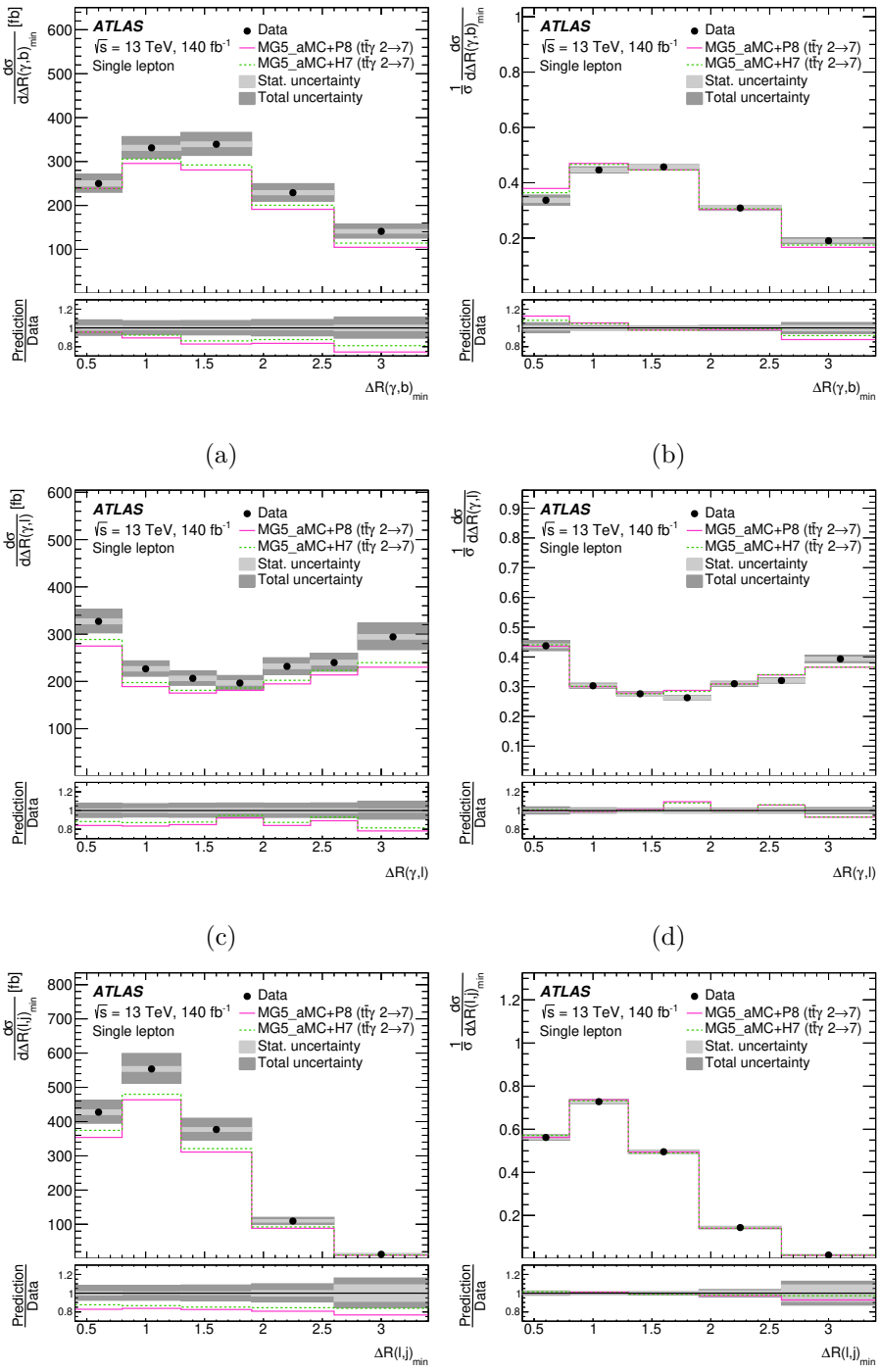

Figure 13. The (a, c, e) absolute and (b, d, f) normalised differential distributions of the total $t\bar{t}\gamma$ production and decay cross-section measured in the fiducial phase space in the single-lepton channel as a function of (a, b) $\Delta R(\gamma, b)_{\text{min}}$, (c, d) $\Delta R(\gamma, \ell)$ and (e, f) $\Delta R(\ell, j)_{\text{min}}$. Data are compared with the $t\bar{t}\gamma$ MadGraph5_aMC@NLO simulation at LO interfaced to Pythia 8 and Herwig 7. The lower panels show the ratios of the predictions to the data. The last bin of the distributions includes the overflow events.

JHEP10(2024)191

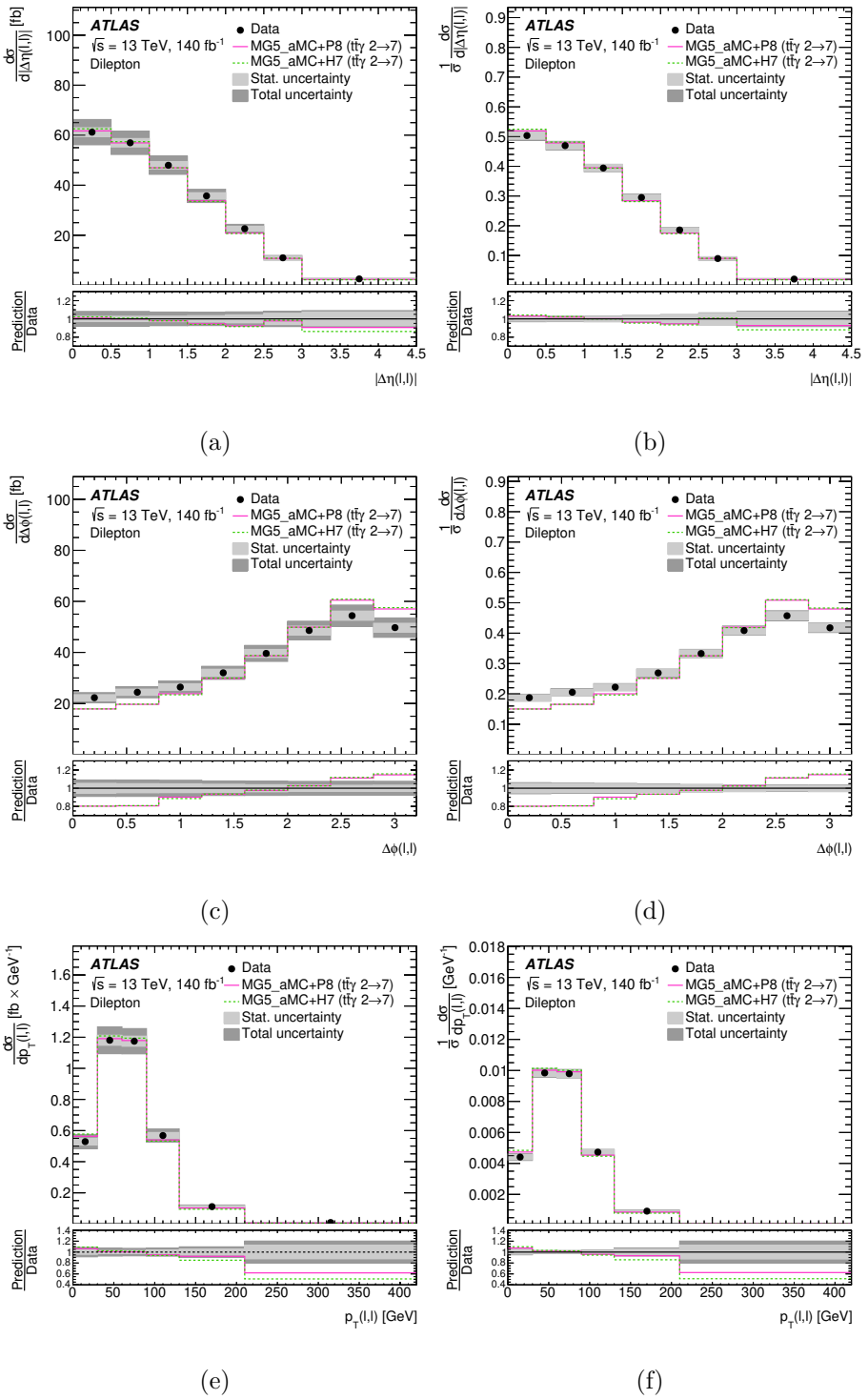

Figure 14. The (a, c, e) absolute and (b, d, f) normalised differential cross-sections of the of the total $t\bar{t}\gamma$ production and decay process measured in the fiducial phase space in the dilepton channel as a function of (a, b) $|\Delta\eta(\ell\ell)|$, (c, d) $\Delta\phi(\ell\ell)$, and the (e, f) p_{T} of the dilepton system. Data are compared with the $t\bar{t}\gamma$ MadGraph5_aMC@NLO simulation at LO interfaced to Pythia 8 and Herwig 7. The lower panels show the ratios of the predictions to the data. The last bin of the distributions includes the overflow events.

JHEP10(2024)191

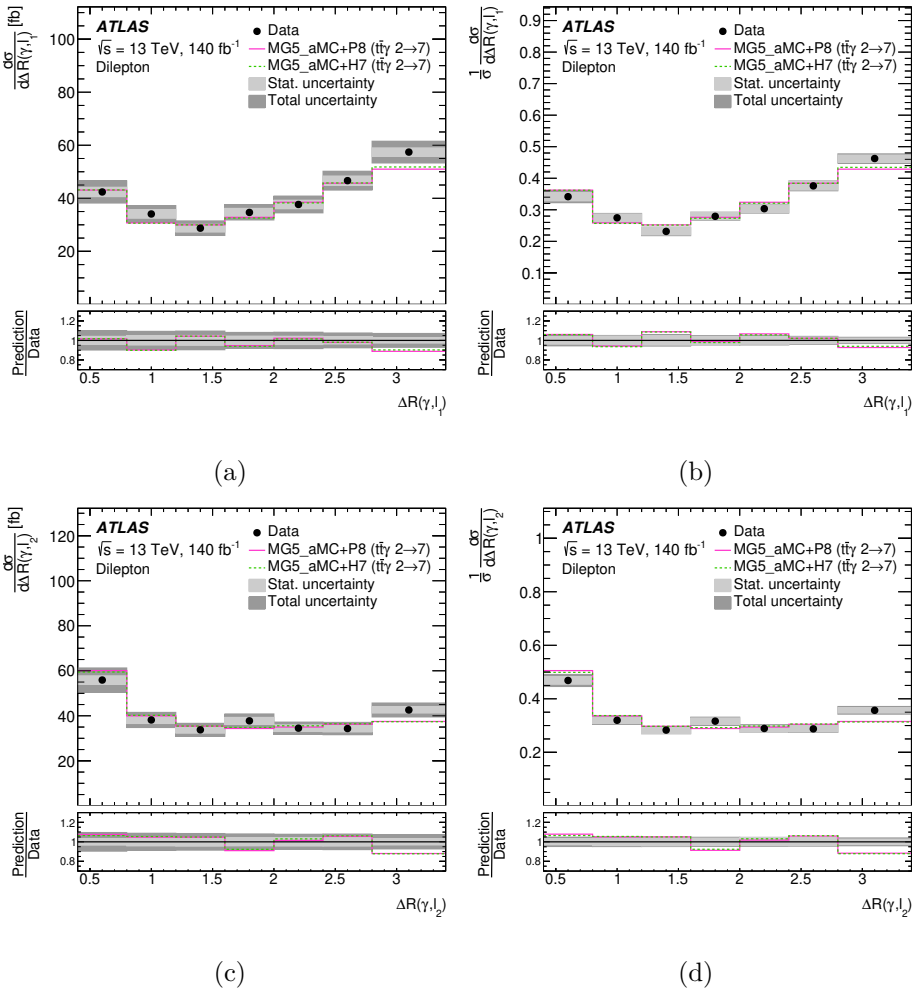

Figure 15. The (a, c) absolute and (b, d) normalised differential cross-sections of the of the total $t\bar{t}\gamma$ production and decay process measured in the fiducial phase space in the dilepton channel as a function of (a, b) $\Delta R(\gamma, \ell_1)$ and (c, d) $\Delta R(\gamma, \ell_2)$. Data are compared with the $t\bar{t}\gamma$ MadGraph5_aMC@NLO simulations at LO interfaced to Pythia 8 and Herwig 7. The lower panels show the ratios of the predictions to the data. The last bin of the distributions includes the overflow events.

JHEP10(2024)191

Variables	Absolute cross-sections				Normalised cross-sections			
	MG5_aMC@NLO+Pythia 8		MG5_aMC@NLO+Herwig 7		MG5_aMC@NLO+Pythia 8		MG5_aMC@NLO+Herwig 7	
	χ^2/ndf	p-value	χ^2/ndf	p-value	χ^2/ndf	p-value	χ^2/ndf	p-value
Single-lepton channel								
$p_{\mathrm{T}}(\gamma)$	12.6/10	0.25	8.5/10	0.58	21.2/9	0.01	12.1/9	0.21
$\lvert\eta(\gamma)\rvert$	13.5/8	0.10	13.3/8	0.10	12.0/7	0.10	12.9/7	0.08
$\Delta R(\gamma,\ell)$	15.3/7	0.03	14.0/7	0.05	13.8/6	0.03	18.6	< 0.01
$\Delta R(\gamma,b)_{\mathrm{min}}$	8.9/5	0.11	6.2/5	0.29	9.3/4	0.05	6.0/4	0.20
$\Delta R(\ell,j)_{\mathrm{min}}$	4.9/5	0.43	3.1/5	0.68	0.8/4	0.93	0.8/4	0.94
$p_{\mathrm{T}}(j_1)$	25.4/5	< 0.01	43.0/5	< 0.01	27.2/4	< 0.01	45.0/4	< 0.01
Dilepton channel								
p_{T} (γ)	7.6/6	0.27	4.9/6	0.56	6.7/5	0.24	4.7/5	0.45
$\lvert\eta(\gamma)\rvert$	5.2/8	0.73	6.0/8	0.64	5.4/7	0.61	6.3/7	0.50
$\Delta R(\gamma,\ell)_{\mathrm{min}}$	23.6/7	< 0.01	22.8/7	< 0.01	20.1/6	< 0.01	19.6/6	< 0.01
$\Delta R(\gamma,\ell_1)$	10.1/7	0.18	8.8/7	0.27	9.8/6	0.13	8.5/6	0.21
$\Delta R(\gamma,\ell_2)$	14.8/7	0.04	15.1/7	0.03	14.3/6	0.03	14.7/6	0.02
$\lvert\Delta\eta(\ell,\ell)\rvert$	3.9/7	0.79	6.7/7	0.46	3.1/6	0.80	5.5/6	0.48
$\Delta\phi(\ell,\ell)$	35.4/8	< 0.01	37.8/8	< 0.01	35.3/7	< 0.01	37.5/7	< 0.01
$p_{\mathrm{T}}(\ell,\ell)$	6.7/6	0.35	12.9/6	0.04	5.9/5	0.32	11.5/5	0.04
$\Delta R(\gamma,b)_{\mathrm{min}}$	1.8/5	0.87	3.7/5	0.59	1.8/4	0.77	3.7/4	0.45
$\Delta R(\ell,j)_{\mathrm{min}}$	6.1/5	0.30	9.2/5	0.10	10.0/4	0.04	12.8/4	0.01
$p_{\mathrm{T}}(j_1)$	10.8/5	0.05	19.2/5	< 0.01	9.8/4	0.04	17.6/4	< 0.01

Table 6. The χ^2/ndf and p-values between the measured absolute and normalised cross-sections of the total $t\bar{t}\gamma$ production and decay process and the LO $2 \to 7$ MadGraph5_aMC@NLO simulation interfaced to Pythia 8 and Herwig 7. They are obtained using the uncertainties of the measured distribution and their correlations.

JHEP10(2024)191

11 EFT interpretation

Physics phenomena beyond the SM might only manifest themselves at an energy scale Λ that is larger than the scales probed at the LHC. In that case, the new states are expected to be produced virtually. In the EFT approach, these virtual effects are parameterized by adding higher-dimensional operators to the SM Lagrangian. Assuming lepton number conservation, the lowest-order EFT operators to contribute have dimension six. Since the interaction strength of an operator of dimension d is proportional to Λ^{4-d}, conventionally chosen to be 1 TeV, higher-dimensional operators are suppressed. The $t\bar{t}\gamma$ production process is expected to be sensitive to several EFT operators [4], but it has the highest sensitivity to the dipole operators C_{tB}, C_{tW}, coupling to the weak hypercharge and isospin gauge bosons, respectively. The $t\bar{t}Z$ production is also modified by the C_{tB} and C_{tW} operators. The electric and magnetic dipole couplings can be expressed in terms of these dimension-6 EFT operators. In particular, the Lagrangian describing the $t\bar{t}X$ vertex (with $X = \gamma, Z$) can be written as:

$$\mathcal{L}_{t\bar{t}X} = e\bar{t}\left[\gamma^{\mu}\left(C^{X}_{1,\mathrm{V}} + \gamma_5 C^{X}_{1,\mathrm{A}}\right) + \frac{i\sigma^{\mu\nu}q_{\nu}}{m_t}\left(C^{X}_{2,\mathrm{V}} + \gamma_5 C^{X}_{2,\mathrm{A}}\right)\right] t X_{\mu}, \tag{11.1}$$

where m_{t} is the top quark mass. The couplings $C^{X}_{1,\mathrm{V}}$ and $C^{X}_{1,\mathrm{A}}$ are fixed in the SM by the quantum numbers of the top quark and the SU(2) × U(1) electroweak symmetry. The $C^{X}_{2,\mathrm{V}}$ and $C^{X}_{2,\mathrm{A}}$ couplings represent the electric and magnetic dipole moments of the top quark (and their weak equivalents), which are absent from the SM at tree-level and receive very small values from higher-order corrections. These anomalous dipole couplings can be expressed as function of the EFT operators as:

$$C^{Z}_{2,\mathrm{V}} = \frac{v^2 m_t}{\sqrt{2} c_w s_w m_Z \Lambda^2}\Re\left[C_{tZ}\right], \quad C^{Z}_{2,\mathrm{A}} = \frac{v^2 m_t}{\sqrt{2} c_w s_w m_Z \Lambda^2}\Im\left[C_{tZ}\right], \tag{11.2}$$

$$C^{\gamma}_{2,\mathrm{V}} = \frac{\sqrt{2} v m_t}{e\Lambda^2}\Re\left[C_{t\gamma}\right], \qquad C^{\gamma}_{2,\mathrm{A}} = \frac{\sqrt{2} v m_t}{e\Lambda^2}\Im\left[C_{t\gamma}\right], \tag{11.3}$$

$$\tag{11.4}$$

where s_w (c_w) is the sine (cosine) of the Weinberg angle, m_Z is the Z boson mass, v is the vacuum expectation value and $C_{t\gamma}$ and C_{tZ} are the EFT operators, which are linear combinations of the dipole operators C_{tB}, C_{tW} introduced in refs. [4, 83]:

$$C_{tZ} = c_w \cdot C_{tW} - s_w \cdot C_{tB}, \tag{11.5}$$

$$C_{t\gamma} = s_w \cdot C_{tW} + c_w \cdot C_{tB}. \tag{11.6}$$

Those relationships hold for both the real and imaginary parts of the coefficients.

Since the C_{tB}, C_{tW} operators most significantly modify the rate and the shape of the photon p_{T} distribution in $t\bar{t}\gamma$ production, this variable is used to set limits on them. This is illustrated in figure 16, where the absolute cross-section as a function of p_{T} (see figure 10(a)) is compared with the SM prediction and predictions where one of the C_{tB}, C_{tW} EFT operators is different from zero.

The $t\bar{t}\gamma$ production cross-section in each bin of the corresponding distributions can be parameterised as

$$\sigma = \sigma_{\mathrm{SM}} + \sum_i C_i \sigma_i + \sum_{i,j} C_i C_j \sigma_{ij}.$$

JHEP10(2024)191

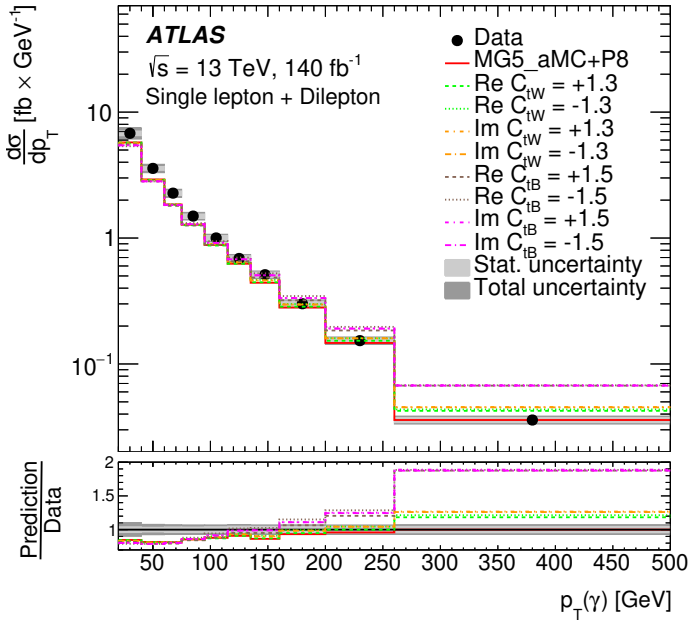

Figure 16. Comparison of the photon p_{T} distribution from the combined measurement in the single-lepton and dilepton channels shown in figure 10 with the SM prediction and predictions where one EFT parameter is different from zero. The values of the coefficients correspond to the largest values considered in the simulation of the samples. The lower panel shows the ratio of the prediction to the data.

The coupling parameters of the EFT operators considered are denoted by C_i, σ_i corresponds to the cross-section of the interference of diagrams with one EFT vertex with diagrams from the SM, and the cross-section σ_{ij} represents the interference of two diagrams with one EFT vertex each or the squares of the amplitudes with one effective vertex for $i = j$. In the following, contributions with $i = j$ are referred to as quadratic terms, while $i \neq j$ are referred to as cross-terms.

The EFTfitter tool [84] is used to obtain the best-fit values of the EFT parameters in a Bayesian statistical framework. For each bin of the p_{T} distribution, the SMEFT prediction of the SM term (σ_{SM}), which is simulated at LO in QCD, is scaled to the NLO cross-section of the nominal $t\bar{t}\gamma$ production sample, thus taking into account both shape and normalisation effects. The real and imaginary parts of the C_{tB} and C_{tW} operators are considered separately.

The fit is performed with the full parameterisation of the $t\bar{t}\gamma$ production cross-section including the linear and quadratic terms and the cross-terms introduced above, for all the operators simultaneously. The analysis shows very little sensitivity when only the linear terms, which represent the interference terms, are considered in the fit when compared with the full quadratic fit. Uncertainties related to the modelling of the EFT samples are not considered in the fit. The results of the global fit (*global mode* in the figures) to the four coefficients are shown in figure 17 as two-dimensional contours. The measured values are in good agreement with the predictions of the SM. As expected, a linear relationship between C_{tW} and C_{tB} is observed (left column).

JHEP10(2024)191

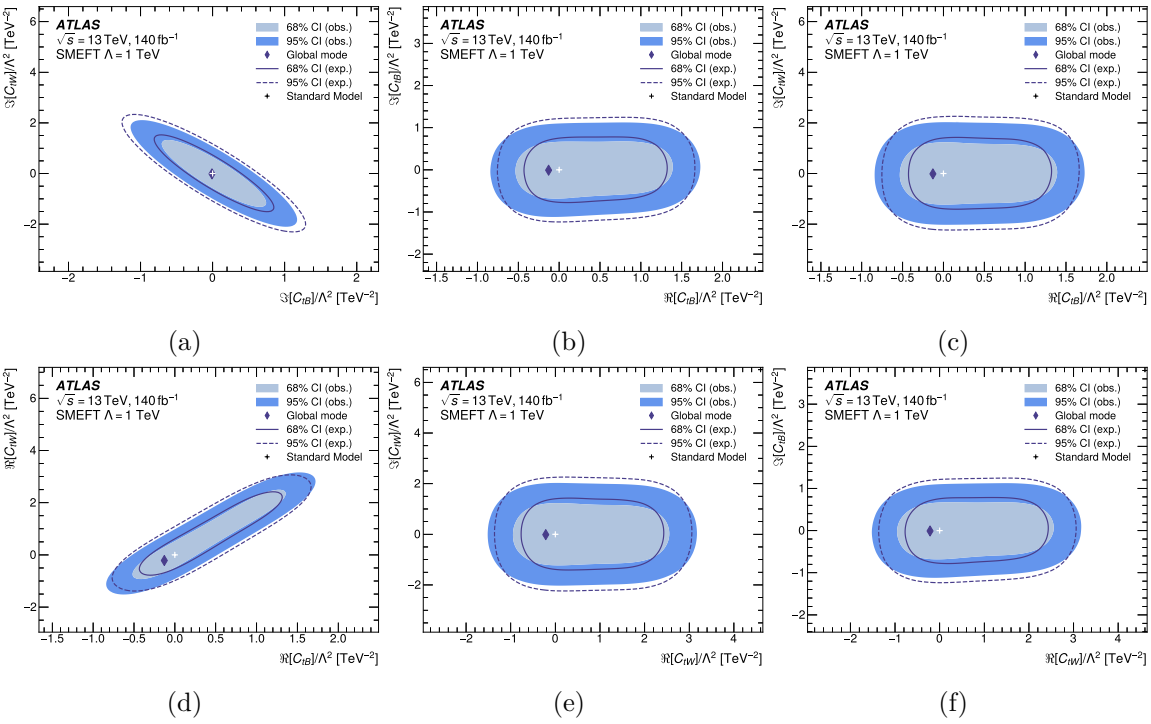

Figure 17. Two-dimensional marginalised posteriors for the C_{tW} and C_{tB} operators from the quadratic fit, indicating the 68% and 95% credible intervals, extracted using the photon p_{T} distribution from the combined measurement in the single-lepton and dilepton channels shown in figure 10. The pairs of operators shown are (a) $\Im[C_{tB}]$,$\Im[C_{tW}]$, (b) $\Re[C_{tB}]$,$\Im[C_{tB}]$, (c) $\Re[C_{tB}]$,$\Im[C_{tW}]$, (d) $\Re[C_{tB}]$,$\Re[C_{tW}]$, (e) $\Re[C_{tW}]$,$\Im[C_{tW}]$ and (f) $\Re[C_{tW}]$,$\Im[C_{tB}]$.

Additionally, the fits where only one EFT parameter is probed at a time, while all others are set to zero, referred to as independent fits, are carried out using the quadratic parameterisations. The observed and expected 68% and 95% credible intervals for the C_{tW} and C_{tB} operators from both sets of fits, the marginalised quadratic fits and the independent quadratic fits, are given in table 7. The marginalised values are obtained by integrating the posterior probability distribution over the other coefficients. The best-fit values for the different coefficients are in agreement with the predictions of the SM despite a slightly larger measured $t\bar{t}\gamma$ production cross-section than the NLO calculation. The constraints on the C_{tB} coefficient are roughly a factor of two better than those on C_{tW}.

The $t\bar{t}Z$ production is also modified by the C_{tB} and C_{tW} operators as mentioned above, providing complementary constraining power. Thus, the limits on EFT parameters are also set using a simultaneous measurement of the photon p_{T} and the Z boson p_{T} using the input data and simulations from the $t\bar{t}Z$ production measurement of ref. [16]. The Z boson p_{T} distribution is measured in $t\bar{t}Z$ events with two, three and four leptons in the final state and is corrected to particle level in a fiducial phase space. The event selection and reconstruction is designed to avoid any statistical overlap with the $t\bar{t}\gamma$ measurement to ease the combination. Both measurements consider the same sources of the systematic uncertainties for all the common objects. Thus, in the simultaneous profile-likelihood fit to the photon and Z boson distributions, all experimental uncertainties are treated as correlated between

JHEP10(2024)191

Wilson coefficient		68% CI (exp.)	95% CI (exp.)	68% CI (obs.)	95% CI (obs.)	Best-fit
$\Re[C_{tW}]$	$\mathcal{O}(\Lambda^{-4})$ (marg.)	$[-0.35, 1.9]$	$[-1.0, 2.7]$	$[-0.55, 1.9]$	$[-1.2, 2.8]$	-0.21
	$\mathcal{O}(\Lambda^{-4})$ (indep.)	$[-0.52, 0.60]$	$[-0.90, 0.98]$	$[-0.44, 0.46]$	$[-0.78, 0.84]$	-0.01
$\Im[C_{tW}]$	$\mathcal{O}(\Lambda^{-4})$ (marg.)	$[-1.1, 1.1]$	$[-1.9, 2.0]$	$[-0.95, 0.95]$	$[-1.8, 1.8]$	-0.01
	$\mathcal{O}(\Lambda^{-4})$ (indep.)	$[-0.58, 0.56]$	$[-0.96, 0.94]$	$[-0.48, 0.44]$	$[-0.84, 0.80]$	-0.01
$\Re[C_{tB}]$	$\mathcal{O}(\Lambda^{-4})$ (marg.)	$[-0.20, 1.0]$	$[-0.58, 1.5]$	$[-0.30, 1.0]$	$[-0.66, 1.5]$	-0.13
	$\mathcal{O}(\Lambda^{-4})$ (indep.)	$[-0.31, 0.31]$	$[-0.51, 0.52]$	$[-0.26, 0.23]$	$[-0.44, 0.44]$	-0.03
$\Im[C_{tB}]$	$\mathcal{O}(\Lambda^{-4})$ (marg.)	$[-0.58, 0.62]$	$[-1.1, 1.1]$	$[-0.50, 0.54]$	$[-0.96, 0.98]$	-0.01
	$\mathcal{O}(\Lambda^{-4})$ (indep.)	$[-0.32, 0.31]$	$[-0.53, 0.51]$	$[-0.26, 0.24]$	$[-0.45, 0.44]$	-0.01

Table 7. Observed and expected 68% and 95% credible intervals on C/Λ^2 [TeV^{-2}] for the C_{tW} and C_{tB} operators obtained from the $t\bar{t}\gamma$ measurement, comparing the results obtained from the marginalised quadratic fit ('marg.') and the independent quadratic fits ('indep.'). Also shown are the best-fit values (global mode) for each operator.

the measurements. The modelling uncertainties of the signal and background processes are uncorrelated owing to the different MC simulations used in both measurements.

After the fit, there are up to 10% correlations between the unfolded bins of the $t\bar{t}Z$ and $t\bar{t}\gamma$ distributions, arising from the correlation of the experimental uncertainties. The measured cross-sections and post-fit values of the systematic uncertainties are not significantly more constrained compared to the results of the individual $t\bar{t}\gamma$ and $t\bar{t}Z$ measurements (see ref. [16]).

The observed and expected 68% and 95% credible intervals for the C_{tW} and C_{tB} operators obtained from the combined measurement are summarised in table 8. The quadratic limits on the real and imaginary parts of the coefficients are similar, with C_{tB} being slightly more constrained than C_{tW}. The combination with $t\bar{t}Z$ slightly improves the limits, in particular the credible intervals for C_{tW} obtained with the independent quadratic fits are reduced by up to 20%. For better visualisation, the results of the marginalised quadratic fits obtained using the photon p_{T} in $t\bar{t}\gamma$ and in combination with $t\bar{t}Z$ are shown in figure 18.

To gauge the importance of each individual measurement in the combination, and to better visualise the interplay between the different directions of EFT sensitivity, the quadratic fits are repeated in terms of the operators C_{tZ} and $C_{t\gamma}$. The C_{tZ} coefficient is probed by the $t\bar{t}Z$ measurement, while $t\bar{t}\gamma$ is sensitive to $C_{t\gamma}$. The comparison of the individual $t\bar{t}Z$ and $t\bar{t}\gamma$ exclusion contours and the combination are shown in figure 19 as a function of C_{tZ} and C_{tW}. The shape of the $t\bar{t}Z$ exclusion contours is driven by the fact that the $t\bar{t}Z$ measurement is mostly sensitive to $\Re[C_{tZ}]$. The imaginary parts of the operators, $\Im[C_{tZ}]$ and $\Im[C_{t\gamma}]$, do not interfere with the SM (CP-odd dipole terms) and, therefore, only the quadratic terms with positive contributions affect the differential cross-section. The $t\bar{t}Z$ measurement is not able to resolve the C_{tZ} and $C_{t\gamma}$, a degenerate structure is observed in e.g., the marginalised posterior

JHEP10(2024)191

Wilson coefficient		68% CI (exp.)	95% CI (exp.)	68% CI (obs.)	95% CI (obs.)	Best-fit
$\Re[C_{tW}]$	$\mathcal{O}(\Lambda^{-4})$ (marg.)	$[-0.50, 1.2]$	$[-1.0, 2.2]$	$[-0.35, 1.8]$	$[-1.1, 2.5]$	1.61
	$\mathcal{O}(\Lambda^{-4})$ (indep.)	$[-0.44, 0.54]$	$[-0.78, 0.86]$	$[-0.28, 0.32]$	$[-0.54, 0.60]$	0.02
$\Im[C_{tW}]$	$\mathcal{O}(\Lambda^{-4})$ (marg.)	$[-1.1, 0.45]$	$[-1.7, 1.2]$	$[-1.3, 0.15]$	$[-1.8, 1.1]$	−0.89
	$\mathcal{O}(\Lambda^{-4})$ (indep.)	$[-0.48, 0.50]$	$[-0.82, 0.82]$	$[-0.32, 0.30]$	$[-0.58, 0.58]$	−0.01
$\Re[C_{tB}]$	$\mathcal{O}(\Lambda^{-4})$ (marg.)	$[-0.28, 0.70]$	$[-0.60, 1.2]$	$[-0.34, 1.2]$	$[-0.68, 1.4]$	0.94
	$\mathcal{O}(\Lambda^{-4})$ (indep.)	$[-0.28, 0.32]$	$[-0.49, 0.52]$	$[-0.24, 0.19]$	$[-0.41, 0.39]$	−0.03
$\Im[C_{tB}]$	$\mathcal{O}(\Lambda^{-4})$ (marg.)	$[-0.34, 0.62]$	$[-0.78, 1.0]$	$[-0.18, 0.72]$	$[-0.64, 1.0]$	0.46
	$\mathcal{O}(\Lambda^{-4})$ (indep.)	$[-0.31, 0.30]$	$[-0.51, 0.51]$	$[-0.23, 0.21]$	$[-0.40, 0.40]$	−0.01

Table 8. Observed and expected 68% and 95% credible intervals on C/Λ^2 [TeV^{-2}] for the C_{tW} and C_{tB} operators obtained from a combined $t\bar{t}Z$ and $t\bar{t}\gamma$ measurements comparing the results obtained from the marginalised global quadratic fit ('marg.') and the independent quadratic fits ('indep.'). Also shown are the best-fit values (global mode) for each operator.

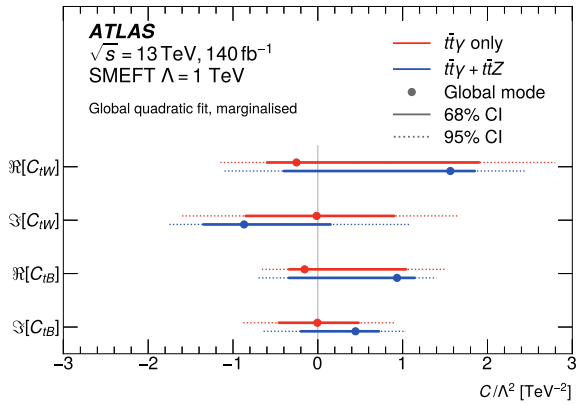

Figure 18. Comparison of the 68% and 95% credible intervals obtained in the marginalised quadratic fits using the photon p_{T} in $t\bar{t}\gamma$ production and using the simultaneous measurement of the p_{T} of the Z boson and the p_{T} of the photon. Also shown are the best-fit values (global mode) for each operator.

of $C_{t\gamma}$ (figure 19(a)). It is resolved by the addition of the $t\bar{t}\gamma$ measurement, as expected. Both $t\bar{t}Z$ and $t\bar{t}\gamma$ lead to the same contour shape in the plane of $\Re[C_{tZ}]$ versus $\Im[C_{tZ}]$ (figure 19(f)), while their combination exhibits a different structure, which highlights the importance of combining measurements with complementary directions of EFT sensitivity.

JHEP10(2024)191

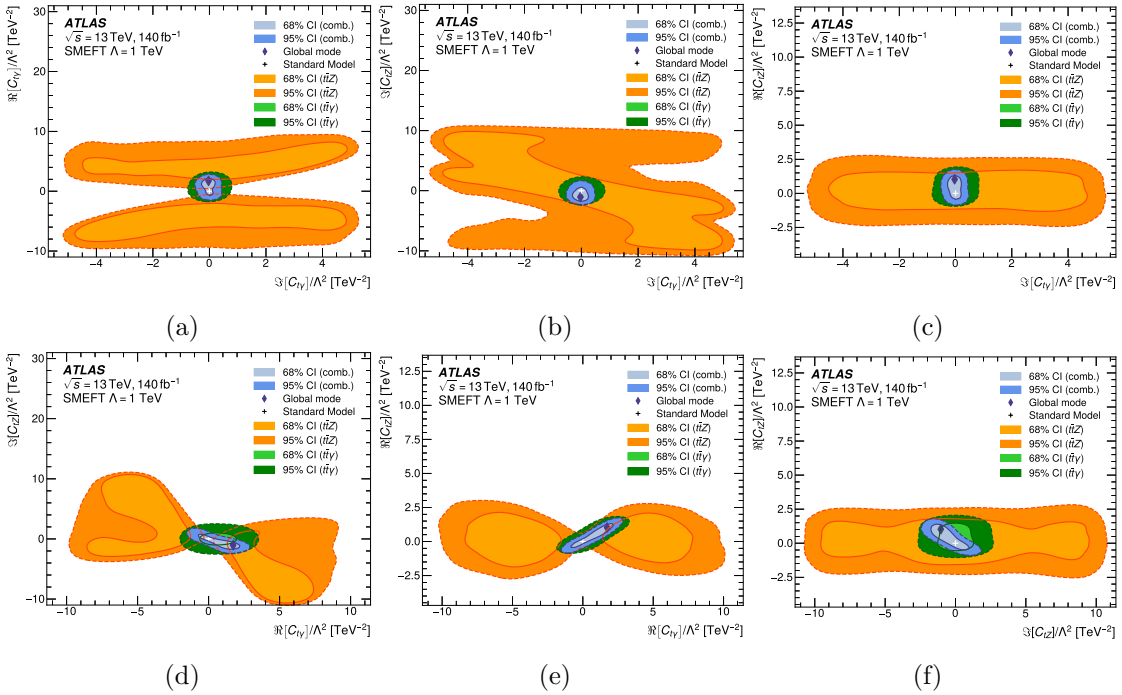

Figure 19. Two-dimensional marginalised posteriors for the $C_{t\gamma}$ and C_{tZ} operators from the quadratic fit, indicating the 68% and 95% credible intervals. The pairs of operators shown are (a) $\Im[C_{t\gamma}]$,$\Re[C_{t\gamma}]$, (b) $\Im[C_{t\gamma}]$,$\Im[C_{tZ}]$, (c) $\Im[C_{t\gamma}]$,$\Re[C_{tZ}]$, (d) $\Re[C_{t\gamma}]$,$\Im[C_{tZ}]$, (e) $\Re[C_{t\gamma}]$,$\Re[C_{tZ}]$ and (f) $\Im[C_{tZ}]$,$\Re[C_{tZ}]$. The individual contributions of the $t\bar{t}Z$ and $t\bar{t}\gamma$ measurements are displayed separately from the result of the full combination. Also shown are the best-fit value (global mode) and the SM prediction.

12 Conclusion

Detailed measurements of the production cross-section of top quark pairs in association with a photon are presented, using a data sample of proton-proton collisions collected with the ATLAS detector at the LHC at $\sqrt{s} = 13$ TeV, corresponding to a total integrated luminosity of 140 fb^{-1}. The cross-section of the $t\bar{t}\gamma$ production process, where the photon is radiated from one of the incoming quarks, or the top quark, is measured for the first time. The inclusive and differential measurements are performed in the single-lepton and dilepton decay channels in fiducial regions at particle level for photon $p_{\mathrm{T}} > 20$ GeV. The combined inclusive fiducial cross-section for the $t\bar{t}\gamma$ production process is $319 \pm 4\,(\mathrm{stat})^{+15}_{-14}(\mathrm{syst})$ fb. The combined $t\bar{t}\gamma$ cross-section for events with photon radiated at any stage of the process is $788 \pm 5\,(\mathrm{stat})\,^{+38}_{-37}\,(\mathrm{syst})$ fb. The MC predictions are in agreement with the measurements within the total uncertainties, although they slightly underestimate the cross-sections.

The differential cross-sections, absolute and normalised, are measured for six variables in the single-lepton and up to eleven variables in the dilepton channel for the $t\bar{t}\gamma$ topology with the photon radiated from an initial-state parton or one of the top quarks and for the $t\bar{t}\gamma$ process regardless of the origin of the photon. They characterise the photon, lepton and jet kinematics as well as the angular separation between the reconstructed objects of the $t\bar{t}\gamma$ event. The shapes of the measured cross-sections are mostly well described by the MC predictions.

JHEP10(2024)191

The differential cross-sections as a function of the photon p_{T} are interpreted in the framework of the SM effective field theory, setting limits on parameters related to the electroweak dipole moments of the top quark. The EFT interpretation is also performed by using a simultaneous fit to the photon p_{T} and the Z boson p_{T} spectra measured in the $t\bar{t}$ production in association with a Z boson.

Acknowledgments

We thank CERN for the very successful operation of the LHC and its injectors, as well as the support staff at CERN and at our institutions worldwide without whom ATLAS could not be operated efficiently.

The crucial computing support from all WLCG partners is acknowledged gratefully, in particular from CERN, the ATLAS Tier-1 facilities at TRIUMF/SFU (Canada), NDGF (Denmark, Norway, Sweden), CC-IN2P3 (France), KIT/GridKA (Germany), INFN-CNAF (Italy), NL-T1 (Netherlands), PIC (Spain), RAL (UK) and BNL (USA), the Tier-2 facilities worldwide and large non-WLCG resource providers. Major contributors of computing resources are listed in ref. [85].

We gratefully acknowledge the support of ANPCyT, Argentina; YerPhI, Armenia; ARC, Australia; BMWFW and FWF, Austria; ANAS, Azerbaijan; CNPq and FAPESP, Brazil; NSERC, NRC and CFI, Canada; CERN; ANID, Chile; CAS, MOST and NSFC, China; Minciencias, Colombia; MEYS CR, Czech Republic; DNRF and DNSRC, Denmark; IN2P3-CNRS and CEA-DRF/IRFU, France; SRNSFG, Georgia; BMBF, HGF and MPG, Germany; GSRI, Greece; RGC and Hong Kong SAR, China; ISF and Benoziyo Center, Israel; INFN, Italy; MEXT and JSPS, Japan; CNRST, Morocco; NWO, Netherlands; RCN, Norway; MEiN, Poland; FCT, Portugal; MNE/IFA, Romania; MESTD, Serbia; MSSR, Slovakia; ARIS and MVZI, Slovenia; DSI/NRF, South Africa; MICIU/AEI, Spain; SRC and Wallenberg Foundation, Sweden; SERI, SNSF and Cantons of Bern and Geneva, Switzerland; NSTC, Taipei; TENMAK, Türkiye; STFC/UKRI, United Kingdom; DOE and NSF, United States of America.

Individual groups and members have received support from BCKDF, CANARIE, CRC and DRAC, Canada; CERN-CZ, PRIMUS 21/SCI/017 and UNCE SCI/013, Czech Republic; COST, ERC, ERDF, Horizon 2020, ICSC-NextGenerationEU and Marie Skłodowska-Curie Actions, European Union; Investissements d'Avenir Labex, Investissements d'Avenir Idex and ANR, France; DFG and AvH Foundation, Germany; Herakleitos, Thales and Aristeia programmes co-financed by EU-ESF and the Greek NSRF, Greece; BSF-NSF and MINERVA, Israel; Norwegian Financial Mechanism 2014–2021, Norway; NCN and NAWA, Poland; La Caixa Banking Foundation, CERCA Programme Generalitat de Catalunya and PROMETEO and GenT Programmes Generalitat Valenciana, Spain; Göran Gustafssons Stiftelse, Sweden; The Royal Society and Leverhulme Trust, United Kingdom.

In addition, individual members wish to acknowledge support from CERN: European Organization for Nuclear Research (CERN PJAS); Chile: Agencia Nacional de Investigación y Desarrollo (FONDECYT 1190886, FONDECYT 1210400, FONDECYT 1230812, FONDECYT 1230987); China: Chinese Ministry of Science and Technology (MOST-2023YFA1605700), National Natural Science Foundation of China (NSFC – 12175119, NSFC 12275265, NSFC-

JHEP10(2024)191

12075060); Czech Republic: PRIMUS Research Programme (PRIMUS/21/SCI/017); EU: H2020 European Research Council (ERC – 101002463); European Union: European Research Council (ERC – 948254, ERC 101089007), Horizon 2020 Framework Programme (MUCCA – CHIST-ERA-19-XAI-00), European Union, Future Artificial Intelligence Research (FAIR-NextGenerationEU PE00000013), Italian Center for High Performance Computing, Big Data and Quantum Computing (ICSC, NextGenerationEU); France: Agence Nationale de la Recherche (ANR-20-CE31-0013, ANR-21-CE31-0013, ANR-21-CE31-0022, ANR-22-EDIR-0002), Investissements d'Avenir Labex (ANR-11-LABX-0012); Germany: Baden-Württemberg Stiftung (BW Stiftung-Postdoc Eliteprogramme), Deutsche Forschungsgemeinschaft (DFG – 469666862, DFG – CR 312/5-2); Italy: Istituto Nazionale di Fisica Nucleare (ICSC, NextGenerationEU), Ministero dell'Università e della Ricerca (PRIN – 20223N7F8K – PNRR M4.C2.1.1); Japan: Japan Society for the Promotion of Science (JSPS KAKENHI JP21H05085, JSPS KAKENHI JP22H01227, JSPS KAKENHI JP22H04944, JSPS KAKENHI JP22KK0227); Netherlands: Netherlands Organisation for Scientific Research (NWO Veni 2020 – VI.Veni.202.179); Norway: Research Council of Norway (RCN-314472); Poland: Polish National Agency for Academic Exchange (PPN/PPO/2020/1/00002/U/00001), Polish National Science Centre (NCN 2021/42/E/ST2/00350, NCN OPUS nr 2022/47/B/ST2/03059, NCN UMO-2019/34/E/ST2/00393, UMO-2020/37/B/ST2/01043, UMO-2021/40/C/ST2/00187, UMO-2022/47/O/ST2/00148); Slovenia: Slovenian Research Agency (ARIS grant J1-3010); Spain: BBVA Foundation (LEO22-1-603), Generalitat Valenciana (Artemisa, FEDER, IDIFEDER/2018/048), Ministry of Science and Innovation (MCIN & NextGenEU PCI2022-135018-2, MICIN & FEDER PID2021-125273NB, RYC2019-028510-I, RYC2020-030254-I, RYC2021-031273-I, RYC2022-038164-I), PROMETEO and GenT Programmes Generalitat Valenciana (CIDEGENT/2019/023, CIDEGENT/2019/027); Sweden: Swedish Research Council (VR 2018-00482, VR 2022-03845, VR 2022-04683, VR grant 2021-03651), Knut and Alice Wallenberg Foundation (KAW 2017.0100, KAW 2018.0157, KAW 2018.0458, KAW 2019.0447, KAW 2022.0358); Switzerland: Swiss National Science Foundation (SNSF – PCEFP2_194658); United Kingdom: Leverhulme Trust (Leverhulme Trust RPG-2020-004); United States of America: U.S. Department of Energy (ECA DE-AC02-76SF00515), Neubauer Family Foundation.

A Variables used in the training of the neural networks

Single lepton	Dilepton
Invariant mass of photon and lepton	ΔR between photon and closest lepton
Photon p_{T}	Invariant mass of photon and closest lepton
ΔR of photon and lepton	Photon p_{T}
Invariant mass of photon and leading PCBT b-jet	Invariant mass of photon and closest b-jet
Sum of invariant masses of the reconstructed top quark and antiquark (4 variables)	Photon energy
Photon energy	Scalar sum of p_{T} of all jets
Sum of squared differences between the top-quark pole mass and reconstructed $t\bar{t}$ mass (4 variables)	p_{T} and energy of the two jets with highest p_{T} (4 variables)
Invariant mass of all jets, the lepton and the photon	ΔR of photon and closest b-jet
H_{T}	$E_{\mathrm{T}}^{\mathrm{miss}}$
Reconstructed leptonic W boson p_{T}	Number of jets
p_{T} and energy of four jets with highest p_{T} (8 variables)	Photon η
ΔR between photon and closest b-jet	Number of b-jets
$E_{\mathrm{T}}^{\mathrm{miss}}$	Photon ϕ
Invariant mass of lepton and closest b-jet	
Number of jets	
Transverse mass of leptonic W boson	
ΔR between lepton and closest b-jet	
Invariant mass of reconstructed W bosons, shifted by the W boson (2 variables)	
Photon η	
PCBT distributions of the four jets with the highest scores (4 variables)	
Photon conversion type	
Number of b-jets	
Photon ϕ	

Table 9. List of the input variables used in the training of the NNs in the (left) single-lepton and (right) dilepton channels. The variables are ordered by separation power between $t\bar{t}\gamma$ production and $t\bar{t}\gamma$ decay or all background processes, respectively.

JHEP10(2024)191

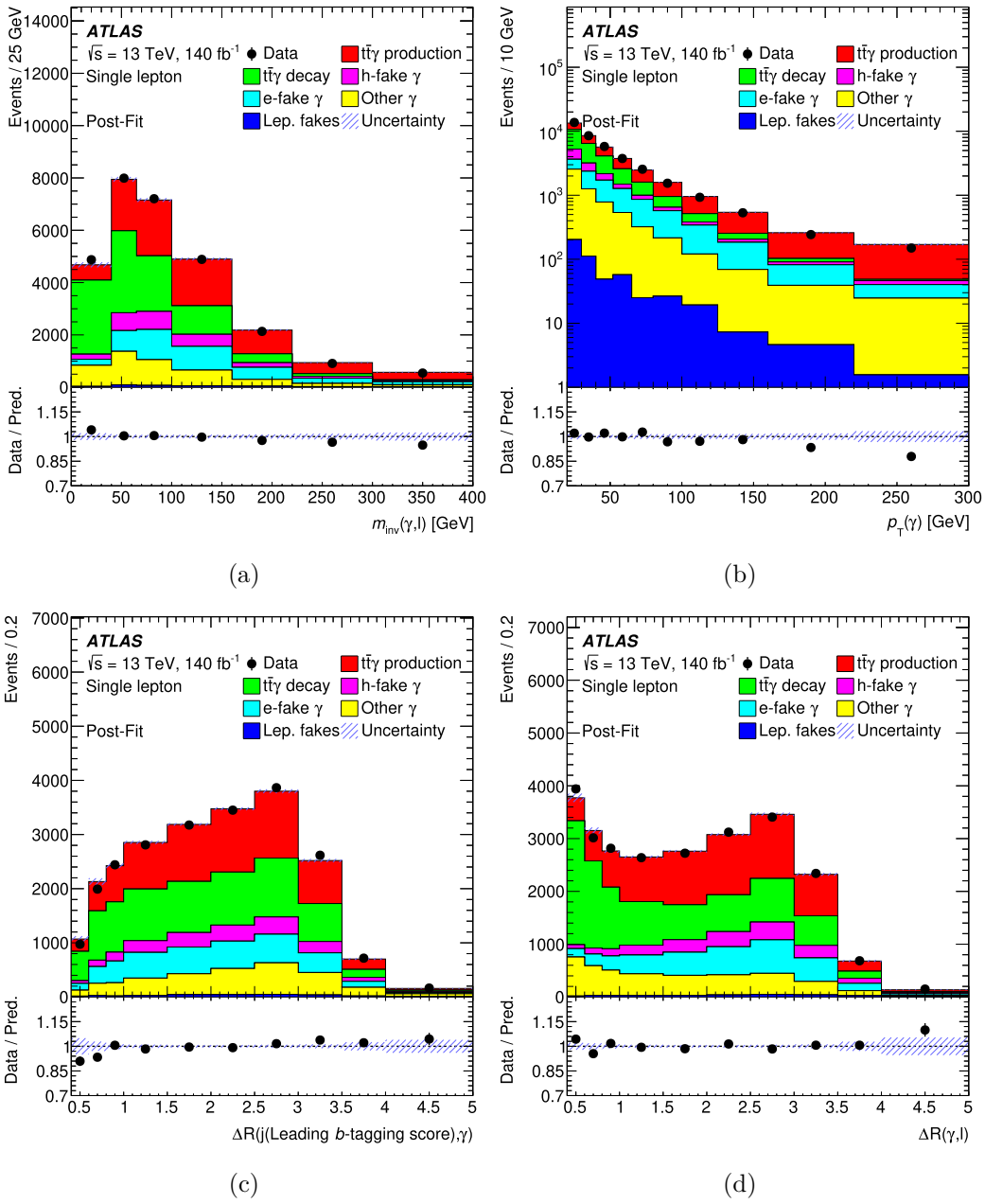

Figure 20. Distributions of the four input variables used in the training of the NN in the single-lepton channel with the largest separation power between $t\bar{t}\gamma$ production and $t\bar{t}\gamma$ decay after the fit to data for the measurement of the $t\bar{t}\gamma$ production cross-section: (a) invariant mass of the photon and lepton system, (b) photon p_{T}, (c) ΔR between the photon and the jet with the highest b-tagging score and (d) $\Delta R(\gamma, \ell)$. The uncertainty band represents the total post-fit uncertainty in the prediction. The lower panels show the ratios of the data to the total post-fit predictions.

JHEP10(2024)191

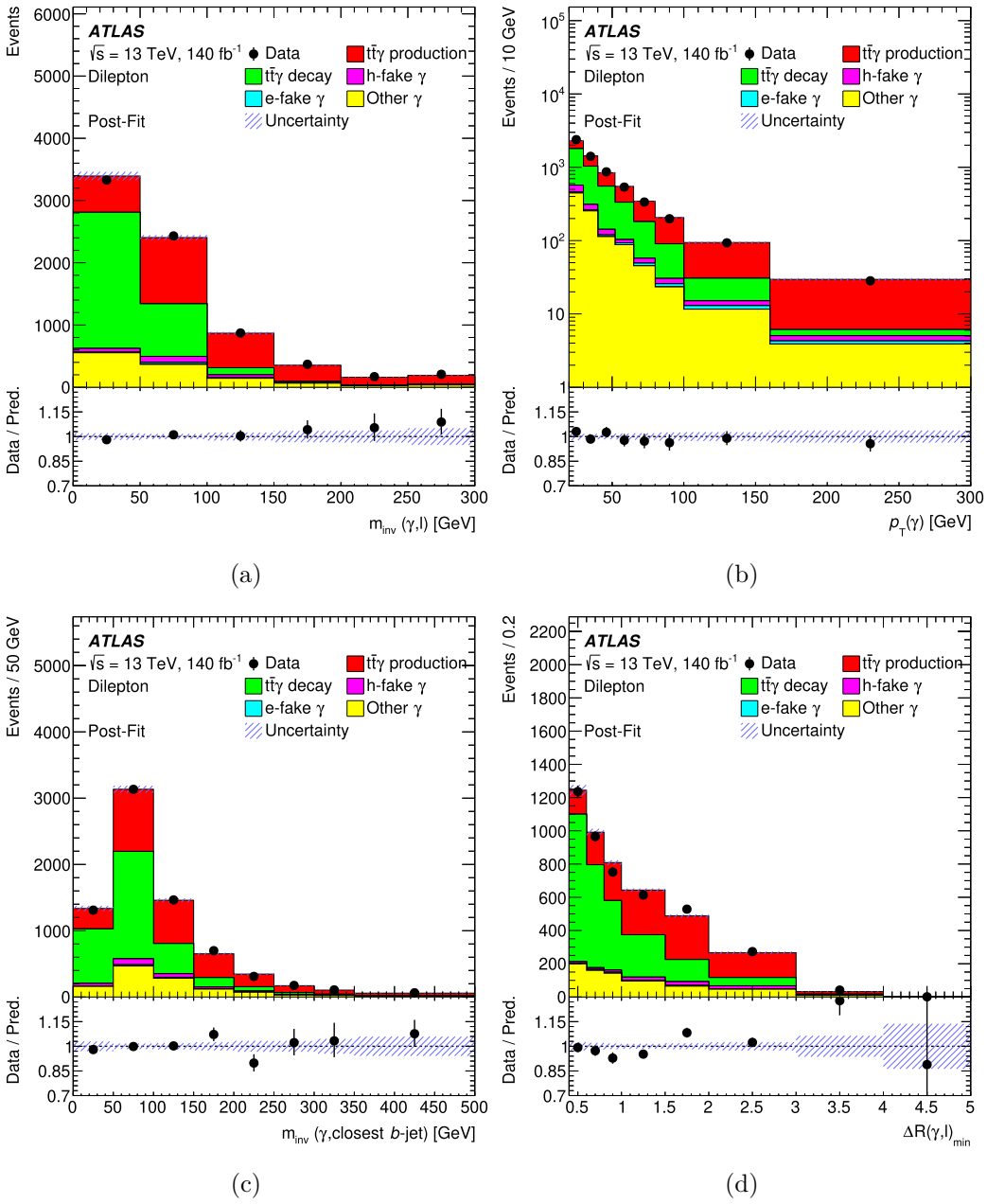

Figure 21. Distributions of the four input variables used in the training of the NN in the dilepton channel with the largest separation power between $t\bar{t}\gamma$ production and the total background after the fit to data for the measurement of the $t\bar{t}\gamma$ production cross-section: (a) invariant mass of the photon and the closest lepton system, (b) photon p_{T}, (c) invariant mass of the photon and the closest b-jet and (d) $\Delta R(\gamma,\ell)_{\mathrm{min}}$. The uncertainty band represents the total post-fit uncertainty in the prediction. The lower panels show the ratios of the data to the total post-fit predictions.

JHEP10(2024)191

B Differential cross-sections for the $t\bar{t}\gamma$ production process

The absolute and normalised cross-sections of the $t\bar{t}\gamma$ production as a function of photon p_{T} and $|\eta|$ and leading jet p_{T} are shown in figure 22 (single-lepton channel) and figure 23 (dilepton channel). They are compared with the MadGraph5_aMC@NLO simulation at NLO interfaced to Pythia 8 and Herwig 7. The agreement between the data and both predictions is similar. Both simulations predict a harder photon p_{T} distribution, while they describe the shape of the photon $|\eta|$ and the p_{T} of a leading jet well.

JHEP10(2024)191

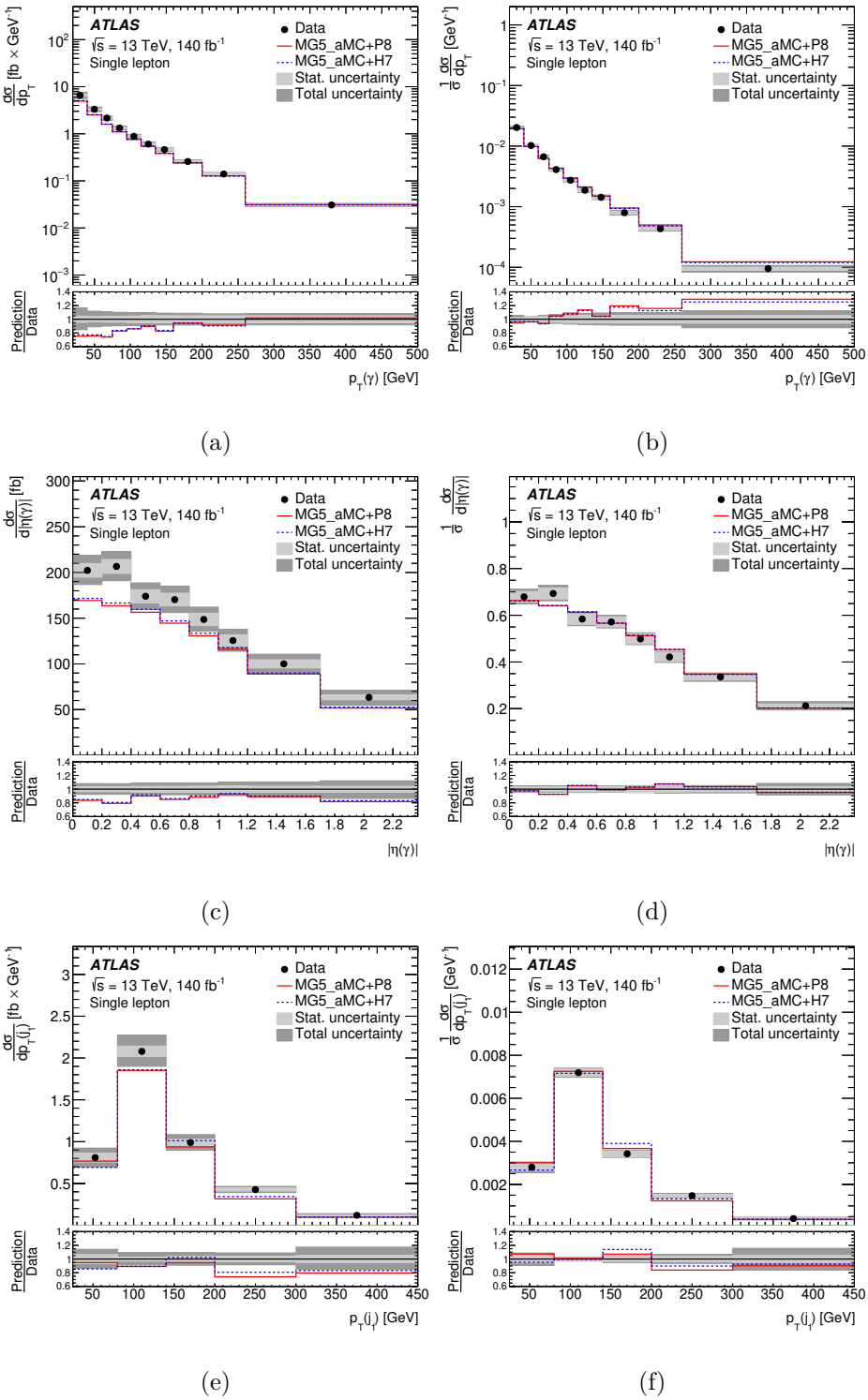

Figure 22. The (a, c, e) absolute and (b, d, f) normalised differential cross-section measured in the fiducial phase space in the single-lepton channel as a function of the (a, b) photon p_{T}, (c, d) photon $|\eta|$ and (e, f) p_{T} of the leading jet. Data are compared with the NLO MadGraph5_aMC@NLO simulation interfaced to Pythia 8 and Herwig 7. The lower panels show the ratios of the predictions to the data. The last bin of the distributions includes the overflow events.

JHEP10(2024)191

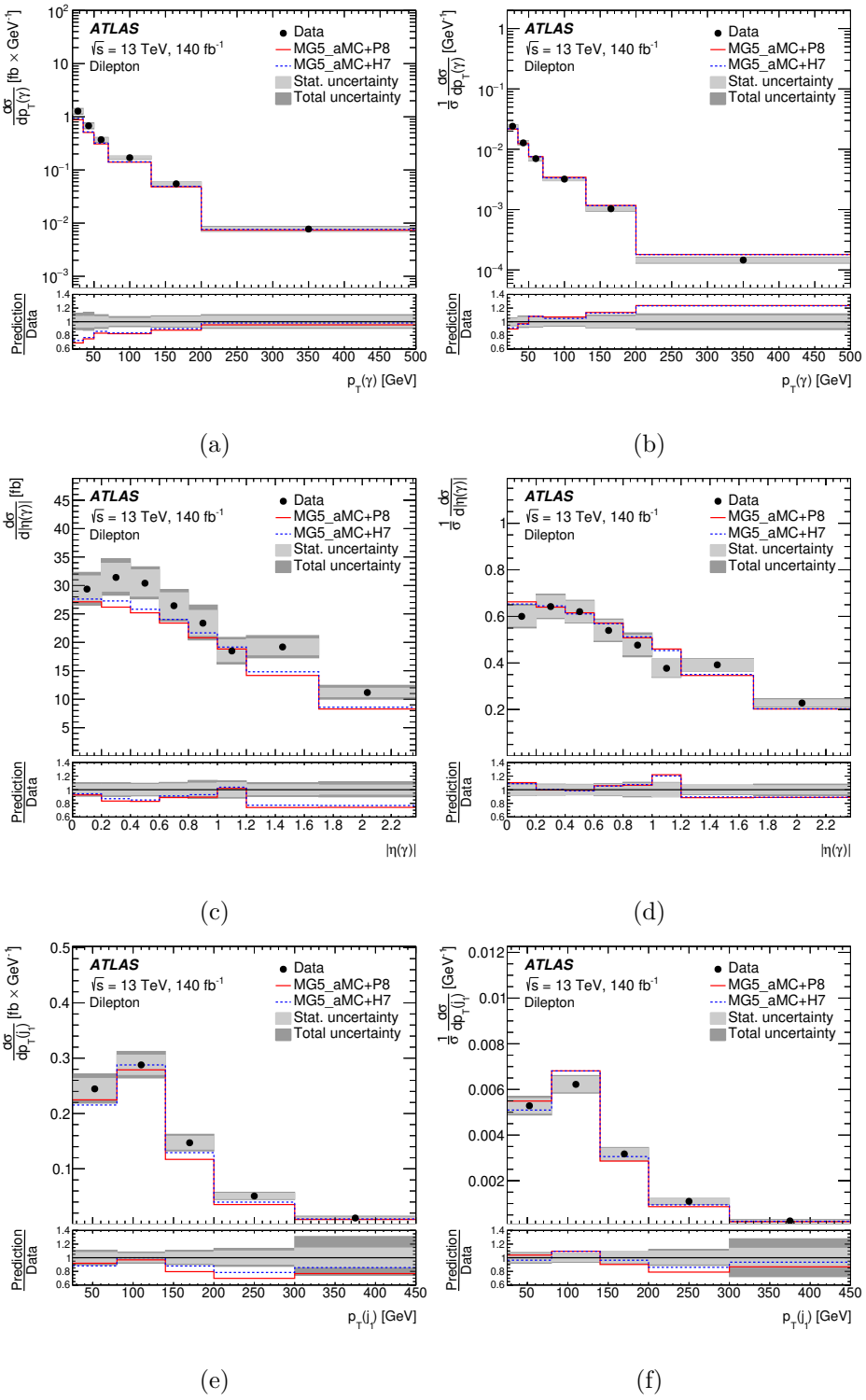

Figure 23. The (a, c, e) absolute and (b, d, f) normalised differential cross-section measured in the fiducial phase space in the dilepton channel as a function of the (a, b) photon p_{T}, (c, d) photon $|\eta|$ and (e, f) leading jet p_{T}. Data are compared with the NLO MadGraph5_aMC@NLO simulation interfaced to Pythia 8 and Herwig 7. The lower panels show the ratios of the predictions to the data. The last bin of the distributions includes the overflow events.

JHEP10(2024)191

C Differential cross-sections for the combined $t\bar{t}\gamma$ production and decay process

The absolute and normalised cross-sections for the sum of the $t\bar{t}\gamma$ production and $t\bar{t}\gamma$ decay measured in the same phase space as the $t\bar{t}\gamma$ production process alone are shown as functions of photon p_{T}, photon $|\eta|$ and leading jet p_{T} in figure 24 and as functions of $\Delta R(\gamma, b)_{\mathrm{min}}$, $\Delta R(\gamma, \ell)$ and $\Delta R(\ell, j)_{\mathrm{min}}$ in figure 25 for the dilepton channel.

JHEP10(2024)191

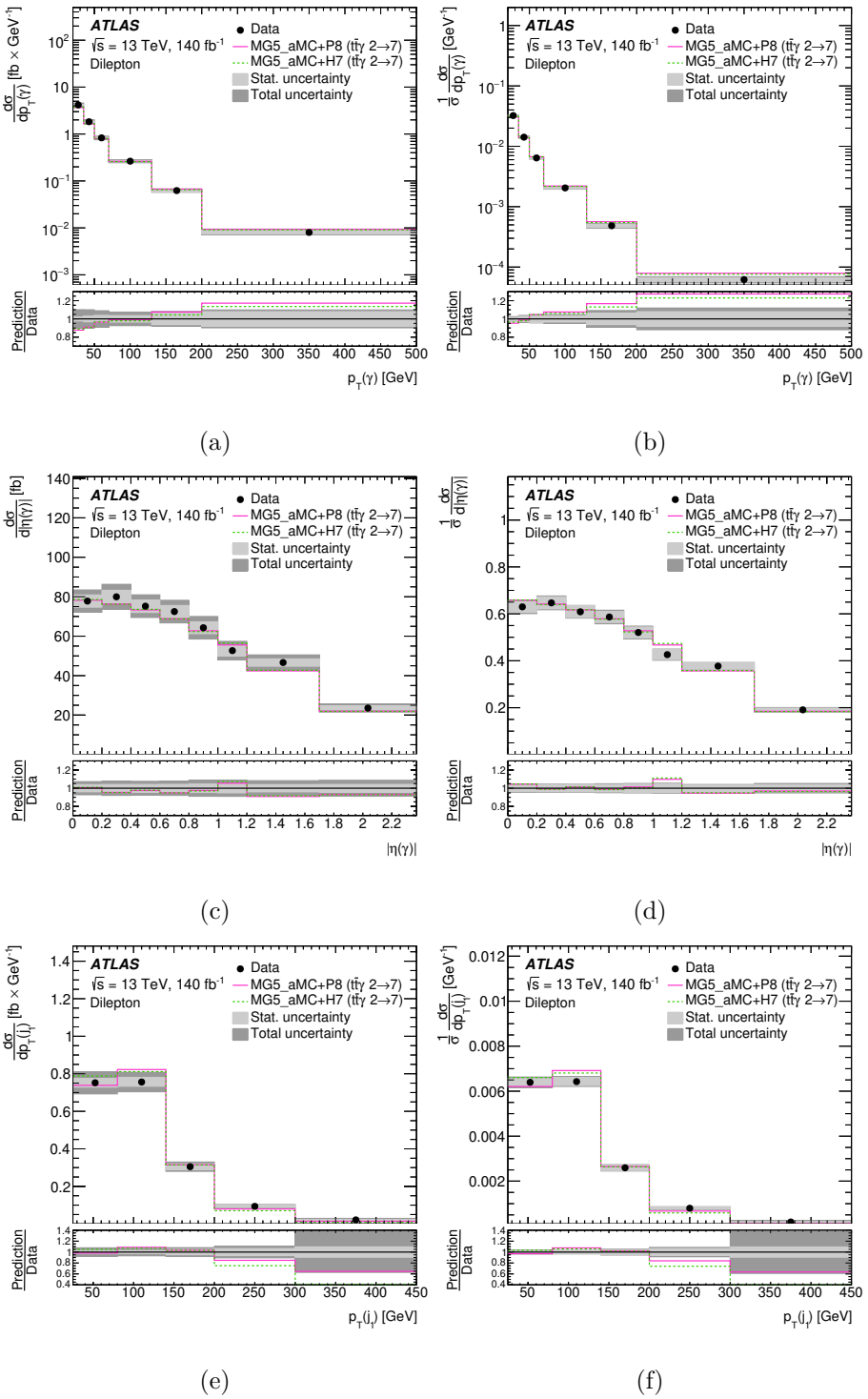

Figure 24. The (a, c, e) absolute and (b, d, f) normalised differential cross-sections of the total $t\bar{t}\gamma$ production and decay measured in the fiducial phase space in the dilepton channel as a function of the (a, b) photon p_{T}, (c, d) photon $|\eta|$ and (e, f) leading jet p_{T}. Data are compared with the $t\bar{t}\gamma$ MadGraph5_aMC@NLO simulation at LO ($t\bar{t}\gamma$ $2 \to 7$ process) interfaced to Pythia 8 and Herwig 7. The lower panels show the ratios of the predictions to the data. The last bin of the distributions includes the overflow events.

JHEP10(2024)191

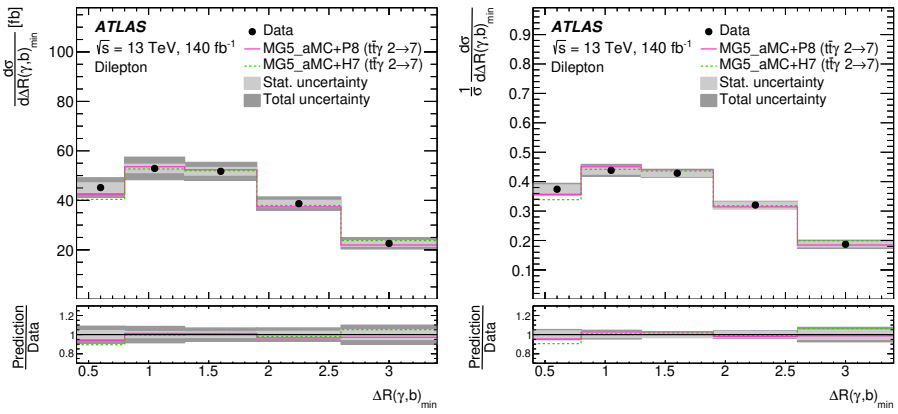

(a) (b)

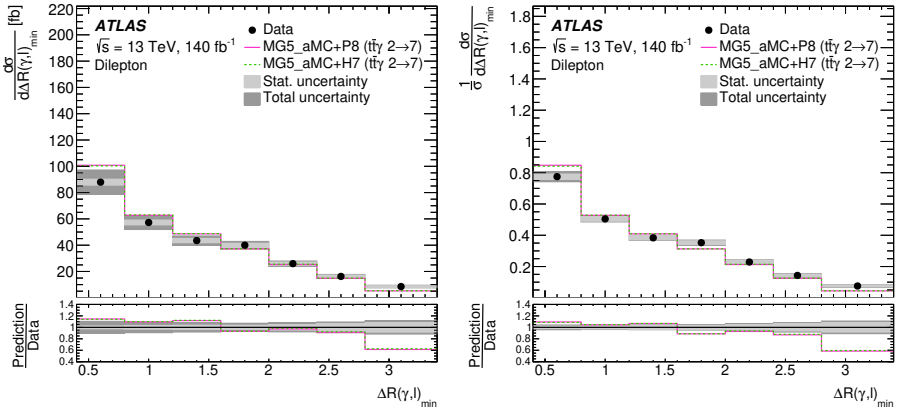

(c) (d)

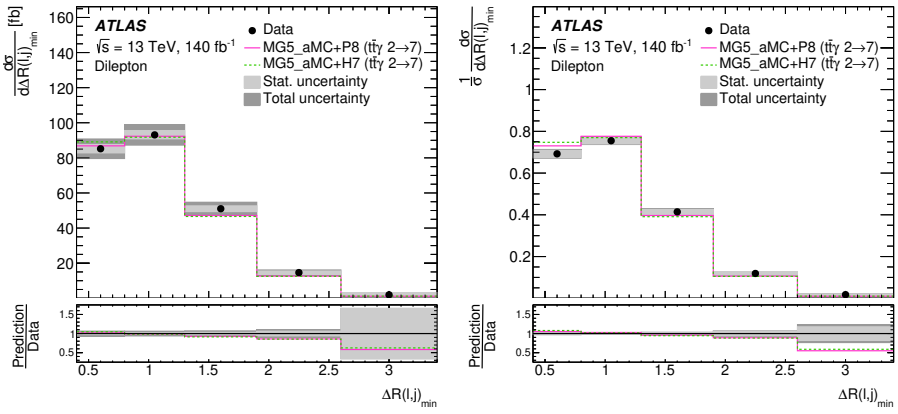

(e) (f)

Figure 25. The (a, c, e) absolute and (b, d, f) normalised differential cross-sections of the total $t\bar{t}\gamma$ production and decay measured in the fiducial phase space in the dilepton channel as a function of (a, b) $\Delta R(\gamma, b)_{\text{min}}$, (c, d) $\Delta R(\gamma, \ell)$ and (e, f) $\Delta R(\ell, j)_{\text{min}}$. Data are compared with the $t\bar{t}\gamma$ MadGraph5_aMC@NLO simulation at LO ($t\bar{t}\gamma$ $2 \to 7$ process) interfaced to Pythia 8 and Herwig 7. The lower panels show the ratios of the predictions to the data. The last bin of the distributions includes the overflow events.

JHEP10(2024)191

Open Access. This article is distributed under the terms of the Creative Commons Attribution License (CC-BY4.0), which permits any use, distribution and reproduction in any medium, provided the original author(s) and source are credited.

References

[1] U. Baur, A. Juste, L.H. Orr and D. Rainwater, *Probing electroweak top quark couplings at hadron colliders*, *Phys. Rev. D* **71** (2005) 054013 [hep-ph/0412021] [INSPIRE].

[2] A.O. Bouzas and F. Larios, *Electromagnetic dipole moments of the top quark*, *Phys. Rev. D* **87** (2013) 074015 [arXiv:1212.6575] [INSPIRE].

[3] M. Schulze and Y. Soreq, *Pinning down electroweak dipole operators of the top quark*, *Eur. Phys. J. C* **76** (2016) 466 [arXiv:1603.08911] [INSPIRE].

[4] O. Bessidskaia Bylund et al., *Probing top quark neutral couplings in the Standard Model Effective Field Theory at NLO in QCD*, *JHEP* **05** (2016) 052 [arXiv:1601.08193] [INSPIRE].

[5] CDF collaboration, *Evidence for $t\bar{t}\gamma$ production and measurement of $\sigma_{t\bar{t}\gamma}/\sigma_{t\bar{t}}$*, *Phys. Rev. D* **84** (2011) 031104 [arXiv:1106.3970] [INSPIRE].

[6] ATLAS collaboration, *Observation of top-quark pair production in association with a photon and measurement of the $t\bar{t}\gamma$ production cross section in pp collisions at $\sqrt{s} = 7$ TeV using the ATLAS detector*, *Phys. Rev. D* **91** (2015) 072007 [arXiv:1502.00586] [INSPIRE].

[7] ATLAS collaboration, *Measurement of the $t\bar{t}\gamma$ production cross section in proton-proton collisions at $\sqrt{s} = 8$ TeV with the ATLAS detector*, *JHEP* **11** (2017) 086 [arXiv:1706.03046] [INSPIRE].

[8] CMS collaboration, *Measurement of the semileptonic $t\bar{t} + \gamma$ production cross section in pp collisions at $\sqrt{s} = 8$ TeV*, *JHEP* **10** (2017) 006 [arXiv:1706.08128] [INSPIRE].

[9] ATLAS collaboration, *Measurements of inclusive and differential fiducial cross-sections of $t\bar{t}\gamma$ production in leptonic final states at $\sqrt{s} = 13$ TeV in ATLAS*, *Eur. Phys. J. C* **79** (2019) 382 [arXiv:1812.01697] [INSPIRE].

[10] ATLAS collaboration, *Measurements of inclusive and differential cross-sections of combined $t\bar{t}\gamma$ and $tW\gamma$ production in the $e\mu$ channel at 13 TeV with the ATLAS detector*, *JHEP* **09** (2020) 049 [arXiv:2007.06946] [INSPIRE].

[11] CMS collaboration, *Measurement of the inclusive and differential $t\bar{t}\gamma$ cross sections in the single-lepton channel and EFT interpretation at $\sqrt{s} = 13$ TeV*, *JHEP* **12** (2021) 180 [arXiv:2107.01508] [INSPIRE].

[12] CMS collaboration, *Measurement of the inclusive and differential $t\bar{t}\gamma$ cross sections in the dilepton channel and effective field theory interpretation in proton-proton collisions at $\sqrt{s} = 13$ TeV*, *JHEP* **05** (2022) 091 [arXiv:2201.07301] [INSPIRE].

[13] ATLAS collaboration, *Measurement of the charge asymmetry in top-quark pair production in association with a photon with the ATLAS experiment*, *Phys. Lett. B* **843** (2023) 137848 [arXiv:2212.10552] [INSPIRE].

[14] G. Bevilacqua et al., *Hard Photons in Hadroproduction of Top Quarks with Realistic Final States*, *JHEP* **10** (2018) 158 [arXiv:1803.09916] [INSPIRE].

[15] G. Bevilacqua et al., *Off-shell vs on-shell modelling of top quarks in photon associated production*, *JHEP* **03** (2020) 154 [arXiv:1912.09999] [INSPIRE].

JHEP10(2024)191

[16] ATLAS collaboration, *Inclusive and differential cross-section measurements of $t\bar{t}Z$ production in pp collisions at $\sqrt{s} = 13$ TeV with the ATLAS detector, including EFT and spin-correlation interpretations*, *JHEP* **07** (2024) 163 [arXiv:2312.04450] [INSPIRE].

[17] ATLAS collaboration, *The ATLAS Experiment at the CERN Large Hadron Collider*, 2008 *JINST* **3** S08003 [INSPIRE].

[18] ATLAS collaboration, *ATLAS Insertable B-Layer: Technical Design Report*, 2010.

[19] ATLAS IBL collaboration, *Production and integration of the ATLAS Insertable B-Layer*, 2018 *JINST* **13** T05008 [arXiv:1803.00844] [INSPIRE].

[20] G. Avoni et al., *The new lucid-2 detector for luminosity measurement and monitoring in atlas*, 2018 *JINST* **13** P07017 [INSPIRE].

[21] ATLAS collaboration, *Performance of the ATLAS trigger system in 2015*, *Eur. Phys. J. C* **77** (2017) 317 [arXiv:1611.09661] [INSPIRE].

[22] ATLAS collaboration, *The ATLAS Collaboration Software and Firmware*, ATL-SOFT-PUB-2021-001, CERN, Geneva (2021).

[23] ATLAS collaboration, *The ATLAS Simulation Infrastructure*, *Eur. Phys. J. C* **70** (2010) 823 [arXiv:1005.4568] [INSPIRE].

[24] GEANT4 collaboration, *GEANT4 — a simulation toolkit*, *Nucl. Instrum. Meth. A* **506** (2003) 250 [INSPIRE].

[25] C. ATLAS et al., *The simulation principle and performance of the ATLAS fast calorimeter simulation FastCaloSim*, ATL-PHYS-PUB-2010-013, CERN, Geneva (2010).

[26] J. Alwall et al., *The automated computation of tree-level and next-to-leading order differential cross sections, and their matching to parton shower simulations*, *JHEP* **07** (2014) 079 [arXiv:1405.0301] [INSPIRE].

[27] S. Frixione, E. Laenen, P. Motylinski and B.R. Webber, *Angular correlations of lepton pairs from vector boson and top quark decays in Monte Carlo simulations*, *JHEP* **04** (2007) 081 [hep-ph/0702198] [INSPIRE].

[28] P. Artoisenet, R. Frederix, O. Mattelaer and R. Rietkerk, *Automatic spin-entangled decays of heavy resonances in Monte Carlo simulations*, *JHEP* **03** (2013) 015 [arXiv:1212.3460] [INSPIRE].

[29] NNPDF collaboration, *Parton distributions for the LHC run II*, *JHEP* **04** (2015) 040 [arXiv:1410.8849] [INSPIRE].

[30] S. Frixione, *Isolated photons in perturbative QCD*, *Phys. Lett. B* **429** (1998) 369 [hep-ph/9801442] [INSPIRE].

[31] J. Pumplin et al., *New Generation of Parton Distributions with Uncertainties from Global QCD Analysis*, *JHEP* **07** (2002) 012 [hep-ph/0201195] [INSPIRE].

[32] P. Nason, *A new method for combining NLO QCD with shower Monte Carlo algorithms*, *JHEP* **11** (2004) 040 [hep-ph/0409146] [INSPIRE].

[33] S. Frixione, P. Nason and G. Ridolfi, *A positive-weight next-to-leading-order Monte Carlo for heavy flavour hadroproduction*, *JHEP* **09** (2007) 126 [arXiv:0707.3088] [INSPIRE].

[34] S. Frixione, P. Nason and C. Oleari, *Matching NLO QCD computations with parton shower simulations: the POWHEG method*, *JHEP* **11** (2007) 070 [arXiv:0709.2092] [INSPIRE].

JHEP10(2024)191

[35] S. Alioli, P. Nason, C. Oleari and E. Re, *A general framework for implementing NLO calculations in shower Monte Carlo programs: the POWHEG BOX*, *JHEP* **06** (2010) 043 [arXiv:1002.2581] [INSPIRE].

[36] ATLAS collaboration, *Studies on top-quark Monte Carlo modelling for Top2016*, ATL-PHYS-PUB-2016-020, CERN, Geneva (2016).

[37] M. Czakon and A. Mitov, *Top++: A program for the calculation of the top-pair cross-section at hadron colliders*, *Comput. Phys. Commun.* **185** (2014) 2930 [arXiv:1112.5675] [INSPIRE].

[38] N. Kidonakis, *Two-loop soft anomalous dimensions for single top quark associated production with a W^- or H^-*, *Phys. Rev. D* **82** (2010) 054018 [arXiv:1005.4451] [INSPIRE].

[39] N. Kidonakis, *Next-to-next-to-leading-logarithm resummation for s-channel single top quark production*, *Phys. Rev. D* **81** (2010) 054028 [arXiv:1001.5034] [INSPIRE].

[40] N. Kidonakis, *Next-to-next-to-leading-order collinear and soft gluon corrections for t-channel single top quark production*, *Phys. Rev. D* **83** (2011) 091503 [arXiv:1103.2792] [INSPIRE].

[41] S. Frixione et al., *Single-top hadroproduction in association with a W boson*, *JHEP* **07** (2008) 029 [arXiv:0805.3067] [INSPIRE].

[42] SHERPA collaboration, *Event generation with Sherpa 2.2*, *SciPost Phys.* **7** (2019) 034 [arXiv:1905.09127] [INSPIRE].

[43] S. Höche, F. Krauss, S. Schumann and F. Siegert, *QCD matrix elements and truncated showers*, *JHEP* **05** (2009) 053 [arXiv:0903.1219] [INSPIRE].

[44] J.M. Campbell and R.K. Ellis, *Update on vector boson pair production at hadron colliders*, *Phys. Rev. D* **60** (1999) 113006 [hep-ph/9905386] [INSPIRE].

[45] ATLAS collaboration, *Measurement of $W^{\pm}$ and Z-boson production cross sections in pp collisions at $\sqrt{s} = 13$ TeV with the ATLAS detector*, *Phys. Lett. B* **759** (2016) 601 [arXiv:1603.09222] [INSPIRE].

[46] I. Brivio, *SMEFTsim 3.0 — a practical guide*, *JHEP* **04** (2021) 073 [arXiv:2012.11343] [INSPIRE].

[47] I. Brivio et al., *Electroweak input parameters*, arXiv:2111.12515 [INSPIRE].

[48] T. Sjöstrand, S. Mrenna and P.Z. Skands, *A brief introduction to PYTHIA 8.1*, *Comput. Phys. Commun.* **178** (2008) 852 [arXiv:0710.3820] [INSPIRE].

[49] ATLAS collaboration, *ATLAS Pythia 8 tunes to 7 TeV data*, ATL-PHYS-PUB-2014-021, CERN, Geneva (2014).

[50] D.J. Lange, *The EvtGen particle decay simulation package*, *Nucl. Instrum. Meth. A* **462** (2001) 152 [INSPIRE].

[51] S. Schumann and F. Krauss, *A parton shower algorithm based on Catani-Seymour dipole factorisation*, *JHEP* **03** (2008) 038 [arXiv:0709.1027] [INSPIRE].

[52] ATLAS collaboration, *The Pythia 8 A3 tune description of ATLAS minimum bias and inelastic measurements incorporating the Donnachie-Landshoff diffractive model*, ATL-PHYS-PUB-2016-017, CERN, Geneva (2016).

[53] ATLAS collaboration, *ATLAS data quality operations and performance for 2015–2018 data-taking*, 2020 *JINST* **15** P04003 [arXiv:1911.04632] [INSPIRE].

[54] ATLAS collaboration, *Luminosity determination in pp collisions at $\sqrt{s} = 13$ TeV using the ATLAS detector at the LHC*, *Eur. Phys. J. C* **83** (2023) 982 [arXiv:2212.09379] [INSPIRE].

JHEP10(2024)191

[55] ATLAS collaboration, *Performance of the ATLAS muon triggers in Run 2*, 2020 *JINST* **15** P09015 [arXiv:2004.13447] [INSPIRE].

[56] ATLAS collaboration, *Performance of electron and photon triggers in ATLAS during LHC Run 2*, *Eur. Phys. J. C* **80** (2020) 47 [arXiv:1909.00761] [INSPIRE].

[57] ATLAS collaboration, *Operation of the ATLAS trigger system in Run 2*, 2020 *JINST* **15** P10004 [arXiv:2007.12539] [INSPIRE].

[58] ATLAS collaboration, *The ATLAS inner detector trigger performance in pp collisions at* 13 *TeV during LHC Run 2*, *Eur. Phys. J. C* **82** (2022) 206 [arXiv:2107.02485] [INSPIRE].

[59] ATLAS collaboration, *Electron and photon performance measurements with the ATLAS detector using the 2015–2017 LHC proton-proton collision data*, 2019 *JINST* **14** P12006 [arXiv:1908.00005] [INSPIRE].

[60] ATLAS collaboration, *Muon reconstruction and identification efficiency in ATLAS using the full Run 2 pp collision data set at* $\sqrt{s} = 13$ *TeV*, *Eur. Phys. J. C* **81** (2021) 578 [arXiv:2012.00578] [INSPIRE].

[61] ATLAS collaboration, *Evidence for the associated production of the Higgs boson and a top quark pair with the ATLAS detector*, *Phys. Rev. D* **97** (2018) 072003 [arXiv:1712.08891] [INSPIRE].

[62] M. Cacciari, G.P. Salam and G. Soyez, *The anti-*k_t *jet clustering algorithm*, *JHEP* **04** (2008) 063 [arXiv:0802.1189] [INSPIRE].

[63] M. Cacciari, G.P. Salam and G. Soyez, *FastJet user manual*, *Eur. Phys. J. C* **72** (2012) 1896 [arXiv:1111.6097] [INSPIRE].

[64] ATLAS collaboration, *Jet reconstruction and performance using particle flow with the ATLAS Detector*, *Eur. Phys. J. C* **77** (2017) 466 [arXiv:1703.10485] [INSPIRE].

[65] ATLAS collaboration, *Jet energy scale and resolution measured in proton-proton collisions at* $\sqrt{s} = 13$ *TeV with the ATLAS detector*, *Eur. Phys. J. C* **81** (2021) 689 [arXiv:2007.02645] [INSPIRE].

[66] ATLAS collaboration, *Performance of pile-up mitigation techniques for jets in pp collisions at* $\sqrt{s} = 8$ *TeV using the ATLAS detector*, *Eur. Phys. J. C* **76** (2016) 581 [arXiv:1510.03823] [INSPIRE].

[67] ATLAS collaboration, *ATLAS flavour-tagging algorithms for the LHC Run 2 pp collision dataset*, *Eur. Phys. J. C* **83** (2023) 681 [arXiv:2211.16345] [INSPIRE].

[68] ATLAS collaboration, E_T^{miss} *performance in the ATLAS detector using 2015–2016 LHC pp collisions*, ATLAS-CONF-2018-023, CERN, Geneva (2018).

[69] ATLAS collaboration, *Measurement of the photon identification efficiencies with the ATLAS detector using LHC Run 2 data collected in 2015 and 2016*, *Eur. Phys. J. C* **79** (2019) 205 [arXiv:1810.05087] [INSPIRE].

[70] CDF collaboration, *Measurement of* $\sigma B(W \to e\nu)$ *and* $\sigma B(Z^0 \to e^+e^-)$ *in* $\bar{p}p$ *collisions at* $\sqrt{s} = 1800$ *GeV*, *Phys. Rev. D* **44** (1991) 29 [INSPIRE].

[71] ATLAS collaboration, *Tools for estimating fake/non-prompt lepton backgrounds with the ATLAS detector at the LHC*, 2023 *JINST* **18** T11004 [arXiv:2211.16178] [INSPIRE].

[72] ATLAS collaboration, *Measurements of b-jet tagging efficiency with the ATLAS detector using* $t\bar{t}$ *events at* $\sqrt{s} = 13$ *TeV*, *JHEP* **08** (2018) 089 [arXiv:1805.01845] [INSPIRE].

JHEP10(2024)191

[73] ATLAS collaboration, *Measurement of the c-jet mistagging efficiency in $t\bar{t}$ events using pp collision data at $\sqrt{s} = 13$ TeV collected with the ATLAS detector*, *Eur. Phys. J. C* **82** (2022) 95 [arXiv:2109.10627] [INSPIRE].

[74] ATLAS collaboration, *Calibration of the light-flavour jet mistagging efficiency of the b-tagging algorithms with Z+jets events using 139 fb^{-1} of ATLAS proton-proton collision data at $\sqrt{s} = 13$ TeV*, *Eur. Phys. J. C* **83** (2023) 728 [arXiv:2301.06319] [INSPIRE].

[75] M. Bähr et al., *Herwig++ physics and manual*, *Eur. Phys. J. C* **58** (2008) 639 [arXiv:0803.0883] [INSPIRE].

[76] J. Bellm et al., *Herwig 7.0/Herwig++ 3.0 release note*, *Eur. Phys. J. C* **76** (2016) 196 [arXiv:1512.01178] [INSPIRE].

[77] ATLAS collaboration, *Improvements in $t\bar{t}$ modelling using NLO+PS Monte Carlo generators for Run 2*, ATL-PHYS-PUB-2018-009, CERN, Geneva (2018).

[78] J. Butterworth et al., *PDF4LHC recommendations for LHC Run II*, *J. Phys. G* **43** (2016) 023001 [arXiv:1510.03865] [INSPIRE].

[79] F. Chollet et al., *Keras*, https://keras.io (2015).

[80] M. Abadi et al., *TensorFlow: Large-scale machine learning on heterogeneous systems*, arXiv:1603.04467.

[81] M. Cacciari, G.P. Salam and G. Soyez, *The catchment area of jets*, *JHEP* **04** (2008) 005 [arXiv:0802.1188] [INSPIRE].

[82] R.J. Barlow and C. Beeston, *Fitting using finite monte carlo samples*, *Comput. Phys. Commun.* **77** (1993) 219 [INSPIRE].

[83] D. Barducci et al., *Interpreting top-quark LHC measurements in the standard-model effective field theory*, arXiv:1802.07237 [INSPIRE].

[84] N. Castro et al., *EFTfitter: A tool for interpreting measurements in the context of effective field theories*, *Eur. Phys. J. C* **76** (2016) 432 [arXiv:1605.05585] [INSPIRE].

[85] ATLAS collaboration, *ATLAS Computing Acknowledgements*, ATL-SOFT-PUB-2023-001, CERN, Geneva (2023).

JHEP10(2024)191

The ATLAS collaboration

G. Aad[103], E. Aakvaag[16], B. Abbott[121], K. Abeling[55], N.J. Abicht[49], S.H. Abidi[29], M. Aboelela[44], A. Aboulhorma[35e], H. Abramowicz[152], H. Abreu[151], Y. Abulaiti[118], B.S. Acharya[69a,69b,l], A. Ackermann[63a], C. Adam Bourdarios[4], L. Adamczyk[86a], S.V. Addepalli[26], M.J. Addison[102], J. Adelman[116], A. Adiguzel[21c], T. Adye[135], A.A. Affolder[137], Y. Afik[39], M.N. Agaras[13], J. Agarwala[73a,73b], A. Aggarwal[101], C. Agheorghiesei[27c], A. Ahmad[36], F. Ahmadov[38,z], W.S. Ahmed[105], S. Ahuja[96], X. Ai[62e], G. Aielli[76a,76b], A. Aikot[164], M. Ait Tamlihat[35e], B. Aitbenchikh[35a], I. Aizenberg[170], M. Akbiyik[101], T.P.A. Åkesson[99], A.V. Akimov[37], D. Akiyama[169], N.N. Akolkar[24], S. Aktas[21a], K. Al Khoury[41], G.L. Alberghi[23b], J. Albert[166], P. Albicocco[53], G.L. Albouy[60], S. Alderweireldt[52], Z.L. Alegria[122], M. Aleksa[36], I.N. Aleksandrov[38], C. Alexa[27b], T. Alexopoulos[10], F. Alfonsi[23b], M. Algren[56], M. Alhroob[142], B. Ali[133], H.M.J. Ali[92], S. Ali[149], S.W. Alibocus[93], M. Aliev[33c], G. Alimonti[71a], W. Alkakhi[55], C. Allaire[66], B.M.M. Allbrooke[147], J.F. Allen[52], C.A. Allendes Flores[138f], P.P. Allport[20], A. Aloisio[72a,72b], F. Alonso[91], C. Alpigiani[139], M. Alvarez Estevez[100], A. Alvarez Fernandez[101], M. Alves Cardoso[56], M.G. Alviggi[72a,72b], M. Aly[102], Y. Amaral Coutinho[83b], A. Ambler[105], C. Amelung[36], M. Amerl[102], C.G. Ames[110], D. Amidei[107], K.J. Amirie[156], S.P. Amor Dos Santos[131a], K.R. Amos[164], S. An[84], V. Ananiev[126], C. Anastopoulos[140], T. Andeen[11], J.K. Anders[36], S.Y. Andrean[47a,47b], A. Andreazza[71a,71b], S. Angelidakis[9], A. Angerami[41,ab], A.V. Anisenkov[37], A. Annovi[74a], C. Antel[56], M.T. Anthony[140], E. Antipov[146], M. Antonelli[53], F. Anulli[75a], M. Aoki[84], T. Aoki[154], J.A. Aparisi Pozo[164], M.A. Aparo[147], L. Aperio Bella[48], C. Appelt[18], A. Apyan[26], S.J. Arbiol Val[87], C. Arcangeletti[53], A.T.H. Arce[51], E. Arena[93], J-F. Arguin[109], S. Argyropoulos[54], J.-H. Arling[48], O. Arnaez[4], H. Arnold[115], G. Artoni[75a,75b], H. Asada[112], K. Asai[119], S. Asai[154], N.A. Asbah[36], K. Assamagan[29], R. Astalos[28a], K.S.V. Astrand[99], S. Atashi[160], R.J. Atkin[33a], M. Atkinson[163], H. Atmani[35f], P.A. Atmasiddha[129], K. Augsten[133], S. Auricchio[72a,72b], A.D. Auriol[20], V.A. Austrup[102], G. Avolio[36], K. Axiotis[56], G. Azuelos[109,af], D. Babal[28b], H. Bachacou[136], K. Bachas[153,p], A. Bachiu[34], F. Backman[47a,47b], A. Badea[39], T.M. Baer[107], P. Bagnaia[75a,75b], M. Bahmani[18], D. Bahner[54], K. Bai[124], A.J. Bailey[164], J.T. Baines[135], L. Baines[95], O.K. Baker[173], E. Bakos[15], D. Bakshi Gupta[8], V. Balakrishnan[121], R. Balasubramanian[115], E.M. Baldin[37], P. Balek[86a], E. Ballabene[23b,23a], F. Balli[136], L.M. Baltes[63a], W.K. Balunas[32], J. Balz[101], E. Banas[87], M. Bandieramonte[130], A. Bandyopadhyay[24], S. Bansal[24], L. Barak[152], M. Barakat[48], E.L. Barberio[106], D. Barberis[57b,57a], M. Barbero[103], M.Z. Barel[115], K.N. Barends[33a], T. Barillari[111], M-S. Barisits[36], T. Barklow[144], P. Baron[123], D.A. Baron Moreno[102], A. Baroncelli[62a], G. Barone[29], A.J. Barr[127], J.D. Barr[97], F. Barreiro[100], J. Barreiro Guimarães da Costa[14a], U. Barron[152], M.G. Barros Teixeira[131a], S. Barsov[37], F. Bartels[63a], R. Bartoldus[144], A.E. Barton[92], P. Bartos[28a], A. Basan[101], M. Baselga[49], A. Bassalat[66,b], M.J. Basso[157a], R.L. Bates[59], S. Batlamous[35e], B. Batool[142], M. Battaglia[137], D. Battulga[18], M. Bauce[75a,75b], M. Bauer[36], P. Bauer[24], L.T. Bazzano Hurrell[30], J.B. Beacham[51], T. Beau[128], J.Y. Beaucamp[91], P.H. Beauchemin[159], P. Bechtle[24], H.P. Beck[19,o],

JHEP10(2024)191

K. Becker[168], A.J. Beddall[82], V.A. Bednyakov[38], C.P. Bee[146], L.J. Beemster[15], T.A. Beermann[36], M. Begalli[83d], M. Begel[29], A. Behera[146], J.K. Behr[48], J.F. Beirer[36], F. Beisiegel[24], M. Belfkir[117b], G. Bella[152], L. Bellagamba[23b], A. Bellerive[34], P. Bellos[20], K. Beloborodov[37], D. Benchekroun[35a], F. Bendebba[35a], Y. Benhammou[152], K.C. Benkendorfer[61], L. Beresford[48], M. Beretta[53], E. Bergeaas Kuutmann[162], N. Berger[4], B. Bergmann[133], J. Beringer[17a], G. Bernardi[5], C. Bernius[144], F.U. Bernlochner[24], F. Bernon[36,103], A. Berrocal Guardia[13], T. Berry[96], P. Berta[134], A. Berthold[50], S. Bethke[111], A. Betti[75a,75b], A.J. Bevan[95], N.K. Bhalla[54], M. Bhamjee[33c], S. Bhatta[146], D.S. Bhattacharya[167], P. Bhattarai[144], K.D. Bhide[54], V.S. Bhopatkar[122], R.M. Bianchi[130], G. Bianco[23b,23a], O. Biebel[110], R. Bielski[124], M. Biglietti[77a], C.S. Billingsley[44], M. Bindi[55], A. Bingul[21b], C. Bini[75a,75b], A. Biondini[93], C.J. Birch-sykes[102], G.A. Bird[32], M. Birman[170], M. Biros[134], S. Biryukov[147], T. Bisanz[49], E. Bisceglie[43b,43a], J.P. Biswal[135], D. Biswas[142], K. Bjørke[126], I. Bloch[48], A. Blue[59], U. Blumenschein[95], J. Blumenthal[101], V.S. Bobrovnikov[37], M. Boehler[54], B. Boehm[167], D. Bogavac[36], A.G. Bogdanchikov[37], C. Bohm[47a], V. Boisvert[96], P. Bokan[36], T. Bold[86a], M. Bomben[5], M. Bona[95], M. Boonekamp[136], C.D. Booth[96], A.G. Borbély[59], I.S. Bordulev[37], H.M. Borecka-Bielska[109], G. Borissov[92], D. Bortoletto[127], D. Boscherini[23b], M. Bosman[13], J.D. Bossio Sola[36], K. Bouaouda[35a], N. Bouchhar[164], J. Boudreau[130], E.V. Bouhova-Thacker[92], D. Boumediene[40], R. Bouquet[57b,57a], A. Boveia[120], J. Boyd[36], D. Boye[29], I.R. Boyko[38], J. Bracinik[20], N. Brahimi[4], G. Brandt[172], O. Brandt[32], F. Braren[48], B. Brau[104], J.E. Brau[124], R. Brener[170], L. Brenner[115], R. Brenner[162], S. Bressler[170], D. Britton[59], D. Britzger[111], I. Brock[24], R. Brock[108], G. Brooijmans[41], E. Brost[29], L.M. Brown[166], L.E. Bruce[61], T.L. Bruckler[127], P.A. Bruckman de Renstrom[87], B. Brüers[48], A. Bruni[23b], G. Bruni[23b], M. Bruschi[23b], N. Bruscino[75a,75b], T. Buanes[16], Q. Buat[139], D. Buchin[111], A.G. Buckley[59], O. Bulekov[37], B.A. Bullard[144], S. Burdin[93], C.D. Burgard[49], A.M. Burger[36], B. Burghgrave[8], O. Burlayenko[54], J.T.P. Burr[32], C.D. Burton[11], J.C. Burzynski[143], E.L. Busch[41], V. Büscher[101], P.J. Bussey[59], J.M. Butler[25], C.M. Buttar[59], J.M. Butterworth[97], W. Buttinger[135], C.J. Buxo Vazquez[108], A.R. Buzykaev[37], S. Cabrera Urbán[164], L. Cadamuro[66], D. Caforio[58], H. Cai[130], Y. Cai[14a,14e], Y. Cai[14c], V.M.M. Cairo[36], O. Cakir[3a], N. Calace[36], P. Calafiura[17a], G. Calderini[128], P. Calfayan[68], G. Callea[59], L.P. Caloba[83b], D. Calvet[40], S. Calvet[40], M. Calvetti[74a,74b], R. Camacho Toro[128], S. Camarda[36], D. Camarero Munoz[26], P. Camarri[76a,76b], M.T. Camerlingo[72a,72b], D. Cameron[36], C. Camincher[166], M. Campanelli[97], A. Camplani[42], V. Canale[72a,72b], A.C. Canbay[3a], E. Canonero[96], J. Cantero[164], Y. Cao[163], F. Capocasa[26], M. Capua[43b,43a], A. Carbone[71a,71b], R. Cardarelli[76a], J.C.J. Cardenas[8], F. Cardillo[164], G. Carducci[43b,43a], T. Carli[36], G. Carlino[72a], J.I. Carlotto[13], B.T. Carlson[130,q], E.M. Carlson[166,157a], L. Carminati[71a,71b], A. Carnelli[136], M. Carnesale[75a,75b], S. Caron[114], E. Carquin[138f], S. Carrá[71a], G. Carratta[23b,23a], A.M. Carroll[124], T.M. Carter[52], M.P. Casado[13,i], M. Caspar[48], F.L. Castillo[4], L. Castillo Garcia[13], V. Castillo Gimenez[164], N.F. Castro[131a,131e], A. Catinaccio[36], J.R. Catmore[126], T. Cavaliere[4], V. Cavaliere[29], N. Cavalli[23b,23a], Y.C. Cekmecelioglu[48], E. Celebi[21a], S. Cella[36], F. Celli[127], M.S. Centonze[70a,70b], V. Cepaitis[56], K. Cerny[123], A.S. Cerqueira[83a], A. Cerri[147],

JHEP10(2024)191

L. Cerrito[76a,76b], F. Cerutti[17a], B. Cervato[142], A. Cervelli[23b], G. Cesarini[53], S.A. Cetin[82], D. Chakraborty[116], J. Chan[17a], W.Y. Chan[154], J.D. Chapman[32], E. Chapon[136], B. Chargeishvili[150b], D.G. Charlton[20], M. Chatterjee[19], C. Chauhan[134], Y. Che[14c], S. Chekanov[6], S.V. Chekulaev[157a], G.A. Chelkov[38,a], A. Chen[107], B. Chen[152], B. Chen[166], H. Chen[14c], H. Chen[29], J. Chen[62c], J. Chen[143], M. Chen[127], S. Chen[154], S.J. Chen[14c], X. Chen[62c,136], X. Chen[14b,ae], Y. Chen[62a], C.L. Cheng[171], H.C. Cheng[64a], S. Cheong[144], A. Cheplakov[38], E. Cheremushkina[48], E. Cherepanova[115], R. Cherkaoui El Moursli[35e], E. Cheu[7], K. Cheung[65], L. Chevalier[136], V. Chiarella[53], G. Chiarelli[74a], N. Chiedde[103], G. Chiodini[70a], A.S. Chisholm[20], A. Chitan[27b], M. Chitishvili[164], M.V. Chizhov[38,r], K. Choi[11], Y. Chou[139], E.Y.S. Chow[114], K.L. Chu[170], M.C. Chu[64a], X. Chu[14a,14e], J. Chudoba[132], J.J. Chwastowski[87], D. Cieri[111], K.M. Ciesla[86a], V. Cindro[94], A. Ciocio[17a], F. Cirotto[72a,72b], Z.H. Citron[170], M. Citterio[71a], D.A. Ciubotaru[27b], A. Clark[56], P.J. Clark[52], C. Clarry[156], J.M. Clavijo Columbie[48], S.E. Clawson[48], C. Clement[47a,47b], J. Clercx[48], Y. Coadou[103], M. Cobal[69a,69c], A. Coccaro[57b], R.F. Coelho Barrue[131a], R. Coelho Lopes De Sa[104], S. Coelli[71a], B. Cole[41], J. Collot[60], P. Conde Muiño[131a,131g], M.P. Connell[33c], S.H. Connell[33c], E.I. Conroy[127], F. Conventi[72a,ag], H.G. Cooke[20], A.M. Cooper-Sarkar[127], A. Cordeiro Oudot Choi[128], L.D. Corpe[40], M. Corradi[75a,75b], F. Corriveau[105,x], A. Cortes-Gonzalez[18], M.J. Costa[164], F. Costanza[4], D. Costanzo[140], B.M. Cote[120], G. Cowan[96], K. Cranmer[171], D. Cremonini[23b,23a], S. Crépé-Renaudin[60], F. Crescioli[128], M. Cristinziani[142], M. Cristoforetti[78a,78b], V. Croft[115], J.E. Crosby[122], G. Crosetti[43b,43a], A. Cueto[100], H. Cui[14a,14e], Z. Cui[7], W.R. Cunningham[59], F. Curcio[164], J.R. Curran[52], P. Czodrowski[36], M.M. Czurylo[36], M.J. Da Cunha Sargedas De Sousa[57b,57a], J.V. Da Fonseca Pinto[83b], C. Da Via[102], W. Dabrowski[86a], T. Dado[49], S. Dahbi[149], T. Dai[107], D. Dal Santo[19], C. Dallapiccola[104], M. Dam[42], G. D'amen[29], V. D'Amico[110], J. Damp[101], J.R. Dandoy[34], M. Danninger[143], V. Dao[36], G. Darbo[57b], S.J. Das[29,ah], F. Dattola[48], S. D'Auria[71a,71b], A. D'Avanzo[72a,72b], C. David[33a], T. Davidek[134], B. Davis-Purcell[34], I. Dawson[95], H.A. Day-hall[133], K. De[8], R. De Asmundis[72a], N. De Biase[48], S. De Castro[23b,23a], N. De Groot[114], P. de Jong[115], H. De la Torre[116], A. De Maria[14c], A. De Salvo[75a], U. De Sanctis[76a,76b], F. De Santis[70a,70b], A. De Santo[147], J.B. De Vivie De Regie[60], D.V. Dedovich[38], J. Degens[93], A.M. Deiana[44], F. Del Corso[23b,23a], J. Del Peso[100], F. Del Rio[63a], L. Delagrange[128], F. Deliot[136], C.M. Delitzsch[49], M. Della Pietra[72a,72b], D. Della Volpe[56], A. Dell'Acqua[36], L. Dell'Asta[71a,71b], M. Delmastro[4], P.A. Delsart[60], S. Demers[173], M. Demichev[38], S.P. Denisov[37], L. D'Eramo[40], D. Derendarz[87], F. Derue[128], P. Dervan[93], K. Desch[24], C. Deutsch[24], F.A. Di Bello[57b,57a], A. Di Ciaccio[76a,76b], L. Di Ciaccio[4], A. Di Domenico[75a,75b], C. Di Donato[72a,72b], A. Di Girolamo[36], G. Di Gregorio[36], A. Di Luca[78a,78b], B. Di Micco[77a,77b], R. Di Nardo[77a,77b], M. Diamantopoulou[34], F.A. Dias[115], T. Dias Do Vale[143], M.A. Diaz[138a,138b], F.G. Diaz Capriles[24], M. Didenko[164], E.B. Diehl[107], S. Díez Cornell[48], C. Diez Pardos[142], C. Dimitriadi[162,24], A. Dimitrievska[20], J. Dingfelder[24], I-M. Dinu[27b], S.J. Dittmeier[63b], F. Dittus[36], M. Divisek[134], F. Djama[103], T. Djobava[150b], C. Doglioni[102,99], A. Dohnalova[28a], J. Dolejsi[134], Z. Dolezal[134], K.M. Dona[39], M. Donadelli[83c], B. Dong[108], J. Donini[40], A. D'Onofrio[72a,72b],

JHEP10(2024)191

M. D'Onofrio[93], J. Dopke[135], A. Doria[72a], N. Dos Santos Fernandes[131a], P. Dougan[102], M.T. Dova[91], A.T. Doyle[59], M.A. Draguet[127], E. Dreyer[170], I. Drivas-koulouris[10], M. Drnevich[118], M. Drozdova[56], D. Du[62a], T.A. du Pree[115], F. Dubinin[37], M. Dubovsky[28a], E. Duchovni[170], G. Duckeck[110], O.A. Ducu[27b], D. Duda[52], A. Dudarev[36], E.R. Duden[26], M. D'uffizi[102], L. Duflot[66], M. Dührssen[36], I. Duminica[27g], A.E. Dumitriu[27b], M. Dunford[63a], S. Dungs[49], K. Dunne[47a,47b], A. Duperrin[103], H. Duran Yildiz[3a], M. Düren[58], A. Durglishvili[150b], B.L. Dwyer[116], G.I. Dyckes[17a], M. Dyndal[86a], B.S. Dziedzic[87], Z.O. Earnshaw[147], G.H. Eberwein[127], B. Eckerova[28a], S. Eggebrecht[55], E. Egidio Purcino De Souza[128], L.F. Ehrke[56], G. Eigen[16], K. Einsweiler[17a], T. Ekelof[162], P.A. Ekman[99], S. El Farkh[35b], Y. El Ghazali[35b], H. El Jarrari[36], A. El Moussaouy[109], V. Ellajosyula[162], M. Ellert[162], F. Ellinghaus[172], N. Ellis[36], J. Elmsheuser[29], M. Elsawy[117a], M. Elsing[36], D. Emeliyanov[135], Y. Enari[154], I. Ene[17a], S. Epari[13], P.A. Erland[87], M. Errenst[172], M. Escalier[66], C. Escobar[164], E. Etzion[152], G. Evans[131a], H. Evans[68], L.S. Evans[96], A. Ezhilov[37], S. Ezzarqtouni[35a], F. Fabbri[23b,23a], L. Fabbri[23b,23a], G. Facini[97], V. Fadeyev[137], R.M. Fakhrutdinov[37], D. Fakoudis[101], S. Falciano[75a], L.F. Falda Ulhoa Coelho[36], P.J. Falke[24], F. Fallavollita[111], J. Faltova[134], C. Fan[163], Y. Fan[14a], Y. Fang[14a,14e], M. Fanti[71a,71b], M. Faraj[69a,69b], Z. Farazpay[98], A. Farbin[8], A. Farilla[77a], T. Farooque[108], S.M. Farrington[52], F. Fassi[35e], D. Fassouliotis[9], M. Faucci Giannelli[76a,76b], W.J. Fawcett[32], L. Fayard[66], P. Federic[134], P. Federicova[132], O.L. Fedin[37,a], M. Feickert[171], L. Feligioni[103], D.E. Fellers[124], C. Feng[62b], M. Feng[14b], Z. Feng[115], M.J. Fenton[160], L. Ferencz[48], R.A.M. Ferguson[92], S.I. Fernandez Luengo[138f], P. Fernandez Martinez[13], M.J.V. Fernoux[103], J. Ferrando[92], A. Ferrari[162], P. Ferrari[115,114], R. Ferrari[73a], D. Ferrere[56], C. Ferretti[107], F. Fiedler[101], P. Fiedler[133], A. Filipčič[94], E.K. Filmer[1], F. Filthaut[114], M.C.N. Fiolhais[131a,131c,c], L. Fiorini[164], W.C. Fisher[108], T. Fitschen[102], P.M. Fitzhugh[136], I. Fleck[142], P. Fleischmann[107], T. Flick[172], M. Flores[33d,ac], L.R. Flores Castillo[64a], L. Flores Sanz De Acedo[36], F.M. Follega[78a,78b], N. Fomin[16], J.H. Foo[156], A. Formica[136], A.C. Forti[102], E. Fortin[36], A.W. Fortman[17a], M.G. Foti[17a], L. Fountas[9,j], D. Fournier[66], H. Fox[92], P. Francavilla[74a,74b], S. Francescato[61], S. Franchellucci[56], M. Franchini[23b,23a], S. Franchino[63a], D. Francis[36], L. Franco[114], V. Franco Lima[36], L. Franconi[48], M. Franklin[61], G. Frattari[26], W.S. Freund[83b], Y.Y. Frid[152], J. Friend[59], N. Fritzsche[50], A. Froch[54], D. Froidevaux[36], J.A. Frost[127], Y. Fu[62a], S. Fuenzalida Garrido[138f], M. Fujimoto[103], K.Y. Fung[64a], E. Furtado De Simas Filho[83e], M. Furukawa[154], J. Fuster[164], A. Gabrielli[23b,23a], A. Gabrielli[156], P. Gadow[36], G. Gagliardi[57b,57a], L.G. Gagnon[17a], S. Galantzan[152], E.J. Gallas[127], B.J. Gallop[135], K.K. Gan[120], S. Ganguly[154], Y. Gao[52], F.M. Garay Walls[138a,138b], B. Garcia[29], C. García[164], A. Garcia Alonso[115], A.G. Garcia Caffaro[173], J.E. García Navarro[164], M. Garcia-Sciveres[17a], G.L. Gardner[129], R.W. Gardner[39], N. Garelli[159], D. Garg[80], R.B. Garg[144,m], J.M. Gargan[52], C.A. Garner[156], C.M. Garvey[33a], P. Gaspar[83b], V.K. Gassmann[159], G. Gaudio[73a], V. Gautam[13], P. Gauzzi[75a,75b], I.L. Gavrilenko[37], A. Gavrilyuk[37], C. Gay[165], G. Gaycken[48], E.N. Gazis[10], A.A. Geanta[27b], C.M. Gee[137], A. Gekow[120], C. Gemme[57b], M.H. Genest[60], A.D. Gentry[113], S. George[96], W.F. George[20], T. Geralis[46], P. Gessinger-Befurt[36], M.E. Geyik[172], M. Ghani[168], K. Ghorbanian[95], A. Ghosal[142],

JHEP10(2024)191

A. Ghosh[160], A. Ghosh[7], B. Giacobbe[23b], S. Giagu[75a,75b], T. Giani[115], P. Giannetti[74a], A. Giannini[62a], S.M. Gibson[96], M. Gignac[137], D.T. Gil[86b], A.K. Gilbert[86a], B.J. Gilbert[41], D. Gillberg[34], G. Gilles[115], L. Ginabat[128], D.M. Gingrich[2,af], M.P. Giordani[69a,69c], P.F. Giraud[136], G. Giugliarelli[69a,69c], D. Giugni[71a], F. Giuli[36], I. Gkialas[9,j], L.K. Gladilin[37], C. Glasman[100], G.R. Gledhill[124], G. Glemža[48], M. Glisic[124], I. Gnesi[43b,f], Y. Go[29], M. Goblirsch-Kolb[36], B. Gocke[49], D. Godin[109], B. Gokturk[21a], S. Goldfarb[106], T. Golling[56], M.G.D. Gololo[33g], D. Golubkov[37], J.P. Gombas[108], A. Gomes[131a,131b], G. Gomes Da Silva[142], A.J. Gomez Delegido[164], R. Gonçalo[131a,131c], L. Gonella[20], A. Gongadze[150c], F. Gonnella[20], J.L. Gonski[144], R.Y. González Andana[52], S. González de la Hoz[164], R. Gonzalez Lopez[93], C. Gonzalez Renteria[17a], M.V. Gonzalez Rodrigues[48], R. Gonzalez Suarez[162], S. Gonzalez-Sevilla[56], L. Goossens[36], B. Gorini[36], E. Gorini[70a,70b], A. Gorišek[94], T.C. Gosart[129], A.T. Goshaw[51], M.I. Gostkin[38], S. Goswami[122], C.A. Gottardo[36], S.A. Gotz[110], M. Gouighri[35b], V. Goumarre[48], A.G. Goussiou[139], N. Govender[33c], I. Grabowska-Bold[86a], K. Graham[34], E. Gramstad[126], S. Grancagnolo[70a,70b], C.M. Grant[1,136], P.M. Gravila[27f], F.G. Gravili[70a,70b], H.M. Gray[17a], M. Greco[70a,70b], C. Grefe[24], I.M. Gregor[48], K.T. Greif[160], P. Grenier[144], S.G. Grewe[111], A.A. Grillo[137], K. Grimm[31], S. Grinstein[13,t], J.-F. Grivaz[66], E. Gross[170], J. Grosse-Knetter[55], J.C. Grundy[127], L. Guan[107], C. Gubbels[165], J.G.R. Guerrero Rojas[164], G. Guerrieri[69a,69c], F. Guescini[111], R. Gugel[101], J.A.M. Guhit[107], A. Guida[18], E. Guilloton[168], S. Guindon[36], F. Guo[14a,14e], J. Guo[62c], L. Guo[48], Y. Guo[107], R. Gupta[48], R. Gupta[130], S. Gurbuz[24], S.S. Gurdasani[54], G. Gustavino[36], M. Guth[56], P. Gutierrez[121], L.F. Gutierrez Zagazeta[129], M. Gutsche[50], C. Gutschow[97], C. Gwenlan[127], C.B. Gwilliam[93], E.S. Haaland[126], A. Haas[118], M. Habedank[48], C. Haber[17a], H.K. Hadavand[8], A. Hadef[50], S. Hadzic[111], A.I. Hagan[92], J.J. Hahn[142], E.H. Haines[97], M. Haleem[167], J. Haley[122], J.J. Hall[140], G.D. Hallewell[103], L. Halser[19], K. Hamano[166], M. Hamer[24], G.N. Hamity[52], E.J. Hampshire[96], J. Han[62b], K. Han[62a], L. Han[14c], L. Han[62a], S. Han[17a], Y.F. Han[156], K. Hanagaki[84], M. Hance[137], D.A. Hangal[41], H. Hanif[143], M.D. Hank[129], J.B. Hansen[42], P.H. Hansen[42], K. Hara[158], D. Harada[56], T. Harenberg[172], S. Harkusha[37], M.L. Harris[104], Y.T. Harris[127], J. Harrison[13], N.M. Harrison[120], P.F. Harrison[168], N.M. Hartman[111], N.M. Hartmann[110], Y. Hasegawa[141], S. Hassan[16], R. Hauser[108], C.M. Hawkes[20], R.J. Hawkings[36], Y. Hayashi[154], S. Hayashida[112], D. Hayden[108], C. Hayes[107], R.L. Hayes[115], C.P. Hays[127], J.M. Hays[95], H.S. Hayward[93], F. He[62a], M. He[14a,14e], Y. He[155], Y. He[48], Y. He[97], N.B. Heatley[95], V. Hedberg[99], A.L. Heggelund[126], N.D. Hehir[95,*], C. Heidegger[54], K.K. Heidegger[54], W.D. Heidorn[81], J. Heilman[34], S. Heim[48], T. Heim[17a], J.G. Heinlein[129], J.J. Heinrich[124], L. Heinrich[111,ad], J. Hejbal[132], A. Held[171], S. Hellesund[16], C.M. Helling[165], S. Hellman[47a,47b], R.C.W. Henderson[92], L. Henkelmann[32], A.M. Henriques Correia[36], H. Herde[99], Y. Hernández Jiménez[146], L.M. Herrmann[24], T. Herrmann[50], G. Herten[54], R. Hertenberger[110], L. Hervas[36], M.E. Hesping[101], N.P. Hessey[157a], E. Hill[156], S.J. Hillier[20], J.R. Hinds[108], F. Hinterkeuser[24], M. Hirose[125], S. Hirose[158], D. Hirschbuehl[172], T.G. Hitchings[102], B. Hiti[94], J. Hobbs[146], R. Hobincu[27e], N. Hod[170], M.C. Hodgkinson[140], B.H. Hodkinson[127], A. Hoecker[36], D.D. Hofer[107], J. Hofer[48], T. Holm[24], M. Holzbock[111],

JHEP10(2024)191

L.B.A.H. Hommels[32], B.P. Honan[102], J. Hong[62c], T.M. Hong[130], B.H. Hooberman[163], W.H. Hopkins[6], Y. Horii[112], S. Hou[149], A.S. Howard[94], J. Howarth[59], J. Hoya[6], M. Hrabovsky[123], A. Hrynevich[48], T. Hryn'ova[4], P.J. Hsu[65], S.-C. Hsu[139], M. Hu[17a], Q. Hu[62a], S. Huang[64b], X. Huang[14a,14e], Y. Huang[140], Y. Huang[14a], Z. Huang[102], Z. Hubacek[133], M. Huebner[24], F. Huegging[24], T.B. Huffman[127], C.A. Hugli[48], M. Huhtinen[36], S.K. Huiberts[16], R. Hulsken[105], N. Huseynov[12], J. Huston[108], J. Huth[61], R. Hyneman[144], G. Iacobucci[56], G. Iakovidis[29], I. Ibragimov[142], L. Iconomidou-Fayard[66], J.P. Iddon[36], P. Iengo[72a,72b], R. Iguchi[154], T. Iizawa[127], Y. Ikegami[84], N. Ilic[156], H. Imam[35a], M. Ince Lezki[56], T. Ingebretsen Carlson[47a,47b], G. Introzzi[73a,73b], M. Iodice[77a], V. Ippolito[75a,75b], R.K. Irwin[93], M. Ishino[154], W. Islam[171], C. Issever[18,48], S. Istin[21a,aj], H. Ito[169], R. Iuppa[78a,78b], A. Ivina[170], J.M. Izen[45], V. Izzo[72a], P. Jacka[132,133], P. Jackson[1], B.P. Jaeger[143], C.S. Jagfeld[110], G. Jain[157a], P. Jain[54], K. Jakobs[54], T. Jakoubek[170], J. Jamieson[59], K.W. Janas[86a], M. Javurkova[104], L. Jeanty[124], J. Jejelava[150a,aa], P. Jenni[54,g], C.E. Jessiman[34], C. Jia[62b], J. Jia[146], X. Jia[61], X. Jia[14a,14e], Z. Jia[14c], C. Jiang[52], S. Jiggins[48], J. Jimenez Pena[13], S. Jin[14c], A. Jinaru[27b], O. Jinnouchi[155], P. Johansson[140], K.A. Johns[7], J.W. Johnson[137], D.M. Jones[147], E. Jones[48], P. Jones[32], R.W.L. Jones[92], T.J. Jones[93], H.L. Joos[55,36], R. Joshi[120], J. Jovicevic[15], X. Ju[17a], J.J. Junggeburth[104], T. Junkermann[63a], A. Juste Rozas[13,t], M.K. Juzek[87], S. Kabana[138e], A. Kaczmarska[87], M. Kado[111], H. Kagan[120], M. Kagan[144], A. Kahn[41], A. Kahn[129], C. Kahra[101], T. Kaji[154], E. Kajomovitz[151], N. Kakati[170], I. Kalaitzidou[54], C.W. Kalderon[29], N.J. Kang[137], D. Kar[33g], K. Karava[127], M.J. Kareem[157b], E. Karentzos[54], I. Karkanias[153], O. Karkout[115], S.N. Karpov[38], Z.M. Karpova[38], V. Kartvelishvili[92], A.N. Karyukhin[37], E. Kasimi[153], J. Katzy[48], S. Kaur[34], K. Kawade[141], M.P. Kawale[121], C. Kawamoto[88], T. Kawamoto[62a], E.F. Kay[36], F.I. Kaya[159], S. Kazakos[108], V.F. Kazanin[37], Y. Ke[146], J.M. Keaveney[33a], R. Keeler[166], G.V. Kehris[61], J.S. Keller[34], A.S. Kelly[97], J.J. Kempster[147], P.D. Kennedy[101], O. Kepka[132], B.P. Kerridge[135], S. Kersten[172], B.P. Kerševan[94], L. Keszeghova[28a], S. Ketabchi Haghighat[156], R.A. Khan[130], A. Khanov[122], A.G. Kharlamov[37], T. Kharlamova[37], E.E. Khoda[139], M. Kholodenko[37], T.J. Khoo[18], G. Khoriauli[167], J. Khubua[150b,*], Y.A.R. Khwaira[66], B. Kibirige[33g], A. Kilgallon[124], D.W. Kim[47a,47b], Y.K. Kim[39], N. Kimura[97], M.K. Kingston[55], A. Kirchhoff[55], C. Kirfel[24], F. Kirfel[24], J. Kirk[135], A.E. Kiryunin[111], C. Kitsaki[10], O. Kivernyk[24], M. Klassen[159], C. Klein[34], L. Klein[167], M.H. Klein[44], S.B. Klein[56], U. Klein[93], P. Klimek[36], A. Klimentov[29], T. Klioutchnikova[36], P. Kluit[115], S. Kluth[111], E. Kneringer[79], T.M. Knight[156], A. Knue[49], R. Kobayashi[88], D. Kobylianskii[170], S.F. Koch[127], M. Kocian[144], P. Kodyš[134], D.M. Koeck[124], P.T. Koenig[24], T. Koffas[34], O. Kolay[50], I. Koletsou[4], T. Komarek[123], K. Köneke[54], A.X.Y. Kong[1], T. Kono[119], N. Konstantinidis[97], P. Kontaxakis[56], B. Konya[99], R. Kopeliansky[41], S. Koperny[86a], K. Korcyl[87], K. Kordas[153,e], A. Korn[97], S. Korn[55], I. Korolkov[13], N. Korotkova[37], B. Kortman[115], O. Kortner[111], S. Kortner[111], W.H. Kostecka[116], V.V. Kostyukhin[142], A. Kotsokechagia[136], A. Kotwal[51], A. Koulouris[36], A. Kourkoumeli-Charalampidi[73a,73b], C. Kourkoumelis[9], E. Kourlitis[111,ad], O. Kovanda[124], R. Kowalewski[166], W. Kozanecki[136], A.S. Kozhin[37], V.A. Kramarenko[37], G. Kramberger[94], P. Kramer[101], M.W. Krasny[128],

JHEP10(2024)191

A. Krasznahorkay[36], J.W. Kraus[172], J.A. Kremer[48], T. Kresse[50], J. Kretzschmar[93], K. Kreul[18], P. Krieger[156], S. Krishnamurthy[104], M. Krivos[134], K. Krizka[20], K. Kroeninger[49], H. Kroha[111], J. Kroll[132], J. Kroll[129], K.S. Krowpman[108], U. Kruchonak[38], H. Krüger[24], N. Krumnack[81], M.C. Kruse[51], O. Kuchinskaia[37], S. Kuday[3a], S. Kuehn[36], R. Kuesters[54], T. Kuhl[48], V. Kukhtin[38], Y. Kulchitsky[37,a], S. Kuleshov[138d,138b], M. Kumar[33g], N. Kumari[48], P. Kumari[157b], A. Kupco[132], T. Kupfer[49], A. Kupich[37], O. Kuprash[54], H. Kurashige[85], L.L. Kurchaninov[157a], O. Kurdysh[66], Y.A. Kurochkin[37], A. Kurova[37], M. Kuze[155], A.K. Kvam[104], J. Kvita[123], T. Kwan[105], N.G. Kyriacou[107], L.A.O. Laatu[103], C. Lacasta[164], F. Lacava[75a,75b], H. Lacker[18], D. Lacour[128], N.N. Lad[97], E. Ladygin[38], A. Lafarge[40], B. Laforge[128], T. Lagouri[173], F.Z. Lahbabi[35a], S. Lai[55], I.K. Lakomiec[86a], N. Lalloue[60], J.E. Lambert[166], S. Lammers[68], W. Lampl[7], C. Lampoudis[153,e], G. Lamprinoudis[101], A.N. Lancaster[116], E. Lançon[29], U. Landgraf[54], M.P.J. Landon[95], V.S. Lang[54], O.K.B. Langrekken[126], A.J. Lankford[160], F. Lanni[36], K. Lantzsch[24], A. Lanza[73a], A. Lapertosa[57b,57a], J.F. Laporte[136], T. Lari[71a], F. Lasagni Manghi[23b], M. Lassnig[36], V. Latonova[132], A. Laudrain[101], A. Laurier[151], S.D. Lawlor[140], Z. Lawrence[102], R. Lazaridou[168], M. Lazzaroni[71a,71b], B. Le[102], E.M. Le Boulicaut[51], L.T. Le Pottier[17a], B. Leban[23b,23a], A. Lebedev[81], M. LeBlanc[102], F. Ledroit-Guillon[60], A.C.A. Lee[97], S.C. Lee[149], S. Lee[47a,47b], T.F. Lee[93], L.L. Leeuw[33c], H.P. Lefebvre[96], M. Lefebvre[166], C. Leggett[17a], G. Lehmann Miotto[36], M. Leigh[56], W.A. Leight[104], W. Leinonen[114], A. Leisos[153,s], M.A.L. Leite[83c], C.E. Leitgeb[18], R. Leitner[134], K.J.C. Leney[44], T. Lenz[24], S. Leone[74a], C. Leonidopoulos[52], A. Leopold[145], C. Leroy[109], R. Les[108], C.G. Lester[32], M. Levchenko[37], J. Levêque[4], L.J. Levinson[170], G. Levrini[23b,23a], M.P. Lewicki[87], C. Lewis[139], D.J. Lewis[4], A. Li[5], B. Li[62b], C. Li[62a], C-Q. Li[111], H. Li[62a], H. Li[62b], H. Li[14c], H. Li[14b], H. Li[62b], J. Li[62c], K. Li[139], L. Li[62c], M. Li[14a,14e], Q.Y. Li[62a], S. Li[14a,14e], S. Li[62d,62c,d], T. Li[5], X. Li[105], Z. Li[127], Z. Li[154], Z. Li[14a,14e], S. Liang[14a,14e], Z. Liang[14a], M. Liberatore[136], B. Liberti[76a], K. Lie[64c], J. Lieber Marin[83e], H. Lien[68], K. Lin[108], R.E. Lindley[7], J.H. Lindon[2], E. Lipeles[129], A. Lipniacka[16], A. Lister[165], J.D. Little[4], B. Liu[14a], B.X. Liu[143], D. Liu[62d,62c], E.H.L. Liu[20], J.B. Liu[62a], J.K.K. Liu[32], K. Liu[62d], K. Liu[62d,62c], M. Liu[62a], M.Y. Liu[62a], P. Liu[14a], Q. Liu[62d,139,62c], X. Liu[62a], X. Liu[62b], Y. Liu[14d,14e], Y.L. Liu[62b], Y.W. Liu[62a], J. Llorente Merino[143], S.L. Lloyd[95], E.M. Lobodzinska[48], P. Loch[7], T. Lohse[18], K. Lohwasser[140], E. Loiacono[48], M. Lokajicek[132,*], J.D. Lomas[20], J.D. Long[163], I. Longarini[160], L. Longo[70a,70b], R. Longo[163], I. Lopez Paz[67], A. Lopez Solis[48], N. Lorenzo Martinez[4], A.M. Lory[110], G. Löschcke Centeno[147], O. Loseva[37], X. Lou[47a,47b], X. Lou[14a,14e], A. Lounis[66], P.A. Love[92], G. Lu[14a,14e], M. Lu[66], S. Lu[129], Y.J. Lu[65], H.J. Lubatti[139], C. Luci[75a,75b], F.L. Lucio Alves[14c], F. Luehring[68], I. Luise[146], O. Lukianchuk[66], O. Lundberg[145], B. Lund-Jensen[145,*], N.A. Luongo[6], M.S. Lutz[36], A.B. Lux[25], D. Lynn[29], R. Lysak[132], E. Lytken[99], V. Lyubushkin[38], T. Lyubushkina[38], M.M. Lyukova[146], M.Firdaus M. Soberi[52], H. Ma[29], K. Ma[62a], L.L. Ma[62b], W. Ma[62a], Y. Ma[122], D.M. Mac Donell[166], G. Maccarrone[53], J.C. MacDonald[101], P.C. Machado De Abreu Farias[83e], R. Madar[40], T. Madula[97], J. Maeda[85], T. Maeno[29], H. Maguire[140], V. Maiboroda[136], A. Maio[131a,131b,131d],

JHEP10(2024)191

K. Maj[86a], O. Majersky[48], S. Majewski[124], N. Makovec[66], V. Maksimovic[15], B. Malaescu[128], Pa. Malecki[87], V.P. Maleev[37], F. Malek[60,n], M. Mali[94], D. Malito[96], U. Mallik[80,*], S. Maltezos[10], S. Malyukov[38], J. Mamuzic[13], G. Mancini[53], M.N. Mancini[26], G. Manco[73a,73b], J.P. Mandalia[95], I. Mandić[94], L. Manhaes de Andrade Filho[83a], I.M. Maniatis[170], J. Manjarres Ramos[90], D.C. Mankad[170], A. Mann[110], S. Manzoni[36], L. Mao[62c], X. Mapekula[33c], A. Marantis[153,s], G. Marchiori[5], M. Marcisovsky[132], C. Marcon[71a], M. Marinescu[20], S. Marium[48], M. Marjanovic[121], M. Markovitch[66], E.J. Marshall[92], Z. Marshall[17a], S. Marti-Garcia[164], T.A. Martin[168], V.J. Martin[52], B. Martin dit Latour[16], L. Martinelli[75a,75b], M. Martinez[13,t], P. Martinez Agullo[164], V.I. Martinez Outschoorn[104], P. Martinez Suarez[13], S. Martin-Haugh[135], G. Martinovicova[134], V.S. Martoiu[27b], A.C. Martyniuk[97], A. Marzin[36], D. Mascione[78a,78b], L. Masetti[101], T. Mashimo[154], J. Masik[102], A.L. Maslennikov[37], P. Massarotti[72a,72b], P. Mastrandrea[74a,74b], A. Mastroberardino[43b,43a], T. Masubuchi[154], T. Mathisen[162], J. Matousek[134], N. Matsuzawa[154], J. Maurer[27b], A.J. Maury[66], B. Maček[94], D.A. Maximov[37], A.E. May[102], R. Mazini[149], I. Maznas[116], M. Mazza[108], S.M. Mazza[137], E. Mazzeo[71a,71b], C. Mc Ginn[29], J.P. Mc Gowan[166], S.P. Mc Kee[107], C.C. McCracken[165], E.F. McDonald[106], A.E. McDougall[115], J.A. Mcfayden[147], R.P. McGovern[129], G. Mchedlidze[150b], R.P. Mckenzie[33g], T.C. Mclachlan[48], D.J. Mclaughlin[97], S.J. McMahon[135], C.M. Mcpartland[93], R.A. McPherson[166,x], S. Mehlhase[110], A. Mehta[93], D. Melini[164], B.R. Mellado Garcia[33g], A.H. Melo[55], F. Meloni[48], A.M. Mendes Jacques Da Costa[102], H.Y. Meng[156], L. Meng[92], S. Menke[111], M. Mentink[36], E. Meoni[43b,43a], G. Mercado[116], C. Merlassino[69a,69c], L. Merola[72a,72b], C. Meroni[71a,71b], J. Metcalfe[6], A.S. Mete[6], C. Meyer[68], J-P. Meyer[136], R.P. Middleton[135], L. Mijović[52], G. Mikenberg[170], M. Mikestikova[132], M. Mikuž[94], H. Mildner[101], A. Milic[36], D.W. Miller[39], E.H. Miller[144], L.S. Miller[34], A. Milov[170], D.A. Milstead[47a,47b], T. Min[14c], A.A. Minaenko[37], I.A. Minashvili[150b], L. Mince[59], A.I. Mincer[118], B. Mindur[86a], M. Mineev[38], Y. Mino[88], L.M. Mir[13], M. Miralles Lopez[59], M. Mironova[17a], A. Mishima[154], M.C. Missio[114], A. Mitra[168], V.A. Mitsou[164], Y. Mitsumori[112], O. Miu[156], P.S. Miyagawa[95], T. Mkrtchyan[63a], M. Mlinarevic[97], T. Mlinarevic[97], M. Mlynarikova[36], S. Mobius[19], P. Mogg[110], M.H. Mohamed Farook[113], A.F. Mohammed[14a,14e], S. Mohapatra[41], G. Mokgatitswane[33g], L. Moleri[170], B. Mondal[142], S. Mondal[133], K. Mönig[48], E. Monnier[103], L. Monsonis Romero[164], J. Montejo Berlingen[13], M. Montella[120], F. Montereali[77a,77b], F. Monticelli[91], S. Monzani[69a,69c], N. Morange[66], A.L. Moreira De Carvalho[48], M. Moreno Llácer[164], C. Moreno Martinez[56], P. Morettini[57b], S. Morgenstern[36], M. Morii[61], M. Morinaga[154], F. Morodei[75a,75b], L. Morvaj[36], P. Moschovakos[36], B. Moser[36], M. Mosidze[150b], T. Moskalets[54], P. Moskvitina[114], J. Moss[31,k], A. Moussa[35d], E.J.W. Moyse[104], O. Mtintsilana[33g], S. Muanza[103], J. Mueller[130], D. Muenstermann[92], R. Müller[19], G.A. Mullier[162], A.J. Mullin[32], J.J. Mullin[129], D.P. Mungo[156], D. Munoz Perez[164], F.J. Munoz Sanchez[102], M. Murin[102], W.J. Murray[168,135], M. Muškinja[94], C. Mwewa[29], A.G. Myagkov[37,a], A.J. Myers[8], G. Myers[107], M. Myska[133], B.P. Nachman[17a], O. Nackenhorst[49], K. Nagai[127], K. Nagano[84], J.L. Nagle[29,ah], E. Nagy[103], A.M. Nairz[36], Y. Nakahama[84], K. Nakamura[84], K. Nakkalil[5], H. Nanjo[125], R. Narayan[44],

JHEP10(2024)191

E.A. Narayanan[113], I. Naryshkin[37], M. Naseri[34], S. Nasri[117b], C. Nass[24], G. Navarro[22a], J. Navarro-Gonzalez[164], R. Nayak[152], A. Nayaz[18], P.Y. Nechaeva[37], F. Nechansky[48], L. Nedic[127], T.J. Neep[20], A. Negri[73a,73b], M. Negrini[23b], C. Nellist[115], C. Nelson[105], K. Nelson[107], S. Nemecek[132], M. Nessi[36,h], M.S. Neubauer[163], F. Neuhaus[101], J. Neundorf[48], R. Newhouse[165], P.R. Newman[20], C.W. Ng[130], Y.W.Y. Ng[48], B. Ngair[117a], H.D.N. Nguyen[109], R.B. Nickerson[127], R. Nicolaidou[136], J. Nielsen[137], M. Niemeyer[55], J. Niermann[55], N. Nikiforou[36], V. Nikolaenko[37,a], I. Nikolic-Audit[128], K. Nikolopoulos[20], P. Nilsson[29], I. Ninca[48], H.R. Nindhito[56], G. Ninio[152], A. Nisati[75a], N. Nishu[2], R. Nisius[111], J-E. Nitschke[50], E.K. Nkadimeng[33g], T. Nobe[154], D.L. Noel[32], T. Nommensen[148], M.B. Norfolk[140], R.R.B. Norisam[97], B.J. Norman[34], M. Noury[35a], J. Novak[94], T. Novak[48], L. Novotny[133], R. Novotny[113], L. Nozka[123], K. Ntekas[160], N.M.J. Nunes De Moura Junior[83b], J. Ocariz[128], A. Ochi[85], I. Ochoa[131a], S. Oerdek[48,u], J.T. Offermann[39], A. Ogrodnik[134], A. Oh[102], C.C. Ohm[145], H. Oide[84], R. Oishi[154], M.L. Ojeda[48], Y. Okumura[154], L.F. Oleiro Seabra[131a], S.A. Olivares Pino[138d], G. Oliveira Correa[13], D. Oliveira Damazio[29], D. Oliveira Goncalves[83a], J.L. Oliver[160], Ö.O. Öncel[54], A.P. O'Neill[19], A. Onofre[131a,131e], P.U.E. Onyisi[11], M.J. Oreglia[39], G.E. Orellana[91], D. Orestano[77a,77b], N. Orlando[13], R.S. Orr[156], V. O'Shea[59], L.M. Osojnak[129], R. Ospanov[62a], G. Otero y Garzon[30], H. Otono[89], P.S. Ott[63a], G.J. Ottino[17a], M. Ouchrif[35d], F. Ould-Saada[126], T. Ovsiannikova[139], M. Owen[59], R.E. Owen[135], K.Y. Oyulmaz[21a], V.E. Ozcan[21a], F. Ozturk[87], N. Ozturk[8], S. Ozturk[82], H.A. Pacey[127], A. Pacheco Pages[13], C. Padilla Aranda[13], G. Padovano[75a,75b], S. Pagan Griso[17a], G. Palacino[68], A. Palazzo[70a,70b], J. Pampel[24], J. Pan[173], T. Pan[64a], D.K. Panchal[11], C.E. Pandini[115], J.G. Panduro Vazquez[96], H.D. Pandya[1], H. Pang[14b], P. Pani[48], G. Panizzo[69a,69c], L. Panwar[128], L. Paolozzi[56], S. Parajuli[163], A. Paramonov[6], C. Paraskevopoulos[53], D. Paredes Hernandez[64b], A. Pareti[73a,73b], K.R. Park[41], T.H. Park[156], M.A. Parker[32], F. Parodi[57b,57a], E.W. Parrish[116], V.A. Parrish[52], J.A. Parsons[41], U. Parzefall[54], B. Pascual Dias[109], L. Pascual Dominguez[152], E. Pasqualucci[75a], S. Passaggio[57b], F. Pastore[96], P. Patel[87], U.M. Patel[51], J.R. Pater[102], T. Pauly[36], C.I. Pazos[159], J. Pearkes[144], M. Pedersen[126], R. Pedro[131a], S.V. Peleganchuk[37], O. Penc[36], E.A. Pender[52], G.D. Penn[173], K.E. Penski[110], M. Penzin[37], B.S. Peralva[83d], A.P. Pereira Peixoto[139], L. Pereira Sanchez[144], D.V. Perepelitsa[29,ah], E. Perez Codina[157a], M. Perganti[10], H. Pernegger[36], O. Perrin[40], K. Peters[48], R.F.Y. Peters[102], B.A. Petersen[36], T.C. Petersen[42], E. Petit[103], V. Petousis[133], C. Petridou[153,e], T. Petru[134], A. Petrukhin[142], M. Pettee[17a], N.E. Pettersson[36], A. Petukhov[37], K. Petukhova[134], R. Pezoa[138f], L. Pezzotti[36], G. Pezzullo[173], T.M. Pham[171], T. Pham[106], P.W. Phillips[135], G. Piacquadio[146], E. Pianori[17a], F. Piazza[124], R. Piegaia[30], D. Pietreanu[27b], A.D. Pilkington[102], M. Pinamonti[69a,69c], J.L. Pinfold[2], B.C. Pinheiro Pereira[131a], A.E. Pinto Pinoargote[101,136], L. Pintucci[69a,69c], K.M. Piper[147], A. Pirttikoski[56], D.A. Pizzi[34], L. Pizzimento[64b], A. Pizzini[115], M.-A. Pleier[29], V. Plesanovs[54], V. Pleskot[134], E. Plotnikova[38], G. Poddar[95], R. Poettgen[99], L. Poggioli[128], I. Pokharel[55], S. Polacek[134], G. Polesello[73a], A. Poley[143,157a], A. Polini[23b], C.S. Pollard[168], Z.B. Pollock[120], E. Pompa Pacchi[75a,75b], D. Ponomarenko[114], L. Pontecorvo[36], S. Popa[27a], G.A. Popeneciu[27d], A. Poreba[36],

JHEP10(2024)191

D.M. Portillo Quintero[157a], S. Pospisil[133], M.A. Postill[140], P. Postolache[27c], K. Potamianos[168], P.A. Potepa[86a], I.N. Potrap[38], C.J. Potter[32], H. Potti[1], J. Poveda[164], M.E. Pozo Astigarraga[36], A. Prades Ibanez[164], J. Pretel[54], D. Price[102], M. Primavera[70a], M.A. Principe Martin[100], R. Privara[123], T. Procter[59], M.L. Proffitt[139], N. Proklova[129], K. Prokofiev[64c], G. Proto[111], J. Proudfoot[6], M. Przybycien[86a], W.W. Przygoda[86b], A. Psallidas[46], J.E. Puddefoot[140], D. Pudzha[37], D. Pyatiizbyantseva[37], J. Qian[107], D. Qichen[102], Y. Qin[13], T. Qiu[52], A. Quadt[55], M. Queitsch-Maitland[102], G. Quetant[56], R.P. Quinn[165], G. Rabanal Bolanos[61], D. Rafanoharana[54], F. Ragusa[71a,71b], J.L. Rainbolt[39], J.A. Raine[56], S. Rajagopalan[29], E. Ramakoti[37], I.A. Ramirez-Berend[34], K. Ran[48,14e], N.P. Rapheeha[33g], H. Rasheed[27b], V. Raskina[128], D.F. Rassloff[63a], A. Rastogi[17a], S. Rave[101], B. Ravina[55], I. Ravinovich[170], M. Raymond[36], A.L. Read[126], N.P. Readioff[140], D.M. Rebuzzi[73a,73b], G. Redlinger[29], A.S. Reed[111], K. Reeves[26], J.A. Reidelsturz[172], D. Reikher[152], A. Rej[49], C. Rembser[36], M. Renda[27b], M.B. Rendel[111], F. Renner[48], A.G. Rennie[160], A.L. Rescia[48], S. Resconi[71a], M. Ressegotti[57b,57a], S. Rettie[36], J.G. Reyes Rivera[108], E. Reynolds[17a], O.L. Rezanova[37], P. Reznicek[134], H. Riani[35d], N. Ribaric[92], E. Ricci[78a,78b], R. Richter[111], S. Richter[47a,47b], E. Richter-Was[86b], M. Ridel[128], S. Ridouani[35d], P. Rieck[118], P. Riedler[36], E.M. Riefel[47a,47b], J.O. Rieger[115], M. Rijssenbeek[146], M. Rimoldi[36], L. Rinaldi[23b,23a], T.T. Rinn[29], M.P. Rinnagel[110], G. Ripellino[162], I. Riu[13], J.C. Rivera Vergara[166], F. Rizatdinova[122], E. Rizvi[95], B.R. Roberts[17a], S.H. Robertson[105,x], D. Robinson[32], C.M. Robles Gajardo[138f], M. Robles Manzano[101], A. Robson[59], A. Rocchi[76a,76b], C. Roda[74a,74b], S. Rodriguez Bosca[36], Y. Rodriguez Garcia[22a], A. Rodriguez Rodriguez[54], A.M. Rodríguez Vera[116], S. Roe[36], J.T. Roemer[160], A.R. Roepe-Gier[137], J. Roggel[172], O. Røhne[126], R.A. Rojas[104], C.P.A. Roland[128], J. Roloff[29], A. Romaniouk[37], E. Romano[73a,73b], M. Romano[23b], A.C. Romero Hernandez[163], N. Rompotis[93], L. Roos[128], S. Rosati[75a], B.J. Rosser[39], E. Rossi[127], E. Rossi[72a,72b], L.P. Rossi[61], L. Rossini[54], R. Rosten[120], M. Rotaru[27b], B. Rottler[54], C. Rougier[90], D. Rousseau[66], D. Rousso[32], A. Roy[163], S. Roy-Garand[156], A. Rozanov[103], Z.M.A. Rozario[59], Y. Rozen[151], A. Rubio Jimenez[164], A.J. Ruby[93], V.H. Ruelas Rivera[18], T.A. Ruggeri[1], A. Ruggiero[127], A. Ruiz-Martinez[164], A. Rummler[36], Z. Rurikova[54], N.A. Rusakovich[38], H.L. Russell[166], G. Russo[75a,75b], J.P. Rutherfoord[7], S. Rutherford Colmenares[32], K. Rybacki[92], M. Rybar[134], E.B. Rye[126], A. Ryzhov[44], J.A. Sabater Iglesias[56], P. Sabatini[164], H.F-W. Sadrozinski[137], F. Safai Tehrani[75a], B. Safarzadeh Samani[135], S. Saha[1], M. Sahinsoy[111], A. Saibel[164], M. Saimpert[136], M. Saito[154], T. Saito[154], A. Sala[71a,71b], D. Salamani[36], A. Salnikov[144], J. Salt[164], A. Salvador Salas[152], D. Salvatore[43b,43a], F. Salvatore[147], A. Salzburger[36], D. Sammel[54], E. Sampson[92], D. Sampsonidis[153,e], D. Sampsonidou[124], J. Sánchez[164], V. Sanchez Sebastian[164], H. Sandaker[126], C.O. Sander[48], J.A. Sandesara[104], M. Sandhoff[172], C. Sandoval[22b], D.P.C. Sankey[135], T. Sano[88], A. Sansoni[53], L. Santi[75a,75b], C. Santoni[40], H. Santos[131a,131b], A. Santra[170], K.A. Saoucha[161], J.G. Saraiva[131a,131d], J. Sardain[7], O. Sasaki[84], K. Sato[158], C. Sauer[63b], F. Sauerburger[54], E. Sauvan[4], P. Savard[156,af], R. Sawada[154], C. Sawyer[135], L. Sawyer[98], I. Sayago Galvan[164], C. Sbarra[23b], A. Sbrizzi[23b,23a], T. Scanlon[97], J. Schaarschmidt[139], U. Schäfer[101], A.C. Schaffer[66,44], D. Schaile[110], R.D. Schamberger[146], C. Scharf[18],

JHEP10(2024)191

M.M. Schefer[19], V.A. Schegelsky[37], D. Scheirich[134], F. Schenck[18], M. Schernau[160], C. Scheulen[55], C. Schiavi[57b,57a], M. Schioppa[43b,43a], B. Schlag[144,m], K.E. Schleicher[54], S. Schlenker[36], J. Schmeing[172], M.A. Schmidt[172], K. Schmieden[101], C. Schmitt[101], N. Schmitt[101], S. Schmitt[48], L. Schoeffel[136], A. Schoening[63b], P.G. Scholer[34], E. Schopf[127], M. Schott[101], J. Schovancova[36], S. Schramm[56], T. Schroer[56], H-C. Schultz-Coulon[63a], M. Schumacher[54], B.A. Schumm[137], Ph. Schune[136], A.J. Schuy[139], H.R. Schwartz[137], A. Schwartzman[144], T.A. Schwarz[107], Ph. Schwemling[136], R. Schwienhorst[108], A. Sciandra[29], G. Sciolla[26], F. Scuri[74a], C.D. Sebastiani[93], K. Sedlaczek[116], P. Seema[18], S.C. Seidel[113], A. Seiden[137], B.D. Seidlitz[41], C. Seitz[48], J.M. Seixas[83b], G. Sekhniaidze[72a], L. Selem[60], N. Semprini-Cesari[23b,23a], D. Sengupta[56], V. Senthilkumar[164], L. Serin[66], L. Serkin[69a,69b], M. Sessa[76a,76b], H. Severini[121], F. Sforza[57b,57a], A. Sfyrla[56], Q. Sha[14a], E. Shabalina[55], A.H. Shah[32], R. Shaheen[145], J.D. Shahinian[129], D. Shaked Renous[170], L.Y. Shan[14a], M. Shapiro[17a], A. Sharma[36], A.S. Sharma[165], P. Sharma[80], P.B. Shatalov[37], K. Shaw[147], S.M. Shaw[102], A. Shcherbakova[37], Q. Shen[62c,5], D.J. Sheppard[143], P. Sherwood[97], L. Shi[97], X. Shi[14a], C.O. Shimmin[173], J.D. Shinner[96], I.P.J. Shipsey[127], S. Shirabe[89], M. Shiyakova[38,v], J. Shlomi[170], M.J. Shochet[39], J. Shojaii[106], D.R. Shope[126], B. Shrestha[121], S. Shrestha[120,ai], E.M. Shrif[33g], M.J. Shroff[166], P. Sicho[132], A.M. Sickles[163], E. Sideras Haddad[33g], A.C. Sidley[115], A. Sidoti[23b], F. Siegert[50], Dj. Sijacki[15], F. Sili[91], J.M. Silva[52], M.V. Silva Oliveira[29], S.B. Silverstein[47a], S. Simion[66], R. Simoniello[36], E.L. Simpson[102], H. Simpson[147], L.R. Simpson[107], N.D. Simpson[99], S. Simsek[82], S. Sindhu[55], P. Sinervo[156], S. Singh[156], S. Sinha[48], S. Sinha[102], M. Sioli[23b,23a], I. Siral[36], E. Sitnikova[48], J. Sjölin[47a,47b], A. Skaf[55], E. Skorda[20], P. Skubic[121], M. Slawinska[87], V. Smakhtin[170], B.H. Smart[135], S.Yu. Smirnov[37], Y. Smirnov[37], L.N. Smirnova[37,a], O. Smirnova[99], A.C. Smith[41], D.R. Smith[160], E.A. Smith[39], H.A. Smith[127], J.L. Smith[102], R. Smith[144], M. Smizanska[92], K. Smolek[133], A.A. Snesarev[37], S.R. Snider[156], H.L. Snoek[115], S. Snyder[29], R. Sobie[166,x], A. Soffer[152], C.A. Solans Sanchez[36], E.Yu. Soldatov[37], U. Soldevila[164], A.A. Solodkov[37], S. Solomon[26], A. Soloshenko[38], K. Solovieva[54], O.V. Solovyanov[40], V. Solovyev[37], P. Sommer[36], A. Sonay[13], W.Y. Song[157b], A. Sopczak[133], A.L. Sopio[97], F. Sopkova[28b], J.D. Sorenson[113], I.R. Sotarriva Alvarez[155], V. Sothilingam[63a], O.J. Soto Sandoval[138c,138b], S. Sottocornola[68], R. Soualah[161], Z. Soumaimi[35e], D. South[48], N. Soybelman[170], S. Spagnolo[70a,70b], M. Spalla[111], D. Sperlich[54], G. Spigo[36], S. Spinali[92], D.P. Spiteri[59], M. Spousta[134], E.J. Staats[34], R. Stamen[63a], A. Stampekis[20], M. Standke[24], E. Stanecka[87], W. Stanek-Maslouska[48], M.V. Stange[50], B. Stanislaus[17a], M.M. Stanitzki[48], B. Stapf[48], E.A. Starchenko[37], G.H. Stark[137], J. Stark[90], P. Staroba[132], P. Starovoitov[63a], S. Stärz[105], R. Staszewski[87], G. Stavropoulos[46], J. Steentoft[162], P. Steinberg[29], B. Stelzer[143,157a], H.J. Stelzer[130], O. Stelzer-Chilton[157a], H. Stenzel[58], T.J. Stevenson[147], G.A. Stewart[36], J.R. Stewart[122], M.C. Stockton[36], G. Stoicea[27b], M. Stolarski[131a], S. Stonjek[111], A. Straessner[50], J. Strandberg[145], S. Strandberg[47a,47b], M. Stratmann[172], M. Strauss[121], T. Strebler[103], P. Strizenec[28b], R. Ströhmer[167], D.M. Strom[124], R. Stroynowski[44], A. Strubig[47a,47b], S.A. Stucci[29], B. Stugu[16], J. Stupak[121], N.A. Styles[48], D. Su[144], S. Su[62a], W. Su[62d], X. Su[62a], D. Suchy[28a],

JHEP10(2024)191

K. Sugizaki[154], V.V. Sulin[37], M.J. Sullivan[93], D.M.S. Sultan[127], L. Sultanaliyeva[37], S. Sultansoy[3b], T. Sumida[88], S. Sun[107], S. Sun[171], O. Sunneborn Gudnadottir[162], N. Sur[103], M.R. Sutton[147], H. Suzuki[158], M. Svatos[132], M. Swiatlowski[157a], T. Swirski[167], I. Sykora[28a], M. Sykora[134], T. Sykora[134], D. Ta[101], K. Tackmann[48,u], A. Taffard[160], R. Tafirout[157a], J.S. Tafoya Vargas[66], Y. Takubo[84], M. Talby[103], A.A. Talyshev[37], K.C. Tam[64b], N.M. Tamir[152], A. Tanaka[154], J. Tanaka[154], R. Tanaka[66], M. Tanasini[57b,57a], Z. Tao[165], S. Tapia Araya[138f], S. Tapprogge[101], A. Tarek Abouelfadl Mohamed[108], S. Tarem[151], K. Tariq[14a], G. Tarna[27b], G.F. Tartarelli[71a], M.J. Tartarin[90], P. Tas[134], M. Tasevsky[132], E. Tassi[43b,43a], A.C. Tate[163], G. Tateno[154], Y. Tayalati[35e,w], G.N. Taylor[106], W. Taylor[157b], A.S. Tee[171], R. Teixeira De Lima[144], P. Teixeira-Dias[96], J.J. Teoh[156], K. Terashi[154], J. Terron[100], S. Terzo[13], M. Testa[53], R.J. Teuscher[156,x], A. Thaler[79], O. Theiner[56], N. Themistokleous[52], T. Theveneaux-Pelzer[103], O. Thielmann[172], D.W. Thomas[96], J.P. Thomas[20], E.A. Thompson[17a], P.D. Thompson[20], E. Thomson[129], R.E. Thornberry[44], Y. Tian[55], V. Tikhomirov[37,a], Yu.A. Tikhonov[37], S. Timoshenko[37], D. Timoshyn[134], E.X.L. Ting[1], P. Tipton[173], S.H. Tlou[33g], K. Todome[155], S. Todorova-Nova[134], S. Todt[50], M. Togawa[84], J. Tojo[89], S. Tokár[28a], K. Tokushuku[84], O. Toldaiev[68], R. Tombs[32], M. Tomoto[84,112], L. Tompkins[144,m], K.W. Topolnicki[86b], E. Torrence[124], H. Torres[90], E. Torró Pastor[164], M. Toscani[30], C. Tosciri[39], M. Tost[11], D.R. Tovey[140], A. Traeet[16], I.S. Trandafir[27b], T. Trefzger[167], A. Tricoli[29], I.M. Trigger[157a], S. Trincaz-Duvoid[128], D.A. Trischuk[26], B. Trocmé[60], L. Truong[33c], M. Trzebinski[87], A. Trzupek[87], F. Tsai[146], M. Tsai[107], A. Tsiamis[153,e], P.V. Tsiareshka[37], S. Tsigaridas[157a], A. Tsirigotis[153,s], V. Tsiskaridze[156], E.G. Tskhadadze[150a], M. Tsopoulou[153], Y. Tsujikawa[88], I.I. Tsukerman[37], V. Tsulaia[17a], S. Tsuno[84], K. Tsuri[119], D. Tsybychev[146], Y. Tu[64b], A. Tudorache[27b], V. Tudorache[27b], A.N. Tuna[61], S. Turchikhin[57b,57a], I. Turk Cakir[3a], R. Turra[71a], T. Turtuvshin[38,y], P.M. Tuts[41], S. Tzamarias[153,e], E. Tzovara[101], F. Ukegawa[158], P.A. Ulloa Poblete[138c,138b], E.N. Umaka[29], G. Unal[36], A. Undrus[29], G. Unel[160], J. Urban[28b], P. Urquijo[106], P. Urrejola[138a], G. Usai[8], R. Ushioda[155], M. Usman[109], Z. Uysal[82], V. Vacek[133], B. Vachon[105], K.O.H. Vadla[126], T. Vafeiadis[36], A. Vaitkus[97], C. Valderanis[110], E. Valdes Santurio[47a,47b], M. Valente[157a], S. Valentinetti[23b,23a], A. Valero[164], E. Valiente Moreno[164], A. Vallier[90], J.A. Valls Ferrer[164], D.R. Van Arneman[115], T.R. Van Daalen[139], A. Van Der Graaf[49], P. Van Gemmeren[6], M. Van Rijnbach[126], S. Van Stroud[97], I. Van Vulpen[115], P. Vana[134], M. Vanadia[76a,76b], W. Vandelli[36], E.R. Vandewall[122], D. Vannicola[152], L. Vannoli[53], R. Vari[75a], E.W. Varnes[7], C. Varni[17b], T. Varol[149], D. Varouchas[66], L. Varriale[164], K.E. Varvell[148], M.E. Vasile[27b], L. Vaslin[84], G.A. Vasquez[166], A. Vasyukov[38], R. Vavricka[101], F. Vazeille[40], T. Vazquez Schroeder[36], J. Veatch[31], V. Vecchio[102], M.J. Veen[104], I. Veliscek[29], L.M. Veloce[156], F. Veloso[131a,131c], S. Veneziano[75a], A. Ventura[70a,70b], S. Ventura Gonzalez[136], A. Verbytskyi[111], M. Verducci[74a,74b], C. Vergis[95], M. Verissimo De Araujo[83b], W. Verkerke[115], J.C. Vermeulen[115], C. Vernieri[144], M. Vessella[104], M.C. Vetterli[143,af], A. Vgenopoulos[153,e], N. Viaux Maira[138f], T. Vickey[140], O.E. Vickey Boeriu[140], G.H.A. Viehhauser[127], L. Vigani[63b], M. Villa[23b,23a], M. Villaplana Perez[164], E.M. Villhauer[52], E. Vilucchi[53], M.G. Vincter[34], G.S. Virdee[20],

JHEP10(2024)191

A. Vishwakarma[52], A. Visibile[115], C. Vittori[36], I. Vivarelli[23b,23a], E. Voevodina[111], F. Vogel[110], J.C. Voigt[50], P. Vokac[133], Yu. Volkotrub[86b], J. Von Ahnen[48], E. Von Toerne[24], B. Vormwald[36], V. Vorobel[134], K. Vorobev[37], M. Vos[164], K. Voss[142], M. Vozak[115], L. Vozdecky[121], N. Vranjes[15], M. Vranjes Milosavljevic[15], M. Vreeswijk[115], N.K. Vu[62d,62c], R. Vuillermet[36], O. Vujinovic[101], I. Vukotic[39], S. Wada[158], C. Wagner[104], J.M. Wagner[17a], W. Wagner[172], S. Wahdan[172], H. Wahlberg[91], M. Wakida[112], J. Walder[135], R. Walker[110], W. Walkowiak[142], A. Wall[129], E.J. Wallin[99], T. Wamorkar[6], A.Z. Wang[137], C. Wang[101], C. Wang[11], H. Wang[17a], J. Wang[64c], R.-J. Wang[101], R. Wang[61], R. Wang[6], S.M. Wang[149], S. Wang[62b], T. Wang[62a], W.T. Wang[80], W. Wang[14a], X. Wang[14c], X. Wang[163], X. Wang[62c], Y. Wang[62d], Y. Wang[14c], Z. Wang[107], Z. Wang[62d,51,62c], Z. Wang[107], A. Warburton[105], R.J. Ward[20], N. Warrack[59], S. Waterhouse[96], A.T. Watson[20], H. Watson[59], M.F. Watson[20], E. Watton[59,135], G. Watts[139], B.M. Waugh[97], J.M. Webb[54], C. Weber[29], H.A. Weber[18], M.S. Weber[19], S.M. Weber[63a], C. Wei[62a], Y. Wei[127], A.R. Weidberg[127], E.J. Weik[118], J. Weingarten[49], M. Weirich[101], C. Weiser[54], C.J. Wells[48], T. Wenaus[29], B. Wendland[49], T. Wengler[36], N.S. Wenke[111], N. Wermes[24], M. Wessels[63a], A.M. Wharton[92], A.S. White[61], A. White[8], M.J. White[1], D. Whiteson[160], L. Wickremasinghe[125], W. Wiedenmann[171], M. Wielers[135], C. Wiglesworth[42], D.J. Wilbern[121], H.G. Wilkens[36], J.J.H. Wilkinson[32], D.M. Williams[41], H.H. Williams[129], S. Williams[32], S. Willocq[104], B.J. Wilson[102], P.J. Windischhofer[39], F.I. Winkel[30], F. Winklmeier[124], B.T. Winter[54], J.K. Winter[102], M. Wittgen[144], M. Wobisch[98], Z. Wolffs[115], J. Wollrath[160], M.W. Wolter[87], H. Wolters[131a,131c], M.C. Wong[137], E.L. Woodward[41], S.D. Worm[48], B.K. Wosiek[87], K.W. Woźniak[87], S. Wozniewski[55], K. Wraight[59], C. Wu[20], M. Wu[14d], M. Wu[114], S.L. Wu[171], X. Wu[56], Y. Wu[62a], Z. Wu[4], J. Wuerzinger[111,ad], T.R. Wyatt[102], B.M. Wynne[52], S. Xella[42], L. Xia[14c], M. Xia[14b], J. Xiang[64c], M. Xie[62a], X. Xie[62a], S. Xin[14a,14e], A. Xiong[124], J. Xiong[17a], D. Xu[14a], H. Xu[62a], L. Xu[62a], R. Xu[129], T. Xu[107], Y. Xu[14b], Z. Xu[52], Z. Xu[14c], B. Yabsley[148], S. Yacoob[33a], Y. Yamaguchi[155], E. Yamashita[154], H. Yamauchi[158], T. Yamazaki[17a], Y. Yamazaki[85], J. Yan[62c], S. Yan[59], Z. Yan[104], H.J. Yang[62c,62d], H.T. Yang[62a], S. Yang[62a], T. Yang[64c], X. Yang[36], X. Yang[14a], Y. Yang[44], Y. Yang[62a], Z. Yang[62a], W-M. Yao[17a], H. Ye[14c], H. Ye[55], J. Ye[14a], S. Ye[29], X. Ye[62a], Y. Yeh[97], I. Yeletskikh[38], B. Yeo[17b], M.R. Yexley[97], P. Yin[41], K. Yorita[169], S. Younas[27b], C.J.S. Young[36], C. Young[144], C. Yu[14a,14e], Y. Yu[62a], M. Yuan[107], R. Yuan[62d], L. Yue[97], M. Zaazoua[62a], B. Zabinski[87], E. Zaid[52], Z.K. Zak[87], T. Zakareishvili[164], N. Zakharchuk[34], S. Zambito[56], J.A. Zamora Saa[138d,138b], J. Zang[154], D. Zanzi[54], O. Zaplatilek[133], C. Zeitnitz[172], H. Zeng[14a], J.C. Zeng[163], D.T. Zenger Jr[26], O. Zenin[37], T. Ženiš[28a], S. Zenz[95], S. Zerradi[35a], D. Zerwas[66], M. Zhai[14a,14e], D.F. Zhang[140], J. Zhang[62b], J. Zhang[6], K. Zhang[14a,14e], L. Zhang[62a], L. Zhang[14c], P. Zhang[14a,14e], R. Zhang[171], S. Zhang[107], S. Zhang[44], T. Zhang[154], X. Zhang[62c], X. Zhang[62b], Y. Zhang[62c,5], Y. Zhang[97], Y. Zhang[14c], Z. Zhang[17a], Z. Zhang[66], H. Zhao[139], T. Zhao[62b], Y. Zhao[137], Z. Zhao[62a], Z. Zhao[62a], A. Zhemchugov[38], J. Zheng[14c], K. Zheng[163], X. Zheng[62a], Z. Zheng[144], D. Zhong[163], B. Zhou[107], H. Zhou[7], N. Zhou[62c], Y. Zhou[14c], Y. Zhou[7], C.G. Zhu[62b], J. Zhu[107], Y. Zhu[62c], Y. Zhu[62a], X. Zhuang[14a], K. Zhukov[37], N.I. Zimine[38], J. Zinsser[63b],

JHEP10(2024)191

M. Ziolkowski[142], L. Živković[15], A. Zoccoli[23b,23a], K. Zoch[61], T.G. Zorbas[140], O. Zormpa[46], W. Zou[41], L. Zwalinski[36]

[1] *Department of Physics, University of Adelaide, Adelaide, Australia*
[2] *Department of Physics, University of Alberta, Edmonton AB, Canada*
[3] [(a)] *Department of Physics, Ankara University, Ankara;* [(b)] *Division of Physics, TOBB University of Economics and Technology, Ankara, Türkiye*
[4] *LAPP, Université Savoie Mont Blanc, CNRS/IN2P3, Annecy, France*
[5] *APC, Université Paris Cité, CNRS/IN2P3, Paris, France*
[6] *High Energy Physics Division, Argonne National Laboratory, Argonne IL, U.S.A.*
[7] *Department of Physics, University of Arizona, Tucson AZ, U.S.A.*
[8] *Department of Physics, University of Texas at Arlington, Arlington TX, U.S.A.*
[9] *Physics Department, National and Kapodistrian University of Athens, Athens, Greece*
[10] *Physics Department, National Technical University of Athens, Zografou, Greece*
[11] *Department of Physics, University of Texas at Austin, Austin TX, U.S.A.*
[12] *Institute of Physics, Azerbaijan Academy of Sciences, Baku, Azerbaijan*
[13] *Institut de Física d'Altes Energies (IFAE), Barcelona Institute of Science and Technology, Barcelona, Spain*
[14] [(a)] *Institute of High Energy Physics, Chinese Academy of Sciences, Beijing;* [(b)] *Physics Department, Tsinghua University, Beijing;* [(c)] *Department of Physics, Nanjing University, Nanjing;* [(d)] *School of Science, Shenzhen Campus of Sun Yat-sen University;* [(e)] *University of Chinese Academy of Science (UCAS), Beijing, China*
[15] *Institute of Physics, University of Belgrade, Belgrade, Serbia*
[16] *Department for Physics and Technology, University of Bergen, Bergen, Norway*
[17] [(a)] *Physics Division, Lawrence Berkeley National Laboratory, Berkeley CA;* [(b)] *University of California, Berkeley CA, U.S.A.*
[18] *Institut für Physik, Humboldt Universität zu Berlin, Berlin, Germany*
[19] *Albert Einstein Center for Fundamental Physics and Laboratory for High Energy Physics, University of Bern, Bern, Switzerland*
[20] *School of Physics and Astronomy, University of Birmingham, Birmingham, U.K.*
[21] [(a)] *Department of Physics, Bogazici University, Istanbul;* [(b)] *Department of Physics Engineering, Gaziantep University, Gaziantep;* [(c)] *Department of Physics, Istanbul University, Istanbul, Türkiye*
[22] [(a)] *Facultad de Ciencias y Centro de Investigaciónes, Universidad Antonio Nariño, Bogotá;* [(b)] *Departamento de Física, Universidad Nacional de Colombia, Bogotá, Colombia*
[23] [(a)] *Dipartimento di Fisica e Astronomia A. Righi, Università di Bologna, Bologna;* [(b)] *INFN Sezione di Bologna, Italy*
[24] *Physikalisches Institut, Universität Bonn, Bonn, Germany*
[25] *Department of Physics, Boston University, Boston MA, U.S.A.*
[26] *Department of Physics, Brandeis University, Waltham MA, U.S.A.*
[27] [(a)] *Transilvania University of Brasov, Brasov;* [(b)] *Horia Hulubei National Institute of Physics and Nuclear Engineering, Bucharest;* [(c)] *Department of Physics, Alexandru Ioan Cuza University of Iasi, Iasi;* [(d)] *National Institute for Research and Development of Isotopic and Molecular Technologies, Physics Department, Cluj-Napoca;* [(e)] *National University of Science and Technology Politechnica, Bucharest;* [(f)] *West University in Timisoara, Timisoara;* [(g)] *Faculty of Physics, University of Bucharest, Bucharest, Romania*
[28] [(a)] *Faculty of Mathematics, Physics and Informatics, Comenius University, Bratislava;* [(b)] *Department of Subnuclear Physics, Institute of Experimental Physics of the Slovak Academy of Sciences, Kosice, Slovak Republic*
[29] *Physics Department, Brookhaven National Laboratory, Upton NY, U.S.A.*
[30] *Universidad de Buenos Aires, Facultad de Ciencias Exactas y Naturales, Departamento de Física, y CONICET, Instituto de Física de Buenos Aires (IFIBA), Buenos Aires, Argentina*
[31] *California State University, CA, U.S.A.*
[32] *Cavendish Laboratory, University of Cambridge, Cambridge, U.K.*
[33] [(a)] *Department of Physics, University of Cape Town, Cape Town;* [(b)] *iThemba Labs, Western*

JHEP10(2024)191

Cape;[(c)] *Department of Mechanical Engineering Science, University of Johannesburg, Johannesburg;*[(d)] *National Institute of Physics, University of the Philippines Diliman (Philippines);*[(e)] *University of South Africa, Department of Physics, Pretoria;*[(f)] *University of Zululand, KwaDlangezwa;*[(g)] *School of Physics, University of the Witwatersrand, Johannesburg, South Africa*

[34] *Department of Physics, Carleton University, Ottawa ON, Canada*

[35] [(a)] *Faculté des Sciences Ain Chock, Université Hassan II de Casablanca;*[(b)] *Faculté des Sciences, Université Ibn-Tofail, Kénitra;*[(c)] *Faculté des Sciences Semlalia, Université Cadi Ayyad, LPHEA-Marrakech;*[(d)] *LPMR, Faculté des Sciences, Université Mohamed Premier, Oujda;*[(e)] *Faculté des sciences, Université Mohammed V, Rabat;*[(f)] *Institute of Applied Physics, Mohammed VI Polytechnic University, Ben Guerir, Morocco*

[36] *CERN, Geneva, Switzerland*

[37] *Affiliated with an institute covered by a cooperation agreement with CERN*

[38] *Affiliated with an international laboratory covered by a cooperation agreement with CERN*

[39] *Enrico Fermi Institute, University of Chicago, Chicago IL, U.S.A.*

[40] *LPC, Université Clermont Auvergne, CNRS/IN2P3, Clermont-Ferrand, France*

[41] *Nevis Laboratory, Columbia University, Irvington NY, U.S.A.*

[42] *Niels Bohr Institute, University of Copenhagen, Copenhagen, Denmark*

[43] [(a)] *Dipartimento di Fisica, Università della Calabria, Rende;*[(b)] *INFN Gruppo Collegato di Cosenza, Laboratori Nazionali di Frascati, Italy*

[44] *Physics Department, Southern Methodist University, Dallas TX, U.S.A.*

[45] *Physics Department, University of Texas at Dallas, Richardson TX, U.S.A.*

[46] *National Centre for Scientific Research "Demokritos", Agia Paraskevi, Greece*

[47] [(a)] *Department of Physics, Stockholm University;*[(b)] *Oskar Klein Centre, Stockholm, Sweden*

[48] *Deutsches Elektronen-Synchrotron DESY, Hamburg and Zeuthen, Germany*

[49] *Fakultät Physik, Technische Universität Dortmund, Dortmund, Germany*

[50] *Institut für Kern- und Teilchenphysik, Technische Universität Dresden, Dresden, Germany*

[51] *Department of Physics, Duke University, Durham NC, U.S.A.*

[52] *SUPA — School of Physics and Astronomy, University of Edinburgh, Edinburgh, U.K.*

[53] *INFN e Laboratori Nazionali di Frascati, Frascati, Italy*

[54] *Physikalisches Institut, Albert-Ludwigs-Universität Freiburg, Freiburg, Germany*

[55] *II. Physikalisches Institut, Georg-August-Universität Göttingen, Göttingen, Germany*

[56] *Département de Physique Nucléaire et Corpusculaire, Université de Genève, Genève, Switzerland*

[57] [(a)] *Dipartimento di Fisica, Università di Genova, Genova;*[(b)] *INFN Sezione di Genova, Italy*

[58] *II. Physikalisches Institut, Justus-Liebig-Universität Giessen, Giessen, Germany*

[59] *SUPA — School of Physics and Astronomy, University of Glasgow, Glasgow, U.K.*

[60] *LPSC, Université Grenoble Alpes, CNRS/IN2P3, Grenoble INP, Grenoble, France*

[61] *Laboratory for Particle Physics and Cosmology, Harvard University, Cambridge MA, U.S.A.*

[62] [(a)] *Department of Modern Physics and State Key Laboratory of Particle Detection and Electronics, University of Science and Technology of China, Hefei;*[(b)] *Institute of Frontier and Interdisciplinary Science and Key Laboratory of Particle Physics and Particle Irradiation (MOE), Shandong University, Qingdao;*[(c)] *School of Physics and Astronomy, Shanghai Jiao Tong University, Key Laboratory for Particle Astrophysics and Cosmology (MOE), SKLPPC, Shanghai;*[(d)] *Tsung-Dao Lee Institute, Shanghai;*[(e)] *School of Physics and Microelectronics, Zhengzhou University, China*

[63] [(a)] *Kirchhoff-Institut für Physik, Ruprecht-Karls-Universität Heidelberg, Heidelberg;*[(b)] *Physikalisches Institut, Ruprecht-Karls-Universität Heidelberg, Heidelberg, Germany*

[64] [(a)] *Department of Physics, Chinese University of Hong Kong, Shatin, N.T., Hong Kong;*[(b)] *Department of Physics, University of Hong Kong, Hong Kong;*[(c)] *Department of Physics and Institute for Advanced Study, Hong Kong University of Science and Technology, Clear Water Bay, Kowloon, Hong Kong, China*

[65] *Department of Physics, National Tsing Hua University, Hsinchu, Taiwan*

[66] *IJCLab, Université Paris-Saclay, CNRS/IN2P3, 91405, Orsay, France*

[67] *Centro Nacional de Microelectrónica (IMB-CNM-CSIC), Barcelona, Spain*

[68] *Department of Physics, Indiana University, Bloomington IN, U.S.A.*

[69] [(a)] *INFN Gruppo Collegato di Udine, Sezione di Trieste, Udine;*[(b)] *ICTP, Trieste;*[(c)] *Dipartimento Politecnico di Ingegneria e Architettura, Università di Udine, Udine, Italy*

JHEP10(2024)191

[70] [(a)] INFN Sezione di Lecce; [(b)] Dipartimento di Matematica e Fisica, Università del Salento, Lecce, Italy
[71] [(a)] INFN Sezione di Milano; [(b)] Dipartimento di Fisica, Università di Milano, Milano, Italy
[72] [(a)] INFN Sezione di Napoli; [(b)] Dipartimento di Fisica, Università di Napoli, Napoli, Italy
[73] [(a)] INFN Sezione di Pavia; [(b)] Dipartimento di Fisica, Università di Pavia, Pavia, Italy
[74] [(a)] INFN Sezione di Pisa; [(b)] Dipartimento di Fisica E. Fermi, Università di Pisa, Pisa, Italy
[75] [(a)] INFN Sezione di Roma; [(b)] Dipartimento di Fisica, Sapienza Università di Roma, Roma, Italy
[76] [(a)] INFN Sezione di Roma Tor Vergata; [(b)] Dipartimento di Fisica, Università di Roma Tor Vergata, Roma, Italy
[77] [(a)] INFN Sezione di Roma Tre; [(b)] Dipartimento di Matematica e Fisica, Università Roma Tre, Roma, Italy
[78] [(a)] INFN-TIFPA; [(b)] Università degli Studi di Trento, Trento, Italy
[79] Universität Innsbruck, Department of Astro and Particle Physics, Innsbruck, Austria
[80] University of Iowa, Iowa City IA, U.S.A.
[81] Department of Physics and Astronomy, Iowa State University, Ames IA, U.S.A.
[82] Istinye University, Sariyer, Istanbul, Türkiye
[83] [(a)] Departamento de Engenharia Elétrica, Universidade Federal de Juiz de Fora (UFJF), Juiz de Fora; [(b)] Universidade Federal do Rio De Janeiro COPPE/EE/IF, Rio de Janeiro; [(c)] Instituto de Física, Universidade de São Paulo, São Paulo; [(d)] Rio de Janeiro State University, Rio de Janeiro; [(e)] Federal University of Bahia, Bahia, Brazil
[84] KEK, High Energy Accelerator Research Organization, Tsukuba, Japan
[85] Graduate School of Science, Kobe University, Kobe, Japan
[86] [(a)] AGH University of Krakow, Faculty of Physics and Applied Computer Science, Krakow; [(b)] Marian Smoluchowski Institute of Physics, Jagiellonian University, Krakow, Poland
[87] Institute of Nuclear Physics Polish Academy of Sciences, Krakow, Poland
[88] Faculty of Science, Kyoto University, Kyoto, Japan
[89] Research Center for Advanced Particle Physics and Department of Physics, Kyushu University, Fukuoka, Japan
[90] L2IT, Université de Toulouse, CNRS/IN2P3, UPS, Toulouse, France
[91] Instituto de Física La Plata, Universidad Nacional de La Plata and CONICET, La Plata, Argentina
[92] Physics Department, Lancaster University, Lancaster, U.K.
[93] Oliver Lodge Laboratory, University of Liverpool, Liverpool, U.K.
[94] Department of Experimental Particle Physics, Jožef Stefan Institute and Department of Physics, University of Ljubljana, Ljubljana, Slovenia
[95] School of Physics and Astronomy, Queen Mary University of London, London, U.K.
[96] Department of Physics, Royal Holloway University of London, Egham, U.K.
[97] Department of Physics and Astronomy, University College London, London, U.K.
[98] Louisiana Tech University, Ruston LA, U.S.A.
[99] Fysiska institutionen, Lunds universitet, Lund, Sweden
[100] Departamento de Física Teorica C-15 and CIAFF, Universidad Autónoma de Madrid, Madrid, Spain
[101] Institut für Physik, Universität Mainz, Mainz, Germany
[102] School of Physics and Astronomy, University of Manchester, Manchester, U.K.
[103] CPPM, Aix-Marseille Université, CNRS/IN2P3, Marseille, France
[104] Department of Physics, University of Massachusetts, Amherst MA, U.S.A.
[105] Department of Physics, McGill University, Montreal QC, Canada
[106] School of Physics, University of Melbourne, Victoria, Australia
[107] Department of Physics, University of Michigan, Ann Arbor MI, U.S.A.
[108] Department of Physics and Astronomy, Michigan State University, East Lansing MI, U.S.A.
[109] Group of Particle Physics, University of Montreal, Montreal QC, Canada
[110] Fakultät für Physik, Ludwig-Maximilians-Universität München, München, Germany
[111] Max-Planck-Institut für Physik (Werner-Heisenberg-Institut), München, Germany
[112] Graduate School of Science and Kobayashi-Maskawa Institute, Nagoya University, Nagoya, Japan
[113] Department of Physics and Astronomy, University of New Mexico, Albuquerque NM, U.S.A.
[114] Institute for Mathematics, Astrophysics and Particle Physics, Radboud University/Nikhef, Nijmegen, Netherlands

JHEP10(2024)191

[115] Nikhef National Institute for Subatomic Physics and University of Amsterdam, Amsterdam, Netherlands
[116] Department of Physics, Northern Illinois University, DeKalb IL, U.S.A.
[117] [(a)] New York University Abu Dhabi, Abu Dhabi;[(b)] United Arab Emirates University, Al Ain, United Arab Emirates
[118] Department of Physics, New York University, New York NY, U.S.A.
[119] Ochanomizu University, Otsuka, Bunkyo-ku, Tokyo, Japan
[120] Ohio State University, Columbus OH, U.S.A.
[121] Homer L. Dodge Department of Physics and Astronomy, University of Oklahoma, Norman OK, U.S.A.
[122] Department of Physics, Oklahoma State University, Stillwater OK, U.S.A.
[123] Palacký University, Joint Laboratory of Optics, Olomouc, Czech Republic
[124] Institute for Fundamental Science, University of Oregon, Eugene, OR, U.S.A.
[125] Graduate School of Science, Osaka University, Osaka, Japan
[126] Department of Physics, University of Oslo, Oslo, Norway
[127] Department of Physics, Oxford University, Oxford, U.K.
[128] LPNHE, Sorbonne Université, Université Paris Cité, CNRS/IN2P3, Paris, France
[129] Department of Physics, University of Pennsylvania, Philadelphia PA, U.S.A.
[130] Department of Physics and Astronomy, University of Pittsburgh, Pittsburgh PA, U.S.A.
[131] [(a)] Laboratório de Instrumentação e Física Experimental de Partículas — LIP, Lisboa;[(b)] Departamento de Física, Faculdade de Ciências, Universidade de Lisboa, Lisboa;[(c)] Departamento de Física, Universidade de Coimbra, Coimbra;[(d)] Centro de Física Nuclear da Universidade de Lisboa, Lisboa;[(e)] Departamento de Física, Universidade do Minho, Braga;[(f)] Departamento de Física Teórica y del Cosmos, Universidad de Granada, Granada (Spain);[(g)] Departamento de Física, Instituto Superior Técnico, Universidade de Lisboa, Lisboa, Portugal
[132] Institute of Physics of the Czech Academy of Sciences, Prague, Czech Republic
[133] Czech Technical University in Prague, Prague, Czech Republic
[134] Charles University, Faculty of Mathematics and Physics, Prague, Czech Republic
[135] Particle Physics Department, Rutherford Appleton Laboratory, Didcot, U.K.
[136] IRFU, CEA, Université Paris-Saclay, Gif-sur-Yvette, France
[137] Santa Cruz Institute for Particle Physics, University of California Santa Cruz, Santa Cruz CA, U.S.A.
[138] [(a)] Departamento de Física, Pontificia Universidad Católica de Chile, Santiago;[(b)] Millennium Institute for Subatomic physics at high energy frontier (SAPHIR), Santiago;[(c)] Instituto de Investigación Multidisciplinario en Ciencia y Tecnología, y Departamento de Física, Universidad de La Serena;[(d)] Universidad Andres Bello, Department of Physics, Santiago;[(e)] Instituto de Alta Investigación, Universidad de Tarapacá, Arica;[(f)] Departamento de Física, Universidad Técnica Federico Santa María, Valparaíso, Chile
[139] Department of Physics, University of Washington, Seattle WA, U.S.A.
[140] Department of Physics and Astronomy, University of Sheffield, Sheffield, U.K.
[141] Department of Physics, Shinshu University, Nagano, Japan
[142] Department Physik, Universität Siegen, Siegen, Germany
[143] Department of Physics, Simon Fraser University, Burnaby BC, Canada
[144] SLAC National Accelerator Laboratory, Stanford CA, U.S.A.
[145] Department of Physics, Royal Institute of Technology, Stockholm, Sweden
[146] Departments of Physics and Astronomy, Stony Brook University, Stony Brook NY, U.S.A.
[147] Department of Physics and Astronomy, University of Sussex, Brighton, U.K.
[148] School of Physics, University of Sydney, Sydney, Australia
[149] Institute of Physics, Academia Sinica, Taipei, Taiwan
[150] [(a)] E. Andronikashvili Institute of Physics, Iv. Javakhishvili Tbilisi State University, Tbilisi;[(b)] High Energy Physics Institute, Tbilisi State University, Tbilisi;[(c)] University of Georgia, Tbilisi, Georgia
[151] Department of Physics, Technion, Israel Institute of Technology, Haifa, Israel
[152] Raymond and Beverly Sackler School of Physics and Astronomy, Tel Aviv University, Tel Aviv, Israel
[153] Department of Physics, Aristotle University of Thessaloniki, Thessaloniki, Greece
[154] International Center for Elementary Particle Physics and Department of Physics, University of Tokyo, Tokyo, Japan

JHEP10(2024)191

[155] Department of Physics, Tokyo Institute of Technology, Tokyo, Japan
[156] Department of Physics, University of Toronto, Toronto ON, Canada
[157] [(a)] TRIUMF, Vancouver BC; [(b)] Department of Physics and Astronomy, York University, Toronto ON, Canada
[158] Division of Physics and Tomonaga Center for the History of the Universe, Faculty of Pure and Applied Sciences, University of Tsukuba, Tsukuba, Japan
[159] Department of Physics and Astronomy, Tufts University, Medford MA, U.S.A.
[160] Department of Physics and Astronomy, University of California Irvine, Irvine CA, U.S.A.
[161] University of Sharjah, Sharjah, United Arab Emirates
[162] Department of Physics and Astronomy, University of Uppsala, Uppsala, Sweden
[163] Department of Physics, University of Illinois, Urbana IL, U.S.A.
[164] Instituto de Física Corpuscular (IFIC), Centro Mixto Universidad de Valencia — CSIC, Valencia, Spain
[165] Department of Physics, University of British Columbia, Vancouver BC, Canada
[166] Department of Physics and Astronomy, University of Victoria, Victoria BC, Canada
[167] Fakultät für Physik und Astronomie, Julius-Maximilians-Universität Würzburg, Würzburg, Germany
[168] Department of Physics, University of Warwick, Coventry, U.K.
[169] Waseda University, Tokyo, Japan
[170] Department of Particle Physics and Astrophysics, Weizmann Institute of Science, Rehovot, Israel
[171] Department of Physics, University of Wisconsin, Madison WI, U.S.A.
[172] Fakultät für Mathematik und Naturwissenschaften, Fachgruppe Physik, Bergische Universität Wuppertal, Wuppertal, Germany
[173] Department of Physics, Yale University, New Haven CT, U.S.A.

[a] Also Affiliated with an institute covered by a cooperation agreement with CERN
[b] Also at An-Najah National University, Nablus, Palestine
[c] Also at Borough of Manhattan Community College, City University of New York, New York NY, U.S.A.
[d] Also at Center for High Energy Physics, Peking University, China
[e] Also at Center for Interdisciplinary Research and Innovation (CIRI-AUTH), Thessaloniki, Greece
[f] Also at Centro Studi e Ricerche Enrico Fermi, Italy
[g] Also at CERN, Geneva, Switzerland
[h] Also at Département de Physique Nucléaire et Corpusculaire, Université de Genève, Genève, Switzerland
[i] Also at Departament de Fisica de la Universitat Autonoma de Barcelona, Barcelona, Spain
[j] Also at Department of Financial and Management Engineering, University of the Aegean, Chios, Greece
[k] Also at Department of Physics, California State University, Sacramento, U.S.A.
[l] Also at Department of Physics, King's College London, London, U.K.
[m] Also at Department of Physics, Stanford University, Stanford CA, U.S.A.
[n] Also at Department of Physics, Stellenbosch University, South Africa
[o] Also at Department of Physics, University of Fribourg, Fribourg, Switzerland
[p] Also at Department of Physics, University of Thessaly, Greece
[q] Also at Department of Physics, Westmont College, Santa Barbara, U.S.A.
[r] Also at Faculty of Physics, Sofia University, 'St. Kliment Ohridski', Sofia, Bulgaria
[s] Also at Hellenic Open University, Patras, Greece
[t] Also at Institucio Catalana de Recerca i Estudis Avancats, ICREA, Barcelona, Spain
[u] Also at Institut für Experimentalphysik, Universität Hamburg, Hamburg, Germany
[v] Also at Institute for Nuclear Research and Nuclear Energy (INRNE) of the Bulgarian Academy of Sciences, Sofia, Bulgaria
[w] Also at Institute of Applied Physics, Mohammed VI Polytechnic University, Ben Guerir, Morocco
[x] Also at Institute of Particle Physics (IPP), Canada
[y] Also at Institute of Physics and Technology, Mongolian Academy of Sciences, Ulaanbaatar, Mongolia
[z] Also at Institute of Physics, Azerbaijan Academy of Sciences, Baku, Azerbaijan
[aa] Also at Institute of Theoretical Physics, Ilia State University, Tbilisi, Georgia
[ab] Also at Lawrence Livermore National Laboratory, Livermore, U.S.A.
[ac] Also at National Institute of Physics, University of the Philippines Diliman (Philippines), Philippines
[ad] Also at Technical University of Munich, Munich, Germany

JHEP10(2024)191

[ae] Also at The Collaborative Innovation Center of Quantum Matter (CICQM), Beijing, China
[af] Also at TRIUMF, Vancouver BC, Canada
[ag] Also at Università di Napoli Parthenope, Napoli, Italy
[ah] Also at University of Colorado Boulder, Department of Physics, Colorado, U.S.A.
[ai] Also at Washington College, Chestertown, MD, U.S.A.
[aj] Also at Yeditepe University, Physics Department, Istanbul, Türkiye
[*] Deceased

JHEP10(2024)191